TURBOPROP PERFORMANCE AND ACOUSTIC EVALUATION FOR A SMALL UNMANNED AIRCRAFT VARIABLE-CYCLE ENGINE

By

MATT DURKEE

Bachelor of Science in Aerospace Engineering
Oklahoma State University
Stillwater, OK
2017

Bachelor of Science in Mechanical Engineering
Oklahoma State University
Stillwater, OK
2017

Submitted to the Faculty of the
Graduate College of the
Oklahoma State University
in partial fulfillment of
the requirements for
the Degree of
MASTER OF SCIENCE
May, 2019

TURBOPROP PERFORMANCE AND ACOUSTIC

EVALUATION FOR A SMALL UNMANNED

AIRCRAFT VARIABLE-CYCLE ENGINE

Thesis Approved:

DR. KURT ROUSER

Thesis Adviser

DR. RICHARD GAETA

DR. JAMEY JACOB

ACKNOWLEDGEMENTS

The author would like to thank Dr. Kurt Rouser and Dr. Rick Gaeta for assistance in the direction of this study. The author would also like to thank research assistants Nick Lucido, Kylar Moody, Connor McCain, Garett Foster, Lauren Jones, Norbert Delatte and Cole Replogle for assistance in engine analysis and tests.

Name: MATT R. DURKEE

Date of Degree: MAY, 2019

Title of Study: TURBOPROP PERFORMANCE AND ACOUSTIC EVALUATION FOR A SMALL UNMANNED AIRCRAFT VARIABLE-CYCLE ENGINE

Major Field: MECHANICAL AND AEROSPACE ENGINEERING

Abstract: Range and endurance of small unmanned aircraft systems (sUAS) driven by gas turbine engines are constrained by high thrust specific fuel consumption (TSFC) resulting from low overall efficiency. This study evaluates the feasibility of a variable-cycle propulsion system to improve the versatility of sUAS by allowing for a dash capability or a lower TSFC when needed. Two variable-cycle concepts are presented, each with the characteristics of a turbojet and a turboprop. These concepts were designed primarily with commercial off-the-shelf components, and parts were tested for operability. The first concept features a turbojet driving a turbine coupled to a propeller. The second concept features a turboprop in its stock configuration with an optional clutch on the propeller shaft. Qualitative results from the variable-cycle concepts show difficulties in engine startup with an aft propeller assembly and higher than nominal temperatures in the stock configuration with a clutched propeller.

To evaluate the effectiveness of the variable-cycle concepts, static performance and acoustic contributions were studied from a small commercial off-the-shelf turboprop. A thermodynamic model and resultant mission analysis are also developed to study performance expectations and potential capabilities. The sensitivity on thrust and SFC for parameters is presented to evaluate the impact of the assumptions. Performance data is used to quantify the expected benefits of each variable-cycle engine mode, and the acoustic signatures of the engines are also a concern from both an annoyance and detection perspective. A thrust stand was designed with the capability to mount various propulsors and measure their thrust. Far field acoustic measurements of the turboprop were acquired simultaneously with thrust measurements. Propwash and exhaust properties and their contributions to noise were studied in a wind tunnel with a traverse pitot probe and a thermocouple. Performance results of this study show approximately a 60% decrease in small turboprop TSFC when compared to turbojets. A notional mission analysis reveals a wider operating range with a variable-cycle engine when compared to a turbojet or turboprop alone. Acoustic data shows distinct blade passing frequencies from turbomachinery and propeller noise which could impact detectability.

TABLE OF CONTENTS

Chapter Page

LIST OF TABLES

Table Page

LIST OF FIGURES

Figure Page

Figure Page

NOMENCLATURE

AR	aspect ratio
α	ratio of primary to secondary flow inlet areas
β	propeller pitch angle, deg
BPF	blade passing frequency, Hz
C_D	drag coefficient
C_L	lift coefficient
CNC	computer numerical control
c_{pc}	specific heat before combustion, BTU/lbm*R
c_{pt}	specific heat after combustion, BTU/lbm*R
d	diameter, in
D	drag, lb
E	aircraft endurance, min
f	frequency, Hz
F	thrust, lb
g	acceleration due to gravity, m/s^2
g_c	gravitational proportionality constant, lbm*ft/lbf*s^2
GSU	ground support unit
γ	ratio of specific heats
h_{PR}	heat capacity of fuel, BTU/lbm
η	efficiency

J	propeller advance ratio
LOT	Level of Technology
M	Mach number
$\dot{m}$	mass flow rate, lbm/s
n	number of blades
OASPL	Overall Sound Pressure Level, dB
p	blade pitch, in
P	pressure, psi
PCA	Parametric Cycle Analysis
Φ	installation losses
r	radius, in
ρ	density, lbm/ft^3
π	pressure ratio
RPM	rotations per minute
s	sample standard deviation
S	wing area, ft^2
SFC	Specific Fuel Consumption
SPL	Sound Pressure Level, dB
sUAS	Small Unmanned Aircraft Systems
T	temperature, °F
TP	turboprop
TSFC	Thrust Specific Fuel Consumption
θ	measurement angle, deg
U	velocity, ft/s
UAS	Unmanned Aircraft Systems
UDF	Unducted Fan

V	velocity, ft/s
VC	Variable-Cycle
Wt	aircraft weight, lb
x_i	variable magnitude
$\bar{x}$	mean value of variable

Subscripts

avg	average
b	combustor, burner
c	compressor
d	diffuser
f	fuel
j	jet
m	mixing region
mech	mechanical shaft
n	nozzle
prop	propeller
t	total or stagnation property
tip	propeller tip
0	ambient, freestream
2	compressor inlet
3	combustor inlet
4	turbine inlet
5	turbine exit
9	nozzle exit
∞	freestream

CHAPTER I

INTRODUCTION

The use of electric motors and batteries has been prominent for propulsion of small unmanned aircraft systems (sUAS) under 50 lb of take-off weight. Range and endurance of sUAS is limited due to the low energy density of batteries. Propulsion systems that use more energy-dense hydrocarbon fuels (about 75 times more dense than batteries) are desirable for increasing range and endurance of sUAS. Small turbojet and turboprop engines (10- to 50-lb thrust class) are commercially available making their use on sUAS feasible. Figure 1 shows an example of a small unmanned aircraft that makes use of a turbojet engine.

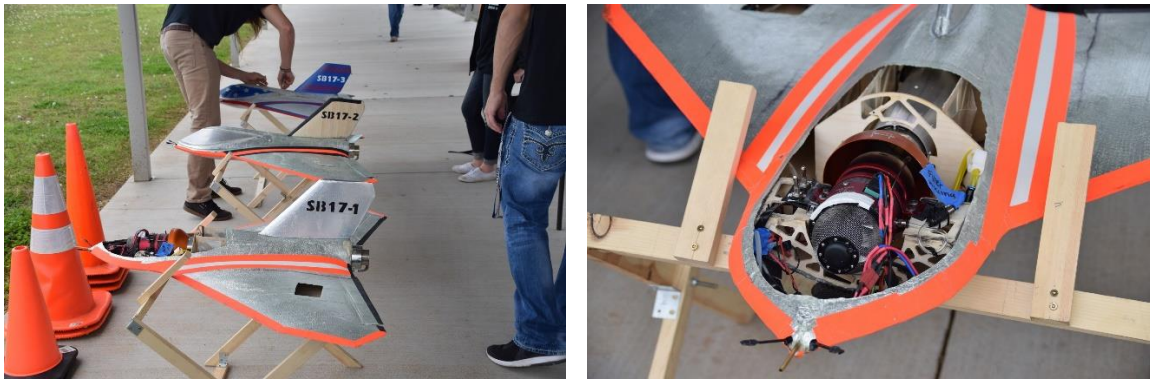

Figure 1. Example of a Small Turbojet Integrated into an Airframe.

Gas turbine propulsion systems are versatile for a range of mission types, so this can open the design space for smaller aircraft. For example, a small turbojet would be appropriate for sUAS

flying a radar avoidance and elimination mission requiring high-speed flight. In contrast, sUAS used for low-speed inspection of oil pipelines are better equipped with a propeller arrangement for lower fuel consumption than a turbojet, and therefore greater range and endurance. A turboprop engine has a similar gas turbine core to that of a turbojet but has a higher power-to-weight ratio than a piston engine and propeller arrangement. The advantage in power-to-weight is more prominent at a large scale but still exists at a small scale. For example, the DA100 piston engine and the KingTech K60TP turboprop both produce 7.3 kW of power, but the DA100 is 6% heavier [1][2][3]. Furthermore, a starter is not included in DA100 weight but is included in the K60TP weight. The K45TP used in the current study is smaller than the K60TP and is capable of producing 5.2 kW.

Figure 2 shows a concept of operation for a notional sUAS mission that would require both the high-speed dash capability of a turbojet and the low fuel consumption inherent to turboprops. This is a military mission in which the UAS needs to quickly achieve proximity to a target and also maintain that proximity for some amount of time. The quick maneuver to a location, or dash, would be carried out in a turbojet mode, and the loiter would make use of a turboprop mode. A variable-cycle propulsion system that has the capability of high-speed dash or low-speed loiter with less fuel consumption would allow sUAS to carry out diverse missions like that shown in Figure 2.

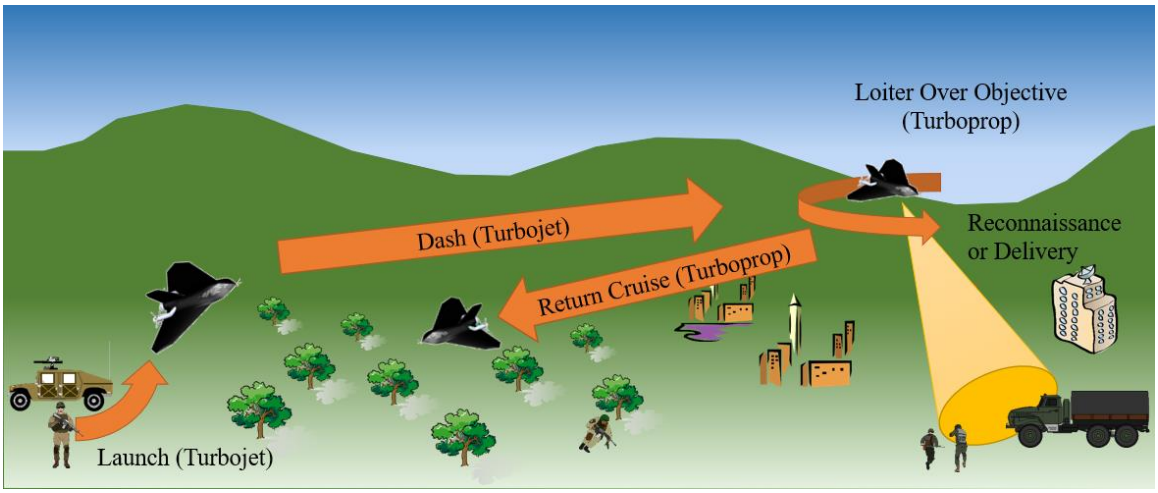

Figure 2. Notional Military Mission for a Variable-Cycle Propulsion System.

Performance and acoustic data are useful for evaluating the effectiveness a design that includes a small gas turbine engine. The current study uses a combined design and research philosophy that features development of variable-cycle concepts and investigation into their accompanying performance and acoustic signature to evaluate the more promising variable-cycle concept. A flow chart of this process can be seen in Figure 3.

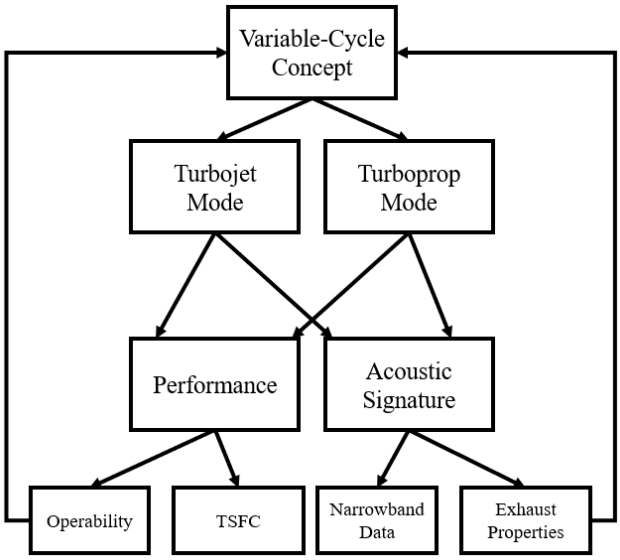

Figure 3. Variable-Cycle Design and Research Flow Chart.

The goal of this study is to evaluate the feasibility of the variable-cycle concept and suggest the most promising configuration. Specific objectives include: 1) experimental evaluation of different propulsion system configurations, 2) computational parametric analysis of turbojet performance and 3) experimental static performance and acoustic analysis of pusher and puller turboprop configurations.

CHAPTER II

BACKGROUND

This chapter reviews the different gas turbine cycles and the theory behind evaluating their performance and acoustics. Previous novel engine designs are studied and relevant theory to the current study's variable-cycle concepts is presented. The review of previous work also includes the contribution of propeller noise and jet noise for turbojet and turboprop noise.

2.1 Gas Turbine Engines

The core of a gas turbine engine includes a compressor, combustor and a turbine. The turbine extracts energy from air flow through the engine after fuel mixing and combustion has occurred. The turbine is typically attached to a shaft to drive the compressor that prepares incoming air for combustion. A turbojet cycle is composed of these three components with the addition of an inlet and a nozzle, as seen in Figure 4. The difference in gas turbine cycles is often due to additional engine components. For example, a turboprop is like a turbojet with the addition of a second turbine (free or power turbine) attached to a shaft that spins a propeller. Simplified schematics of these two cycles can be seen in Figure 4.

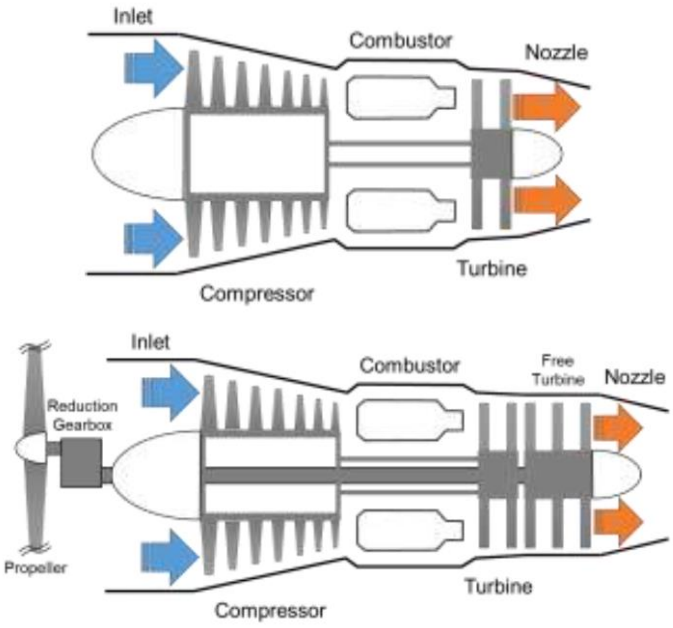

Figure 4. Turbojet Schematic (top) and Turboprop Schematic (bottom).

Turbojets inherently have high-speed exhaust but also a higher thrust specific fuel consumption (TSFC), or SFC when uninstalled [4]. SFC considers the fuel consumption divided by thrust, shown in Equation 1. Turboprops have a lower SFC but have a smaller range of flight speeds due to relatively low-speed exhaust. A turboprop's lower fuel consumption can be seen in Figure 5 (left) and a turbojet's higher specific thrust can be seen in Figure 5 (right) from Mattingly [4]. SFC is inversely related to range and endurance as shown by the simplified, linear-averaged relations in Equation 2. In summary, aircraft with turbojets are traditionally high-speed with low range and endurance, and aircraft with turboprops are low-speed with high range and endurance. A versatile aircraft would feature the benefits of both of these modes. These relations motivate the current study, and SFC will be used to evaluate the different forms of propulsion.

$$SFC \equiv \frac{\dot{m}_f}{F} \tag{1}$$

$$E = \frac{\Delta W t_f}{TSFC * D_{avg}} \qquad R = \frac{\Delta W t_f}{TSFC * D_{avg}} * V_{\infty} \tag{2}$$

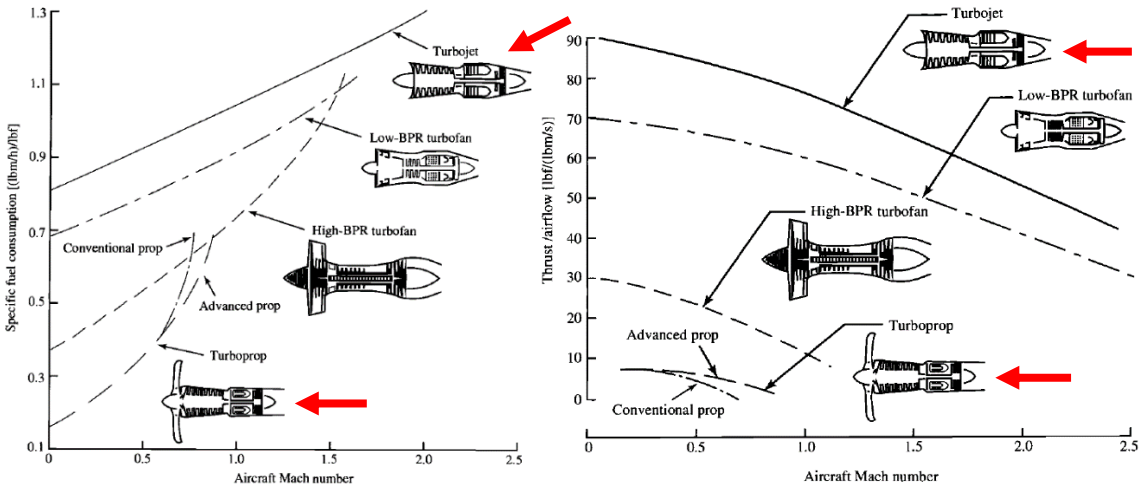

Figure 5. Specific Fuel Consumption and Specific Thrust vs Flight Speed for Several Different Gas Turbine Engines [4].

Mattingly [4] defines Level of Technology (LOT) for analysis of gas turbines. LOT is a way of representing figures of merit and expected losses across components in gas turbines. For example, in an ideal analysis, the total pressure ratio across an exhaust nozzle (π_n) is assumed to be 1. In other words, the nozzle does not cause a drop in total pressure. Figure 6 shows different levels of technology that account for real effects in gas turbine components. The different levels of technology are essentially representations of technical capabilities in 20-year increments in history beginning in 1945. For example, LOT 3 is component figures of merit from the time period 1985-2005. The table also takes into account varying design types and resultant figures of merit. Thus, Figure 6 shows that a fixed-area convergent nozzle with LOT 3 would have a π_n of 0.98. Various LOT is chosen for components in the analytical section of the current study due to considerations like small-scale analysis and modern manufacturing.

Component	Figure of merit	Type[a]	Level of technology[b] 1	2	3	4
Diffuser	$\pi_{d\,max}$	A	0.90	0.95	0.98	0.995
		B	0.88	0.93	0.96	0.98
		C	0.85	0.90	0.94	0.96
Compressor	e_c		0.80	0.84	0.88	0.90
Fan	e_f		0.78	0.82	0.86	0.89
Burner	π_b		0.90	0.92	0.94	0.95
	η_b		0.88	0.94	0.99	0.999
Turbine	e_t	Uncooled	0.80	0.85	0.89	0.90
		Cooled		0.83	0.87	0.89
Afterburner	π_{AB}		0.90	0.92	0.94	0.95
	η_{AB}		0.85	0.91	0.96	0.99
Nozzle		D	0.95	0.97	0.98	0.995
	π_n	E	0.93	0.96	0.97	0.98
		F	0.90	0.93	0.95	0.97
Mechanical shaft	η_m	Shaft only	0.95	0.97	0.99	0.995
		With power takeoff	0.90	0.92	0.95	0.97
Maximum T_{t4}		(K)	1110	1390	1780	2000
		(R)	2000	2500	3200	3600
Maximum T_{t7}		(K)	1390	1670	2000	2220
		(R)	2500	3000	3600	4000

[a]A = subsonic aircraft with engines in nacelles
B = subsonic aircraft with engine(s) in airframe
C = supersonic aircraft with engine(s) in airframe
D = fixed-area convergent nozzle
E = variable-area convergent nozzle
F = variable-area convergent-divergent nozzle

Figure 6. Levels of Technology for Gas Turbine Engines [4].

2.2 Variable-Cycle Engine Design

Variable-cycle engines have been explored for larger scale aircraft. These engines typically involve variable systems that adjust the bypass ratio of the engine, enabling dual-mode operation between turbofan and turbojet. For example, the performance of a selective-bleed turbofan for the conceptual S-95 aircraft was studied by Wood and Pelidis [5]. They proposed an engine with two different bypass flow areas and accompanying valves that would change the bypass ratio from 0.4 to 1. Simulations in a gas turbine design software showed that the low-bypass mode met speed requirements for the conceptual aircraft, but the high-bypass mode resulted in 48% less SFC and 5% less specific thrust when the high speed was not needed. A comparable variable bleed system is also in development on the GE ADVENT engine with a prototype already tested in the 1990s [6]. Although these two examples feature ducted rotors, performance results and versatility of the concepts in the current study are expected to be similar.

The design of one of the variable-cycle concepts in the current study is influenced by an aft open rotor similar to the Unducted Fan (UDF) from the Advanced Turboprop Project [7]. Aft propellers were driven directly by counterrotating turbine stages in the gas turbine core. Figure 7 shows flight tests that were conducted on a Boeing 727 aircraft at Mach 0.6 and 35,000 ft. The project reports a TSFC 30% lower than a comparable turbofan at the time effectively due to high bypass ratios. The UDF concept takes advantage of exposed fan blades but does not vary the cycle of the gas turbine. Another concept in the current study uses an optional clutch on an exposed rotor. This effectively extracts more work from the engine core like the F135 lift fan [8] although the current study produces thrust in the same direction with and without the clutch.

Figure 7. Unducted Fan Flight Tests during the Advanced Turboprop Project [7].

2.2.1 Propeller Theory and Definitions

A relevant quantity for propeller selection is propeller efficiency which is a ratio of power (P) out of and into the propeller, as shown in Equation 3 [3][9].

$$\eta_{prop} = \frac{P_{out}}{P_{in}} \tag{3}$$

Propeller efficiency depends on advance ratio. Advance ratio is a dimensionless quantity that can be used to compare propellers with different diameters, rotational speeds and freestream speeds. It is important to select a propeller that is optimized for the advance ratio corresponding to expected flight and rotational speeds.

$$J \equiv \frac{V_\infty}{n * d_{tip}} \tag{4}$$

Other relevant dimensions for propellers used in the current study include tip diameter and pitch. The tip-to-tip diameter is denoted as d_{tip}. Propeller pitch angle (β) is the angle between the rotational speed vector and the propeller chord. Blade pitch (p) is a function of blade pitch angle according to the equation $p = 2\pi r\ tan(\beta)$), where r is the radius from the centerline. For example, an 18x12 propeller has a d_{tip} equal to 18 in and a p of 12 in. Figure 8 shows blade geometry and nomenclature. For the assemblies in this current study, the power output of the jet engine is P_{in} for the propeller. The KingTech K45TP engine outputs a maximum of 5.2kW at 6500 engine rotations per minute (RPM) [2]. The 20x10 and 20x12 propellers in the current study perform at their maximum efficiency near 6500 RPM and 5.2kW.

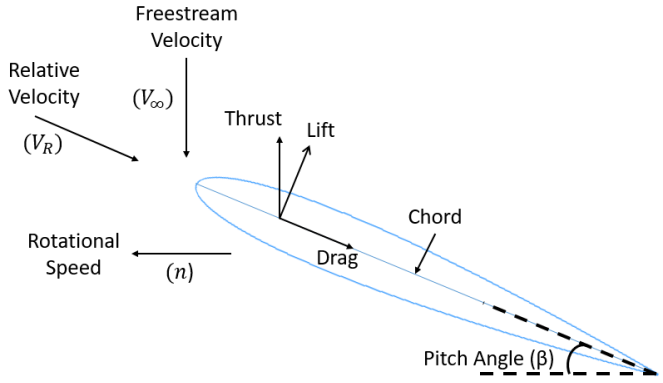

Figure 8. Propeller Definitions.

2.2.2 Ejector Theory

One of the concepts in the current study incorporates an ejector for passive thrust augmentation of a variable-cycle concept. Ejectors augment thrust by entraining freestream air into turbojet exhaust without any added power or fuel. Heiser found thrust augmentation in ejectors to be a function of mass entrainment from secondary mass flow over a bellmouth inlet, as shown in Figure 9 [3][10]. Heiser noted that secondary flow is a function of the secondary flow area. The ratio of primary to secondary flow area at an inlet is defined as α. As 1/α increases, thrust augmentation increases. Therefore, a higher ratio of secondary to primary flow area augments thrust. This current study uses an ejector but replaces the diffuser with an aft rotor assembly.

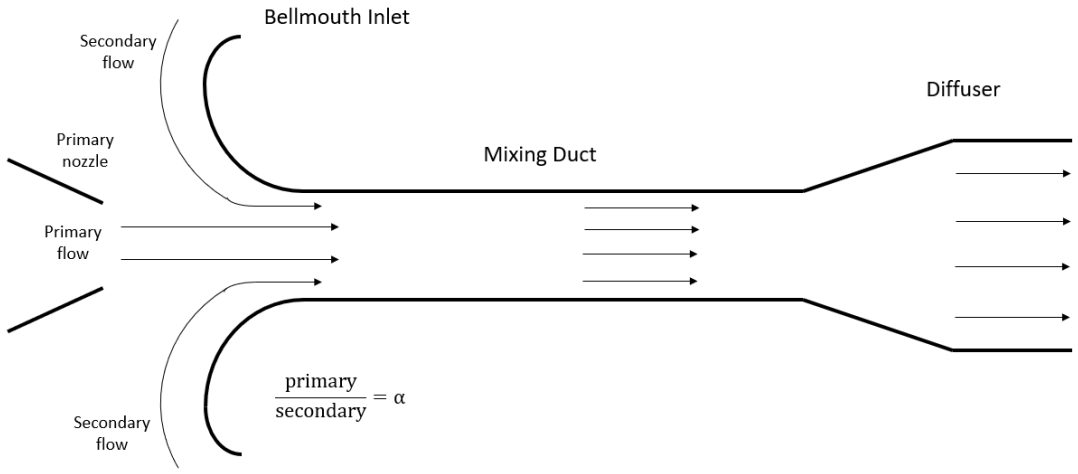

Figure 9. Ejector Nomenclature.

Another consideration for ejector assemblies is the inlet shape. Blaire and Cahoon studied various shapes for bellmouth inlets commonly used in ejectors [3][11]. There were three bellmouth profiles tested: radial, aerofoil and elliptical. Comparisons were made by measuring mass flow rates through pipes with these varying inlet geometries. The pipe without a bellmouth inlet had a mass flow rate of 30.02 gm/s (0.066 lbm/s); whereas, the simple radius inlet had 34.83 gm/s (0.077 lbm/s), and the elliptical profile inlet had 36.15 gm/s (0.080 lbm/s). All bellmouth inlet

geometries provided an increased mass flow rate over the pipe alone, but the elliptical profile yielded the largest increase. The elliptical profile had a 20% increase in mass flow over the pipe alone, whereas the simple radius had only a 16% increase. This current study uses an elliptical profile for a bellmouth inlet on a variable-cycle concept to maximize mass flow entrainment. The location of an aft ejector assembly from the turbojet nozzle exit plane is another design parameter. Oglesby found the ideal thrust augmentation distance for a jet pipe [3][12]. Oglesby used a KingTech K45 and a Grumania-brand jet pipe on a static test stand to measure thrust. The difference in thrust with the jet pipe over the engine alone at various locations showed the resulting thrust augmentation as a function of distance. Figure 10 shows results with percent difference in thrust over the engine alone. Positive distance (shown on the x-axis) occurs when the jet pipe inlet is upstream of the engine nozzle exit plane. In other words, a positive distance in Figure 10 corresponds to the jet pipe overlapping the engine nozzle exit plane. The ideal distance to place a jet pipe for thrust augmentation occurs when the jet pipe inlet is 1.5 in upstream of the engine nozzle exit plane.

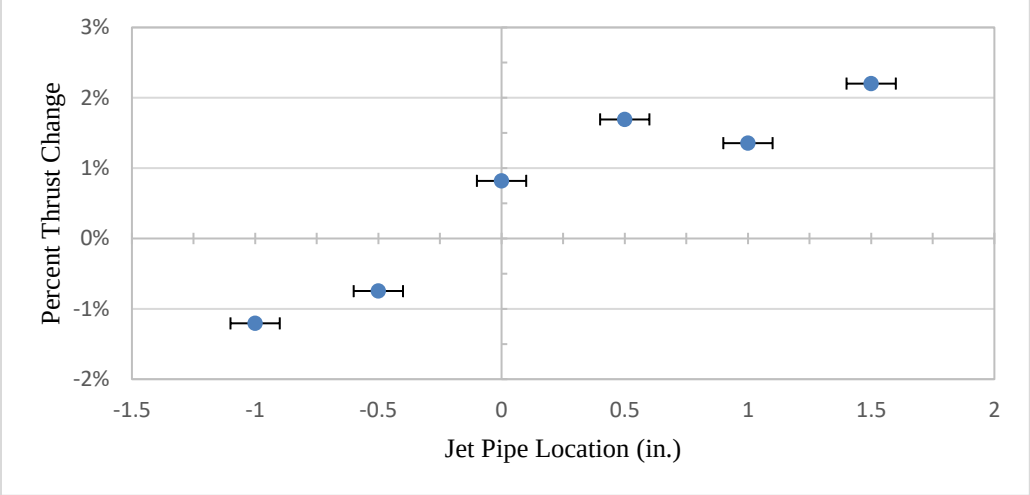

Figure 10. Thrust Augmentation of Jet Pipe with Varying Distance [12].

This distance for maximum thrust augmentation is the same when a bellmouth inlet is added to the jet pipe [13]. The location of the bellmouth/jet pipe assembly in this current study is located at the same distance from the nozzle exit plane.

2.3 Acoustic Theory

2.3.1 Jet Noise

Lighthill showed that a jet of air has acoustic intensity that is a function of various properties of the jet as shown in Equation 5 [14]. Important trends to note for this study are dependence on jet velocity (U_j) and dependence on angle (θ) of measurement. For example, faster jets have a higher sound pressure level (SPL), and increasing angle from the jetstream yields lower noise up to 90°.

$$I \propto \frac{\rho_m^2 U_j^8 d_j^2}{\rho_o a_o^5 r^2} \frac{1}{|1-M_c \cos(\theta)|^5} \tag{5}$$

Jet noise is expected to be a large contributor to the acoustic signature of small turbojets (or the turbojet mode of a variable-cycle engine), and a potential contributor to turboprop noise. The current study will test a turboprop whose exhaust and propwash have properties of a jet. Acoustic data from a small turbojet is also presented as a baseline for the turbojet mode in a variable-cycle engine.

Ahuja and Bushell showed Equation 8 proportionalities experimentally [15]. Using a test rig that produces a low-turbulence jet in an anechoic chamber, the authors measured jet noise with several microphones in the quarter-circle downstream of the jet. Measurements were taken at a 6-foot radius from the nozzle. Figure 11 shows Overall Sound Pressure Level (OASPL) data from jet diameters of 2.84 in, 2.4 in and 1.52 in. The data is in good agreement with predictions by Lighthill with regard to jet diameter, jet velocity and angle of measurement. The KingTech K45 used in this current study has a nozzle diameter of 2 in, and measurements were taken at an 5-foot

radius. Although Ahuja and Bushell measured jets much colder than K45 exhaust, expected trends are similar to Figure 11.

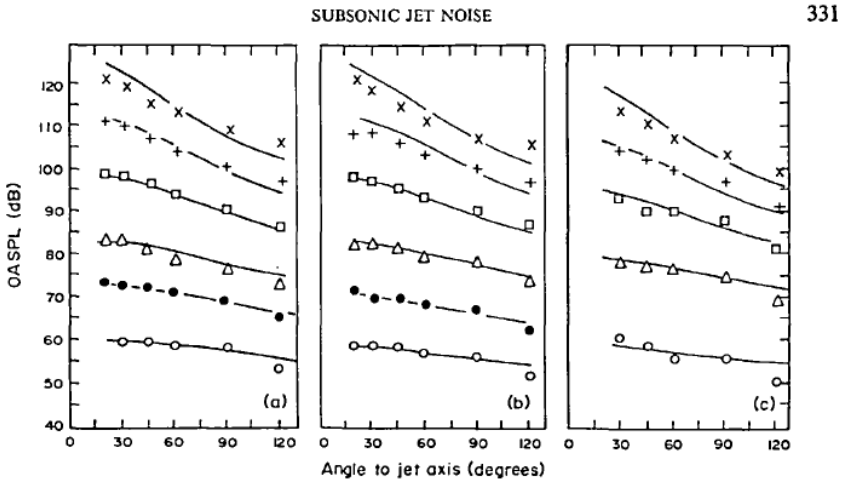

Figure 16. Directivities of OASPL's for "clean" jet noise. (a) $D = 2{\cdot}84$ in; (b) $D = 2{\cdot}40$ in; (c) $D = 1{\cdot}52$ in. Values for V_j: ×, 1000 ft/s;+, 800 ft/s; □, 600 ft/s; △, 400 ft/s; ●, 300 ft/s; ○, 200 ft/s. ——, Theory $V_j^8 (1 - M_c \cos\theta)^{-5}$.

Figure 11. OASPL for Several Jet Diameters, Velocities and Angles [15].

2.3.2 Propeller Noise

Isolated propeller spectra are presented in Sinibaldi and Marino [16]. Propeller tests were conducted with 60 cm propellers in an anechoic chamber with the only noise sources being the motor and the propeller. Propellers have two components of noise: harmonics of the blade passing frequency (BPF) and broadband noise. The BPF and its harmonics are seen as spikes in the frequency spectra shown in Figure 12. The broadband component of propeller noise is the rest of the propeller's frequency spectrum.

Other results in Sinibaldi and Marino include the effect of angle on propeller noise. The angle convention is different than the current study; 90° is in line with the propeller plane and 0° is directly aft of the propeller or in the propeller wake. The highest power spectral density in Figure 12 is at 0° or directly aft of the propeller. The remaining power spectral densities are from greatest to least as follows: 30°, 90° and 60°. This means that broadband noise from the propeller

wake dominates the BPF tones in the rear arc of acoustic measurement. Propellers in the current study are of similar size. It is expected that propeller noise will be a large part of turboprop noise and trends with changing angle of measurement will be similar. The concept of BPF is also apparent in turbomachinery noise which is expected from turbojets and turboprops.

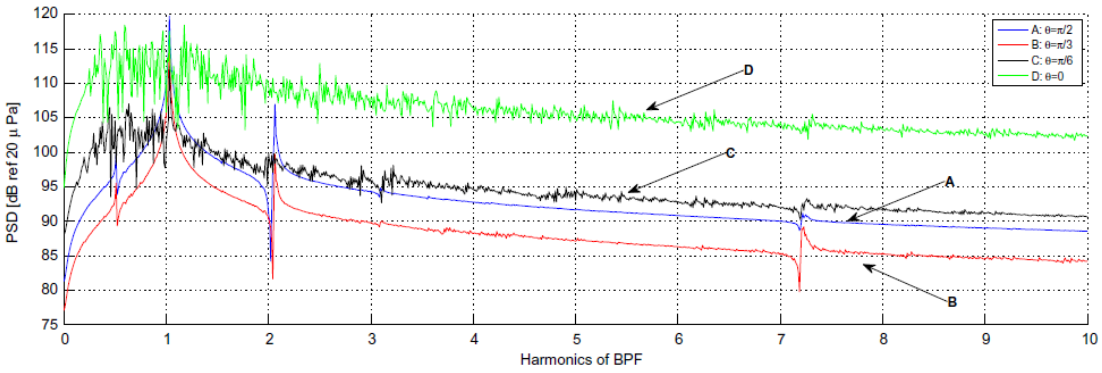

Figure 12. Propeller Frequency Spectra vs Angle [16].

2.3.3 Turboprop Noise

Clark and Scott [17] studied propeller noise from a large turboprop engine analytically and experimentally. Aerodynamic predictions of an SR-3 propeller blade from the advanced turboprop project were used by modified acoustic software to predict far field noise of the turboprop. Experiments included wind tunnel tests of the SR-3 turboprop and flight tests on a JetStar aircraft. Experimental measurements included the noise of the entire turboprop. Figure 13 shows predicted and experimental data of the BPF and overall sound pressure level (OASPL). These parameters were measured forward and aft of the turboprop's propeller plane. The most noticeable trend is a higher OASPL aft of the propeller plane. Since the analytical results included the propeller alone and show good agreement with experimental results, it can be assumed that the propeller is the primary contribution to turboprop noise. While Clark and Scott did not examine noise from specific components of the turboprop, the propeller is expected to be a large contributor to turboprop noise in the current study.

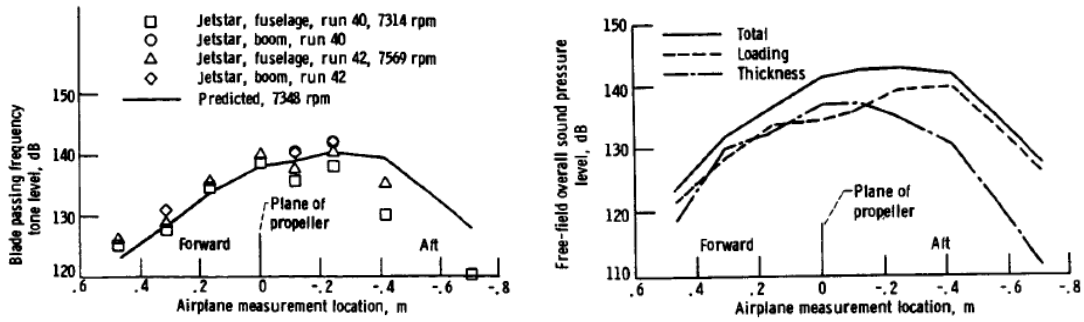

Figure 13. Turboprop SPL with Varying Location [17].

CHAPTER III

ANALYTICAL STUDY

This chapter contains a parametric cycle analysis (PCA) of a small turbojet and an analysis of a notional, variable-cycle mission that uses the results from the PCA. These analytical results are useful for examining effects of component modification and predicting capabilities of a variable-cycle engine on a notional military mission.

3.1 Parametric Cycle Analysis

A PCA of a real engine from Mattingly uses thermodynamic relations to predict performance of gas turbine engines [4]. A PCA assumes one-dimensional flow on either side of each engine component. Additionally, a perfect gas with a constant specific heat is assumed, but different specific heats are used before and after the combustor. The nozzle is assumed to be perfectly expanded. PCA equations make use of station numbers of the engine. For example, T_{t4} is the total temperature at station 4, the exit of the combustor and the inlet of the turbine. Figure 14 shows station numbers used for a turbojet PCA. Pressure ratio across components is denoted by π. For example, P_{t4}/P_{t3} is labeled as π_b and is the pressure ratio before and after the burner. π_c is the pressure ratio across the compressor, or P_{t3}/P_{t2}. In the current study, a PCA is used to model a small turbojet.

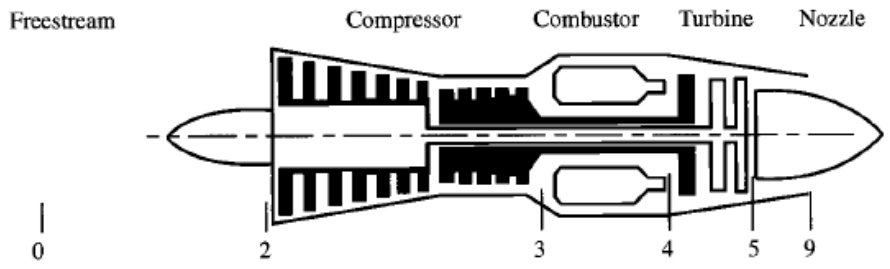

Figure 14. Station Numbers of a Turbojet Engine.

Primary inputs for a PCA are a flight condition (M_0, P_0, T_0), compressor pressure ratio (π_c) and turbine inlet temperature (T_{t4}). Using the flight condition and π_c, total temperatures on either side of the compressor can be found:

$$\frac{T_{t0}}{T_0} = 1 + \frac{\gamma_c - 1}{2} M_0^2 \qquad \frac{P_{t0}}{P_0} = \left(\frac{T_{t0}}{T_0}\right)^{\frac{\gamma_c}{\gamma_c - 1}} \tag{6}$$

$$T_{t2} = T_{t0} \qquad \frac{T_{t3}}{T_{t2}} = \pi_c^{\frac{\gamma_c - 1}{\gamma_c e_c}} \qquad T_{t3} = \frac{T_{t3}}{T_{t2}} T_{t2} \tag{7}$$

Using the thermal energy release by the fuel during combustion and conservation of energy, fuel-air ratio can be found with:

$$f = \frac{c_{pt} T_{t4} - c_{pc} T_{t3}}{h_{PR} \eta_b - c_{pt} T_{t4}} \tag{8}$$

T_{t5} can be found with a power balance between the compressor and the turbine assuming negligible mass flow rate of fuel:

$$c_{pc}(T_{t3} - T_{t2}) \eta_{mech} = c_{pt}(T_{t4} - T_{t5}) \tag{9}$$

Exit properties are found with the ratio of total pressure to static pressure at the exit and assuming no total temperature loss after the turbine:

$$\frac{P_{t9}}{P_9} = \frac{P_{t0}}{P_0}\pi_d\pi_c\pi_b\pi_t\pi_n\frac{P_0}{P_9} \qquad T_{t5} = T_{t9} \qquad \frac{T_{t9}}{T_9} = \frac{P_{t9}}{P_9}^{\frac{\gamma_t - 1}{\gamma_t}} \tag{10}$$

Where $P_9/P_0 = 1$ assuming the nozzle is perfectly expanded. V_9 and specific thrust can then be found with:

$$V_9 = \sqrt{(T_{t9} - T_9)2g_c c_{pt}} \qquad \frac{F}{\dot{m}_0} = \frac{(1+f)V_9 - V_{dash}}{g_c} \tag{11}$$

Lastly, SFC is calculated by:

$$SFC = \frac{f}{\frac{F}{\dot{m}_0}} \tag{12}$$

The flight condition of 150 mph and 2000 ft was selected based on recent aircraft that use small turbojet engines [12]. The compressor pressure ratio was estimated using values from turbojets of similar size [18].

A real PCA also uses LOT to represent component figures of merit. LOT 3 was used for terms related to the inlet, compressor, turbine and nozzle. These components likely use modern machining methods, therefore the losses related to them are modern. Losses related to the combustor used LOT 2 because of the size of the engines used on UAS. LOT 1 was used for the turbine inlet temperature because the turbine is uncooled. LOT and other assumed values can be seen in Table 1.

V_{dash}	**150 mph**	**π_n**	**0.98**	**γ_t**	**1.36**
Altitude	**2000 ft**	**$\pi_{d,max}$**	**0.96**	**c_{pc}**	**0.24 $\frac{BTU}{lbm*R}$**
π_c	**2.1**	**e_c**	**0.88**		
T_{t4}	**1400 °F**	**e_t**	**0.89**	**c_{pt}**	**0.275 $\frac{BTU}{lbm*R}$**
π_b	**0.92**	**η_{mech}**	**0.99**		
η_b	**0.94**	**γ_c**	**1.4**	**h_{PR}**	**18400 BTU/lbm**

Table 1. Inputs for Turbojet PCA.

Detailed calculations using these equations can be seen in Appendix A.

Results of the PCA for a small turbojet were compared to a KingTech K45 turbojet [2]. The PCA resulted in the same thrust (10 lb) but an SFC 12% higher than the K45 turbojet (2.29 1/hr). Information from the model can be expected to have error on the same order of magnitude. This is likely because the published values for a K45 were taken at different flight conditions than those used in the PCA.

The PCA can also be used to predict thrust and SFC if a K45-like engine is modified to be variable-cycle. For example, Figure 15 shows the effect on thrust and SFC with a custom nozzle that has more pressure drop than LOT 3.

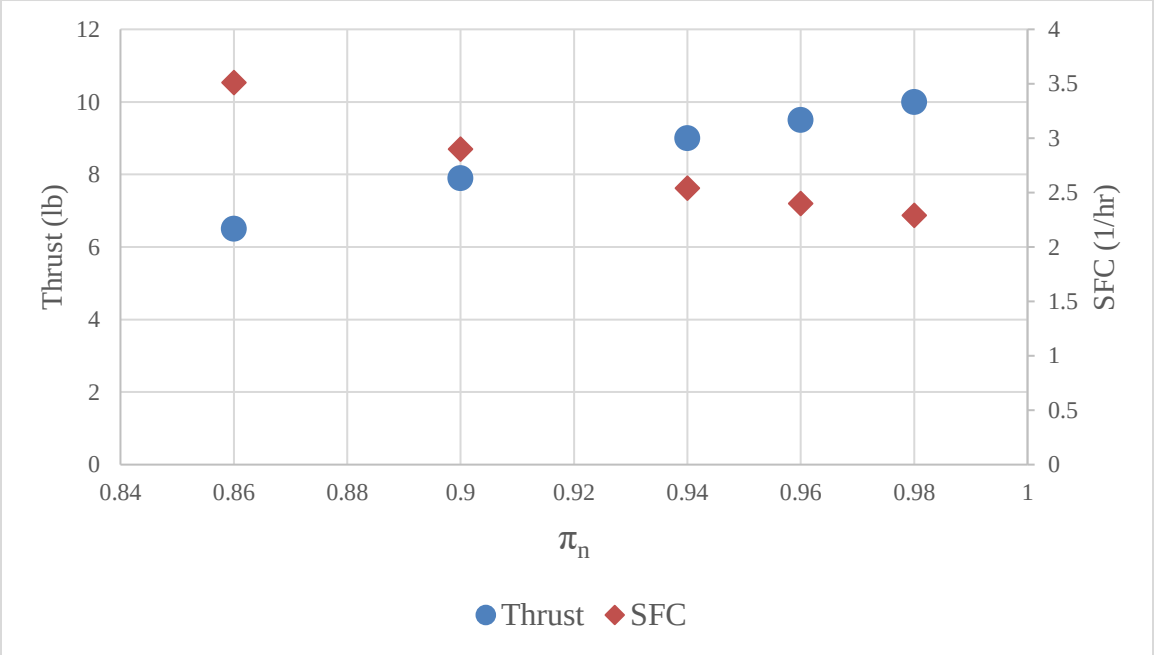

Figure 15. Effect of Nozzle Losses on Thrust and SFC.

An alternative design that increases losses at the nozzle would have a large effect on thrust. This is relevant to vehicle design that needs a certain amount of thrust to maintain lift for a delivery, for example. The change in SFC would have a minor effect on mission endurance since a dash mission leg is relatively short compared to a loiter leg.

3.1.1 Sensitivity Study

To examine the uncertainty in the choice of parameters, the change in SFC and thrust of the engine model is presented with a percent change in several parameters. The X-axes in Figure 16 and Figure 17 represent a percent change in each parameter so all parameters can be plotted on the same graph. With this method, the most driving factors have steeper slopes on the plot. For example, Figure 16 and Figure 17 show that π_b has a steep slope and therefore a relatively large influence on SFC and thrust. Since information on burner efficiency of small turbojets is not readily available, this could be a large factor in the accuracy of the model. One pressure loss term (π_b) and one polytropic efficiency (e_c) are presented because changes in similar terms (π_n, e_t) result in similar changes to SFC and thrust. For example, changes in pressure terms in Equation 10 have the same effect on P_{t9}/P_9 and therefore T_9, V_9 and thrust. Other results show that T_{t4} has a large effect on thrust and a minor effect on SFC. The sensitivity study as a whole also helps understand the driving factors for increased small turbojet efficiency in general.

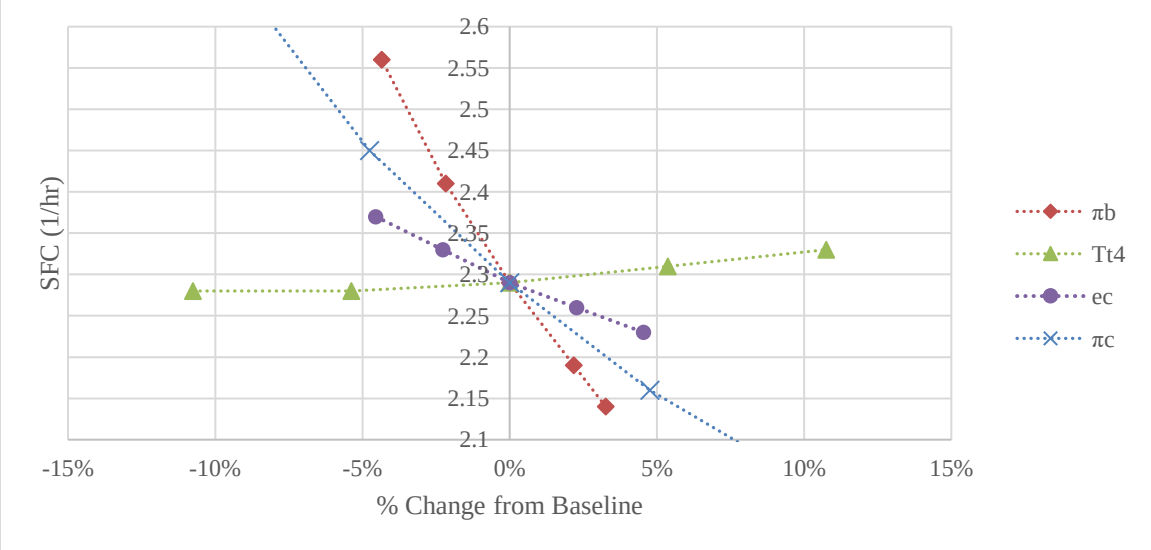

Figure 16. Effect of Parameter Changes on SFC.

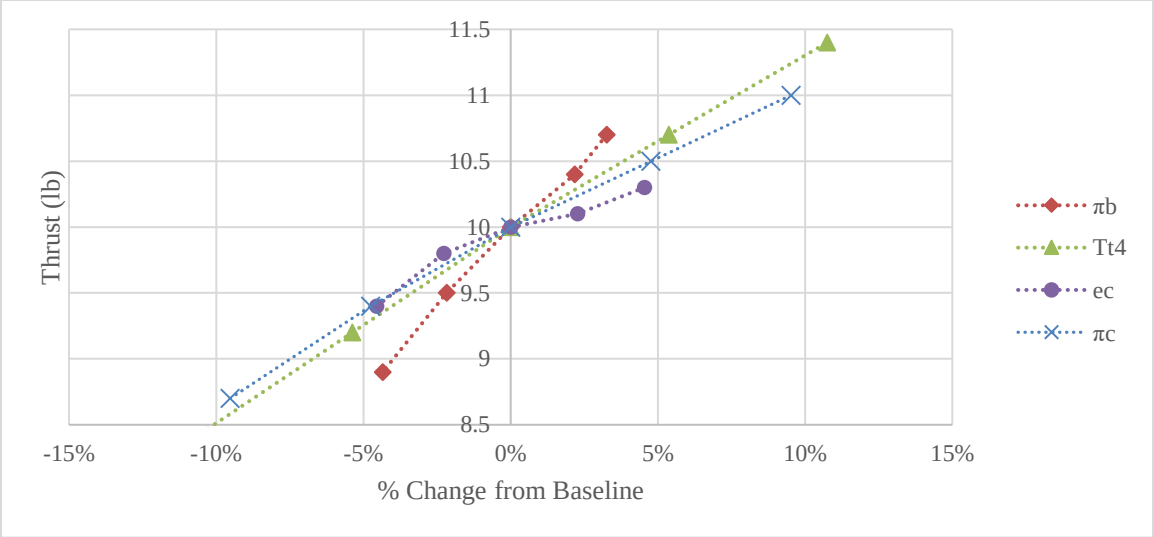

Figure 17. Effect of Parameter Changes on Thrust.

3.2 Mission Analysis

Using the notional mission from Figure 2 and installation losses of 5%, an analysis according to Mattingly [4] was conducted to study the impact of a variable-cycle engine on sUAS range and endurance. Figure 18 shows a benchmark aircraft that was used for aerodynamic elements of the analysis, and Figure 19 shows the station numbers for the mission legs.

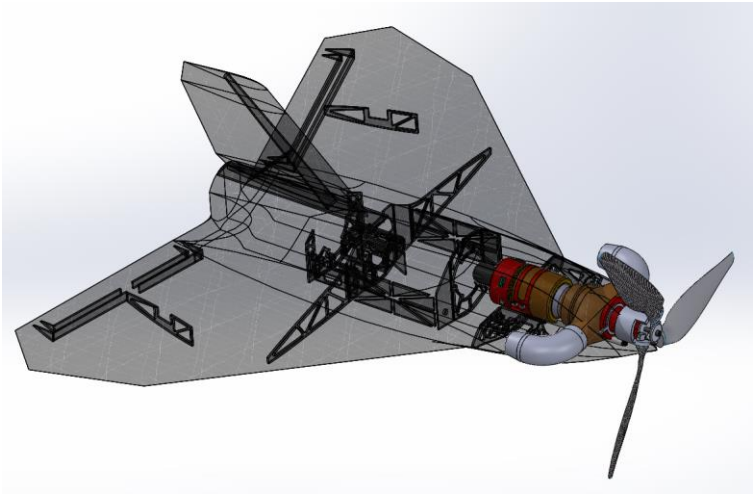

Figure 18. Notional Aircraft for Variable Cycle Engine.

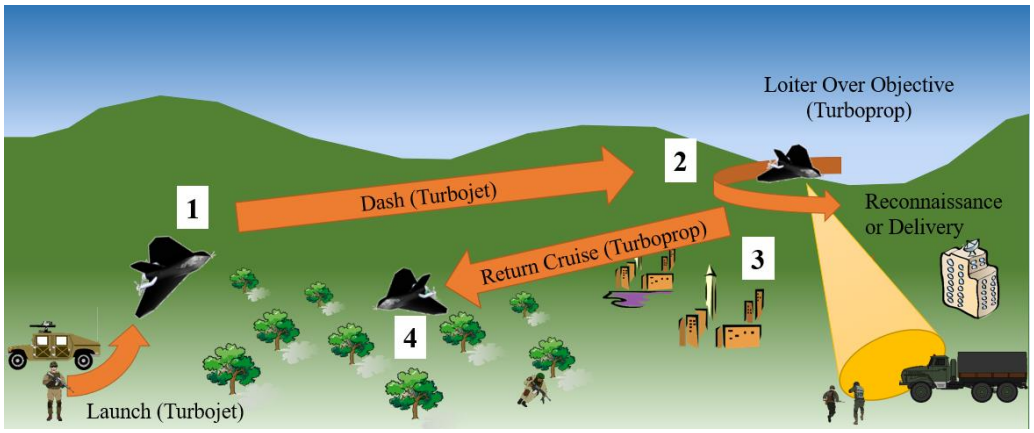

Figure 19. Notional Mission Legs for Variable-Cycle Engine Mission (bottom).

Primary inputs for the mission analysis include aircraft characteristics, engine SFC, flight condition and desired range of the first leg. SFC for the turbojet (dash) leg of the mission used the results from the PCA (π_n LOT 3). The SFC for the turboprop legs used a partial throttle estimate for the K45TP turboprop [19]. For the mission analysis calculations, lift was assumed to equal weight for all mission legs therefore:

$$C_L = \frac{2Wt}{\rho_0 V^2 S} \qquad C_D = C_{D0} + K{C_L}^2 \tag{13}$$

where W is the aircraft weight at a mission leg, S is the wing area and V is that leg's flight velocity.

The Breguet range equation was used to solve for fuel burn during mission legs and loiter time.

$$R = \frac{V}{g}\frac{1-\Phi}{SFC}\frac{C_L}{C_D}\ln\frac{Wt_1}{Wt_2} \tag{14}$$

where Φ is the installation losses. Equation 14 was used without the velocity term for endurance of the loiter leg of the mission and was also used to solve for the change in aircraft weight (fuel burn) given a range to dash. A summary of assumed values can be seen in Table 2.

V_{dash}	150 mph	C_{d0}	0.013
Altitude	2000 ft	AR	2
W_{empty}	12 lb	M_{loiter}	0.05
W_{fuel}	6 lb	$W_{factor4}$	1.02
S	3 ft^2	Φ	5%
SFC_{dash}	2.29 $\frac{1}{hr}$	$SFC_{2\text{-}4}$	1 $\frac{1}{hr}$

Table 2. Assumed Values for Mission Analysis.

The detailed calculations in Appendix A output several mission characteristics, namely length of loiter when given an initial cruise range. The results of the mission analysis give rise to a tradeoff between loiter endurance and range capability of the dash leg. This is essentially an operating envelope for the aircraft on a delivery or reconnaissance mission. For example, Figure 20 shows that a Variable-Cycle delivery mission requiring no loiter is capable of a 100-mile range. Alternatively, a mission that requires as much loiter endurance as possible can achieve about 35 minutes of loiter if the range is kept at 10 miles. For the comparison to aircraft that use only a turbojet or turboprop, all parameters were kept the same except for two. SFC was 2.29/hr for the entire turbojet mission and 1/hr for the entire turboprop mission. Additionally, the dash leg velocity was changed to Mach 0.05 in the turboprop-only scenario.

Mission analysis results show less loiter time at all points for the turbojet mode when compared to a variable-cycle mission. However, the turbojet envelope features a similar negative correlation in loiter endurance as dash range is increased. Turboprop-only loiter endurance decreases more quickly with increased range. Although the turboprop has a much lower SFC, total fuel used on the dash/cruise legs increases significantly with range because of the low flight speed. This leaves significantly less fuel for the loiter leg with increasing range. In addition to better range and endurance in general, the variable-cycle engine also has the advantage of dash in the first leg. These results show the effectiveness of a variable-cycle engine on a diverse mission involving dash, loiter and low-speed return cruise.

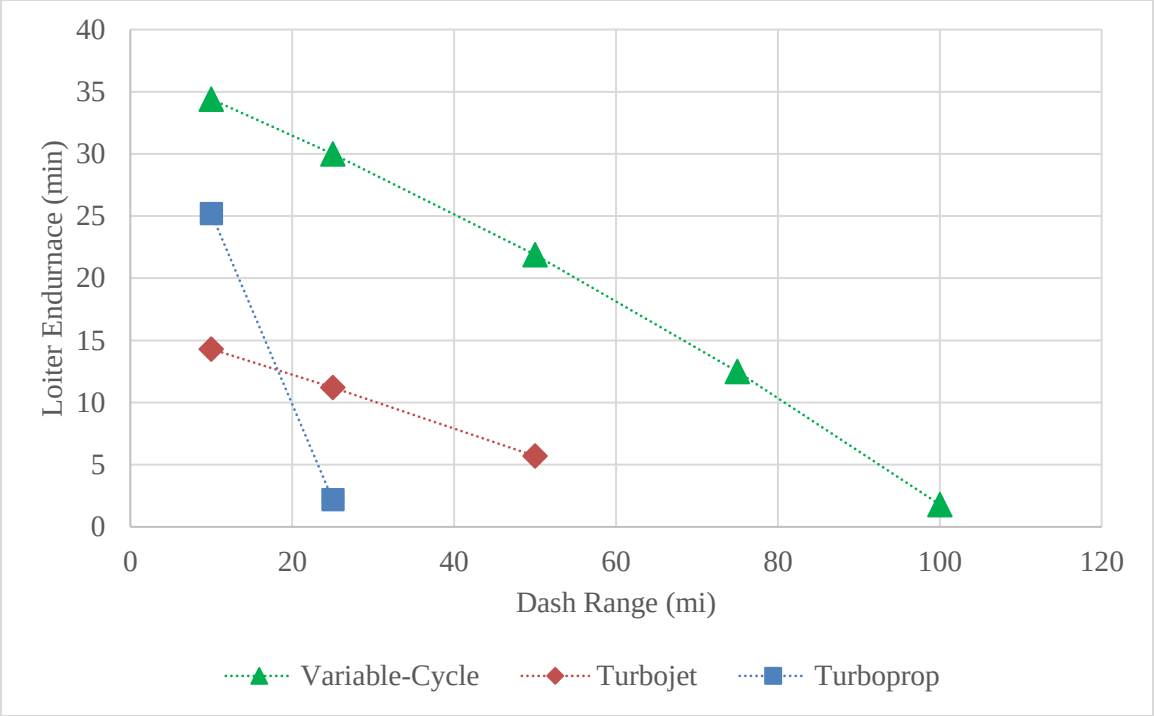

Figure 20. Various Mission Leg Lengths in terms of Dash Range and Loiter Endurance.

CHAPTER IV

EXPERIMENTAL METHODOLOGY

This chapter presents various test stands, propulsor configurations and experimental setups used in the study.

4.1 Moment Arm Thrust Stand Design

Because of the comparisons among different types of propulsion systems, a versatile, custom stand for measuring thrust was desired. In previous work, thrust stands often featured load cells reading force in the same axis as the thrust produced. To avoid impingement on the inlet and exit airflow of gas turbine engines and propellers, load cells are typically mounted offset from the thrust axis. This increases uncertainty of the thrust measurement due to the propulsor's thrust causing unmeasured torque on the load cell instead of pure directional force. To minimize this bias error, load cells commonly measure thrust as close to the thrust axis as possible. This results in unique load cell mounts for every engine depending on the engine's size and mounts. The current study explores a concept in which the thrust measurement is not in the same axis as the thrust produced which allows for unchanging attachment of the load cell.

4.1.1 Basic Concept

A “moment arm” concept was used for measurement of thrust produced by the various configurations in the current study. This concept makes use of the fact that the load measurement is entirely off-axis from the thrust of the propulsor. A simplified schematic of the concept can be seen in Figure 21.

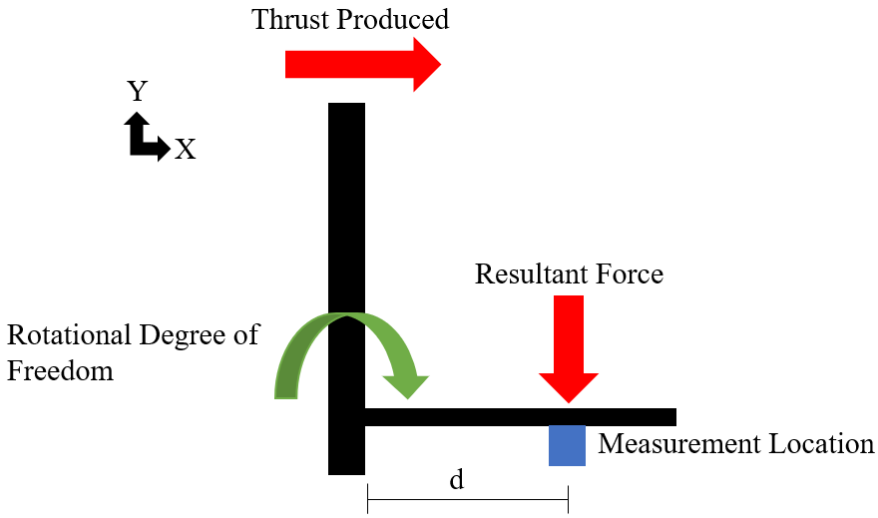

Figure 21. Simplified Moment Arm Stand Schematic.

The basic elements of the moment arm stand concept are a vertical arm supporting thrust in the x-axis and horizontal arm supporting a resultant load in the y-axis due to a rotational degree of freedom. The advantage of this setup is that any size or type of mount for any engine may be placed on top of the stand without changing the location of or reattaching the measurement device. In other words, different configurations require different mounting schemes for the propulsion system but use an unchanging mount for the load cell. The only disadvantage is that different propulsion systems and their accompanying mounts each require a unique calibration, but that is that case with most thrust stand designs.

4.1.2 Practical Considerations

An important consideration for the moment arm stand is to size the horizontal ‘arm’ length based on the measurement location. This measurement in pounds on the load cell is a function of thrust produced and the distance of the measurement along the horizontal arm, denoted ‘d’ in Figure 21. Figure 22 shows the expected reading of the load cell on the y-axis given varying thrust values and varying distance along the horizontal arm, d.

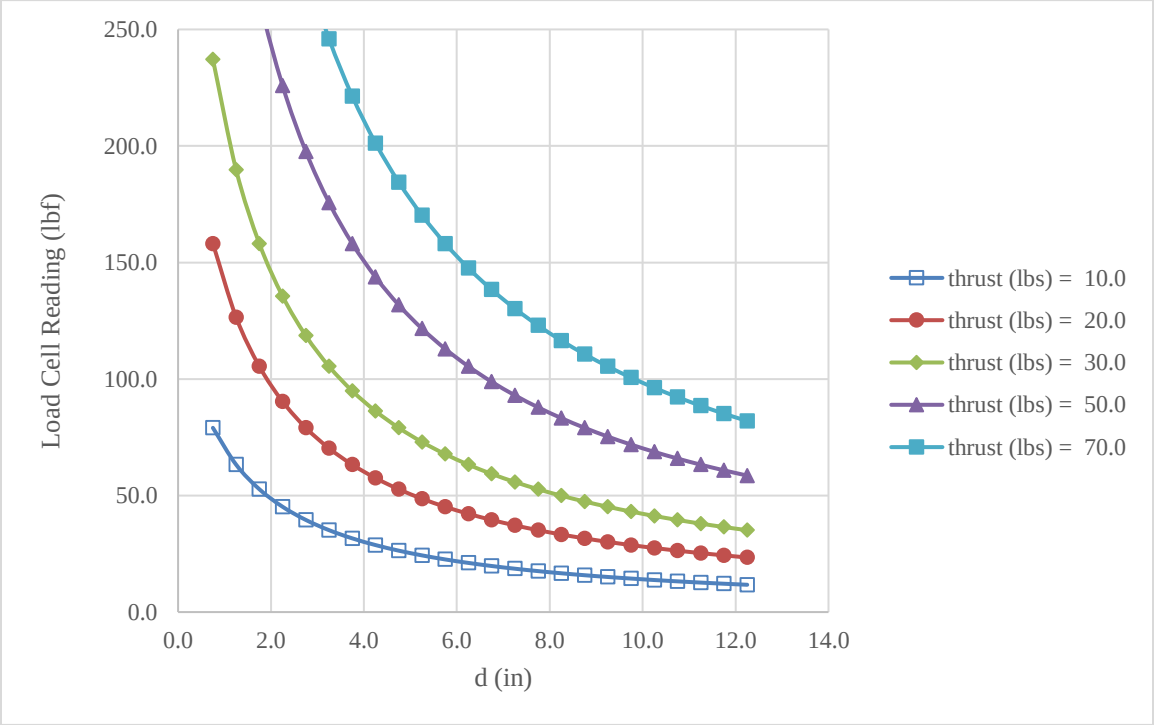

Figure 22. Load Cell Reading in Pounds against Various Parameters.

The resultant load cell reading was calculated from summation of forces and moments about the rotational axis. The summation took into account forces from thrust produced, the weight of a rigid horizontal arm and the weight of a notional propulsor that could be expected for use on this moment arm stand. The distance from the root of the horizontal arm to the center of rotation was also added to ‘d’ for the reaction force of the load cell. Thrust values from hobby aircraft propulsors typically do not exceed 70 lbf.

After a distance of 10 inches along the horizontal arm, load cell reading levels off with further increased distance, so a horizontal arm length longer than 12 inches was not needed. At a distance of 4 inches, many thrust levels give distinct load cell readings in approximately the middle of range of a 250 lbf load cell. For this reason, the measurement location was chosen to be 4 inches from the vertical arm and a 250 lbf load cell was chosen. In the future, a different location along the horizontal arm could be chosen for the load cell mount if very high thrust valued are expected.

4.1.3 Final Assembly

The moment arm stand will be described from bottom to top. Mounted Roller Bearings were attached to an optical table that has several threaded holes one inch apart. Steel rods were machined to fit inside the inner diameter of the roller bearings and those machined rods were welded onto a collar that attached to the stand. The collar featured three steel plates welded at 90 degree angles to fit around the vertical arm. 12 inches of steel U-Channel was also welded to the collar. This U-Channel is the horizontal arm to which the load cell is mounted. After being welded together, the rods, collar and U-Channel were one solid part that was bolted to the vertical arm which was made of T-Slotted Extruded Aluminum. This solid part can be seen attached to the vertical arm in Figure 23.

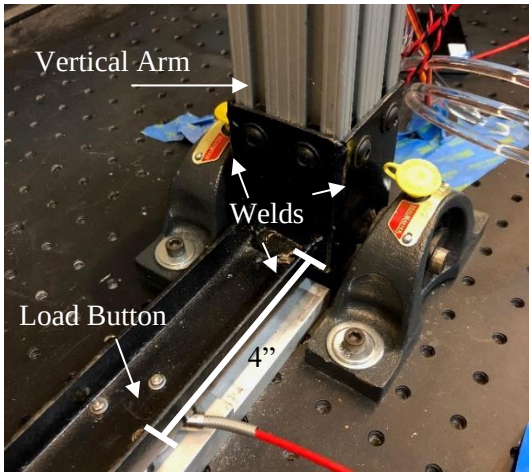

Figure 23. Moment Arm Stand Collar and Welded Attachments.

An upper horizontal arm is typically attached to the vertical arm for ease of mounting different propulsors. The vertical arm is sized so that propulsors are located in the center of the wind tunnel test section described in Section 4.4. The horizontal arm is 12 inches in length to move the propeller farther from the vertical arm and therefore reduce interactions with the rest of the stand. The upper mounts for the propulsors will be described in depth in each propulsor's section. A Futek LLB400 "load button" type load cell with threaded holes was bolted 4 inches from the base of the U-Channel for thrust measurements as seen in Figure 23. The load button was wired to a Futek IAA100 amplifier which was connected to a National Instruments USB-6211 to be read on a computer with LabVIEW software. It is important to note that this type of load cell is rated for 250 lb in compression only. This means that thrust can only be measured in one direction on the stand. The fully assembled stand with an off-the-shelf turboprop engine mounted is shown in Figure 24. Annotations show the thrust produced and the location of the load cells resultant measurement.

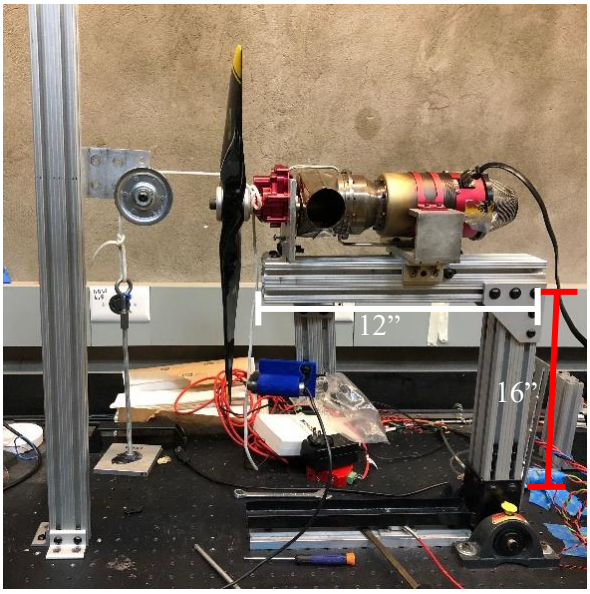

Figure 24. Fully Assembled Moment Arm Thrust Stand.

4.1.4 Calibration

Although the manufacturer calibrates the Futek LLB400 load button for a direct load, the thrust produced by the mounted propulsor is not equal to the force on the moment arm stand's load button. A summation of forces and moments would allow for an estimation of thrust produced, but a more exact calibration can be accomplished by pulling on the stand with known weights. A cable and pulley were used to load the stand with known weights in a similar manner to thrust produced. Figure 25 shows the calibration setup for two of the configurations used in this study. A calibration curve with weight vs. voltage was created for each configuration, so that load button voltage could be converted to pounds of thrust produced during testing. The stand was not calibrated up to the thrust levels of some configurations because of limitations with the weight plate size. However, calibration curves were very linear, so experimenters extrapolated for these higher thrust values. These various calibration curves can be seen in Appendix B.

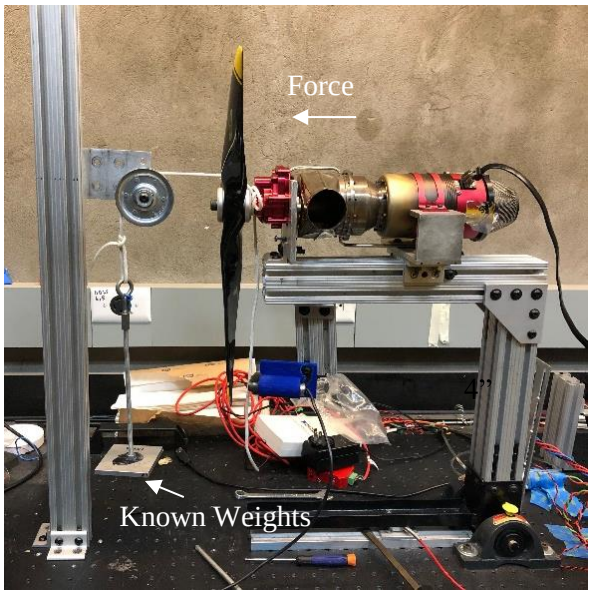

Figure 25. Example Calibration Setup; TP Tractor.

4.2 Test Configurations and Thrust Setup

Different propulsors were used to study the feasibility of a variable-cycle engine. In addition to the attempted variable-cycle assemblies themselves, noise and thrust of off-the-shelf gas turbines and propellers were investigated. The K45TP and K45 are studied because of their use on the variable-cycle concepts. Observations drawn from these engines apply to the variable-cycle concepts presented. Additionally, a propeller driven by an electric motor is studied to view the effect of the propeller on turboprop noise. All propulsors used in the current study and their descriptions can be seen in Table 3.

VC	Attempted Concepts for Variable-Cycle
TP Tractor	**K45TP Turboprop with Tractor Propeller**
TP Pusher	**K45TP Turboprop with Pusher Propeller**
Electric Tractor	**Tractor Propeller driven by Electric Motor**
K45	**Baseline Small Turbojet**

Table 3. Names and Descriptions of All Configurations.

4.2.1 Variable-Cycle Concepts

Concept 1

The first proof of concept for a variable-cycle engine featured a small turbojet engine with exhaust that could be directed into an aft propeller assembly or directed into the atmosphere. Figure 26 shows a KingTech K45TP turboprop engine and a K45 turbojet engine. The red body of these two engines is approximately 3 inches in diameter.

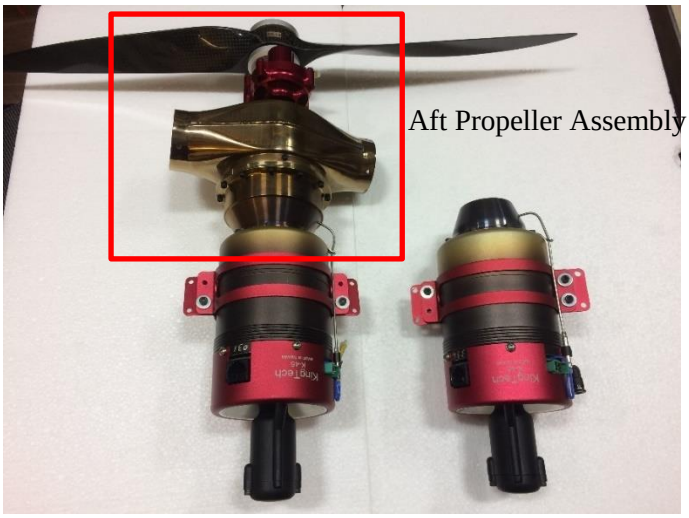

Figure 26. K45TP Turboprop (left) and K45 Turbojet (right).

The aft propeller assembly of the turboprop is boxed in Figure 26. This assembly houses a turbine which drives a shaft, and a propeller is typically attached to this shaft. Exhaust ducts can be seen facing outward from the engine near the middle of the assembly. This assembly was detached from the rest of the turboprop and mounted downstream of the turbojet. When the turbojet's exhaust is directed into the aft propeller assembly, the concept functions as a turboprop. When the turbojet's exhaust is directed into the atmosphere, the concept functions as a turbojet. A Solidworks model of Variable-Cycle Concept 1 can be seen in Figure 27 with turbojet mode on the left and turboprop mode on the right.

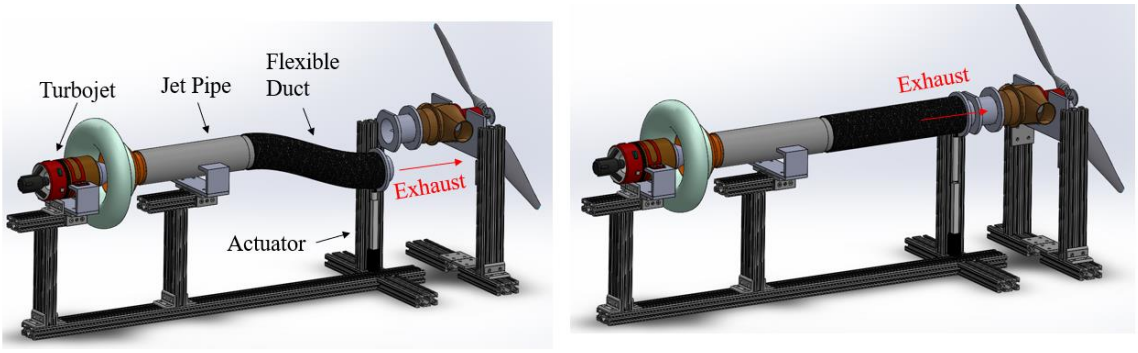

Figure 27. Solidworks Model of Variable-Cycle Concept 1.

In addition to the turbojet, a jet pipe with a custom bellmouth inlet can be seen in Figure 27. Jet pipes are typically used by R/C hobbyists to duct high temperature exhaust out of an airframe and are known to entrain ambient air [12]. This effectively functions as an ejector for thrust augmentation purposes [13][19]. Also shown is flexible ducting for redirection of the turbojet exhaust and a linear actuator for control.

Concept 1 also features several custom fittings.

1. Turbojet and Jet Pipe Mounts

The turbojet and jet pipe were mounted on the T-Slotted Extruded Aluminum with custom aluminum right-angle mounts attached to linear bearings that can be slid onto the Extruded Aluminum. The turbojet collar and jet pipe collar were bolted to the right-angle mounts to hold the turbojet and jet pipe in place.

2. Aft Propeller Assembly Mount

A plate with bolt holes is used to hold the aft propeller assembly in place. This plate can be slid into vertical T-Slotted Extruded Aluminum or bolted to horizontal T-Slotted Extruded Aluminum by use of a 90 degree bracket. Figure 27 shows the plate slid in vertically.

3. Exhaust Nozzle

At the downstream end of the flexible duct, a custom nozzle was used for clamping the flex duct outlet, attaching to the actuator, accelerating exhaust in turbojet mode and for joining the exhaust path to the propeller assembly in turboprop mode.

4. Aft Propeller Assembly Cone and Cone Housing

The aft propeller assembly has a hub because the turbine stator and rotor are in the outer annulus. A custom cone was fabricated and fit into the hub of the aft propeller assembly to direct the full-

annular exhaust through the jet pipe into the outer annulus. The cone housing was bolted to the aft propeller assembly and can be seen just upstream of the aft propeller assembly in Figure 27.

Turbojet engine startup was attempted with several different component combinations. Qualitative data from Concept 1 was gathered and can be found in the results section.

Concept 2

The second proof of concept for a variable-cycle propulsion system featured the K45TP assembled in its stock configuration. A custom clutch locks the propeller, and therefore locks the free turbine shaft, while exhaust travels out of the custom nozzle to produce thrust. With the shaft locked, this concept functions as a turbojet, and once the shaft is released, the engine will operate in its stock configuration as a turboprop. Figure 28 (left) shows a notional design for an exhaust nozzle that will provide thrust when the propeller is locked and for a clutch that can be moved forward or aft to lock or unlock the propeller. The concept will likely require folding propellers as shown in Figure 28 (right) to reduce drag during turbojet mode. This concept is intended to switch from turbojet mode to turboprop mode but will likely not return to turbojet mode because of difficulties clutching the propeller after it has been released. The resultant mission for an aircraft using this concept would therefore feature a dash to a location and a cruise in turboprop mode for the rest of the mission. Notional missions include high-speed deliveries or surveillance in which a high-speed return is not required.

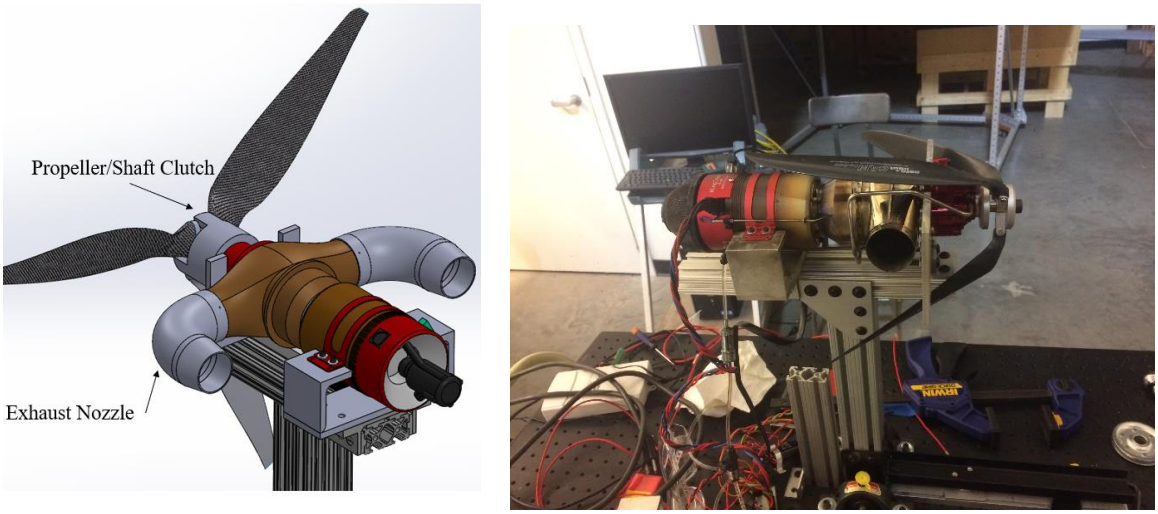

Figure 28. Solidworks Model of Variable-Cycle Concept 2 (left) and Folding Propellers for Turbojet Mode (right).

4.2.2 Turboprop Tractor

A commercially available KingTech K45TP was used to study turboprop thrust and noise. This engine is approximately 13 inches long and the manufacturer notes that the shaft operates up to about 7000 RPM [2]. All TP configurations take advantage of the aft propeller assembly plate and the right-angle mounts from Section 4.2.1.1 to hold the K45TP in place. Figure 29 shows the turboprop in a Tractor configuration because the propeller produces thrust that pulls the rest of the turboprop. The TP Tractor configuration used a 20x10 3-bladed wooden propeller. When compared to the electric motor, the TP Tractor configuration used a 20x12 2-bladed carbon fiber propeller.

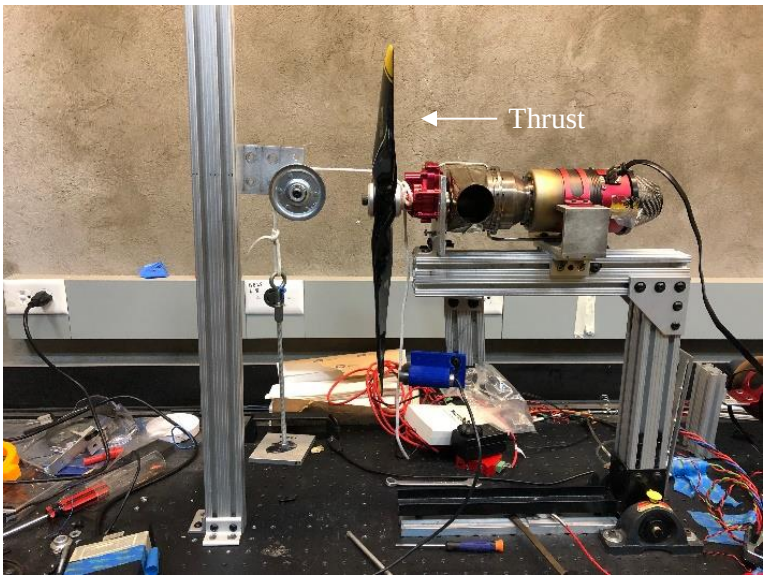

Figure 29. TP Tractor Configuration Mounted on Moment Arm Stand.

4.2.3 Turboprop Pusher

The TP Pusher configuration mounts similarly to the TP Tractor configuration but makes use of a propeller that pushes the turboprop engine. The 20x10 3-bladed wooden propeller is identical to the TP Tractor configuration except for propeller blade design that produces thrust in the opposite direction. Since the moment arm stand's load button only measures in compression, the upper horizontal arm of the stand had to be reversed and the lower horizontal arm had to be preloaded with a weight to avoid the stand tipping over. Load cell reading with the engines off is subtracted from each throttle setting's thrust value. In other words, differences in pre-load or drag from ambient wind is subtracted from the final thrust values to view the force produced by the engine only. The TP Pusher configuration can be seen in Figure 30 with thrust direction and the preload weight labeled.

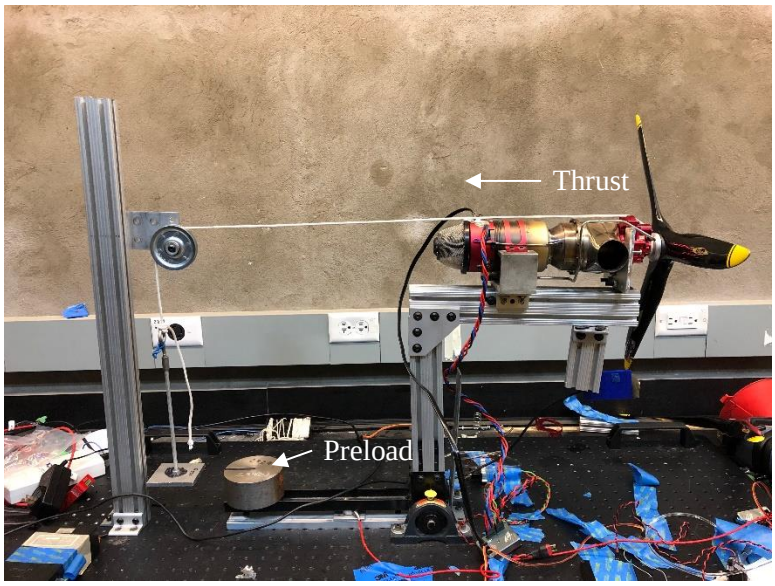

Figure 30. TP Pusher Configuration Mounted on Moment Arm Stand.

4.2.4 Electric Motor

To measure propeller noise without the turboprop, an electric motor was mounted on the moment arm stand. The motor was bolted to an aluminum plate that also had a slot for wires. 90 degree brackets attached the aluminum plate to the T-Slotted Aluminum Extrusion. The same 2-bladed 20x12 carbon fiber propeller from the TP Tractor configuration was attached to a Rimfire 50cc electric motor. This electric motor was throttled by a Castle speed controller powered by a 44.4V battery. An optical RPM sensor was also attached to match previously acquired turboprop RPM during testing. The Electric Tractor configuration with the RPM sensor, motor and speed controller can be seen in Figure 31.

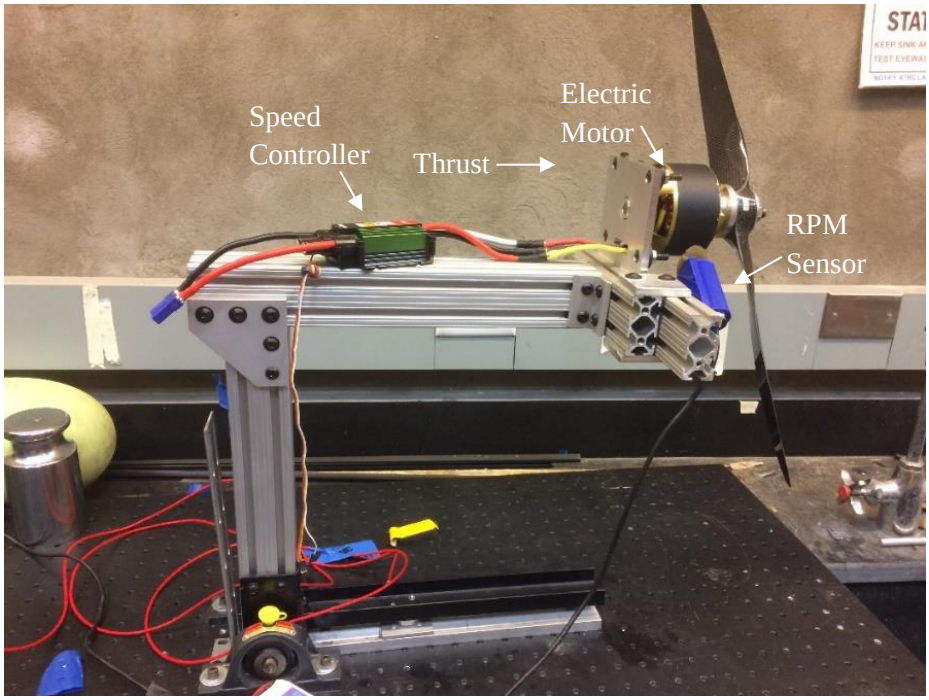

Figure 31. Electric Tractor Configuration Mounted on Moment Arm Stand.

4.2.5 Secondary Thrust Stand

A KingTech K45 was tested to view the expected acoustic signature from the turbojet mode of a variable-cycle engine. Acoustic data was gathered from the K45 turbojet before the fabrication of the moment arm stand used in the current study, so an existent thrust stand was used. The K45 thrust stand uses welded steel plates to mount the engine and an Omega LCCD-100 load cell that is rated to 100 pounds in tension and compression. The engine and engine mount act as a rigid body that puts the load cell in tension. A model of the K45 mounted on the steel thrust stand can be seen in Figure 32.

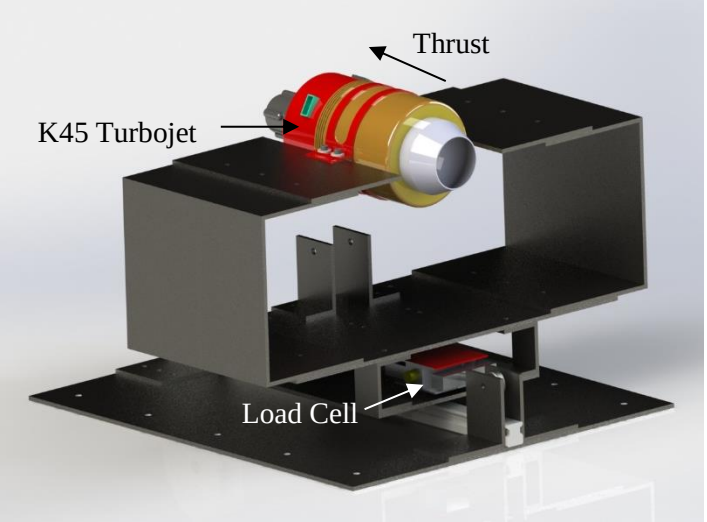

Figure 32. K45 on Existent Thrust Stand.

4.2.6 Test Procedures

The procedures for testing the different gas turbines was identical and the electric motor operation was similar. This section outlines the procedures for throttling the propulsors and for data acquisition.

1. Gas Turbine Operation

To run the engine, the fuel line was first attached from the fuel tank to the engine. Second, batteries were connected to power the engine control unit and wireless receiver. Then, the fuel line was primed manually using the Ground Support Unit (GSU). The wireless engine controller was then turned on, after which the throttle channel was trimmed up on the controller to prepare for fuel flow. Finally, the engine initiation sequence was prompted according to the KingTech Engine Manual [2].

2. Electric Motor Operation

To run the electric motor, the speed controller was attached to a 44.4V power source and throttled with the same wireless engine controller that was used to power the gas turbine engines. Acoustic

and thrust data from the Electric Tractor configuration was only gathered at one thrust level due to battery capacity constraints.

3. Sampling

For the gas turbine engines, thrust and acoustic data was gathered at four engine throttle settings: idle (0%), 50%, 75% and 100%. Throttle settings were not an exact input, so engine core RPM and engine thrust are presented. Data collection began once the exhaust temperature readout on the GSU stopped fluctuating. This is an approximate equilibrium for the engine.

For the propeller driven by the electric motor, propeller RPM was matched to approximately that of previously achieved turboprop propeller RPM.

Acoustic data was gathered for 30 seconds, and thrust data was gathered for approximately five seconds at equilibrium. Thrust data was sampled at 100 Hz. The load cell signal was sent to a data acquisition system, with results viewable through LabVIEW software. Acoustic data was converted to narrowband frequency spectrum with National Instruments SignalExpress. A Hanning window with root mean square averaging and linear weighting was used to export to the acoustic data into data analysis software.

4.3 Acoustic Setup

All acoustic data was gathered outdoors at the Oklahoma State University Design and Manufacturing Lab. Testing was done on multiple days that had winds less than 10 mph and temperatures of 20-30 °F. Multiple GRAS 46AD 1/2” CCP Pressure Standard Microphones were used to measure noise. Microphones were placed at a constant distance from the propulsors but at different angles. The angle convention used in the current study is as follows: 0° is forward or in the thrust direction of the propulsors, and 180° is aft or directly in the exhaust. The microphones were placed at consistent distance of 18 feet from the propulsors to ensure far field acoustic

measurements of the 20-inch diameter propeller. Thrust stands were mounted to a table in a grass field to the northwest of the lab. This reduces reflectivity from structures or vehicles. Background noise from a nearby power plant is present in the ambient data but is well below the broadband noise of the propulsors.

Six total microphones were used in acoustic testing in a semi-circle around the table and thrust stand as shown in Figure 33.

Figure 33. Acoustic Testing Microphone Semi-Circle.

Three microphones were placed in a quarter-circle around the inlet and three more in a quarter-circle around the exhaust nozzle. In summary, the microphones were placed at 30°, 60°, 90°, 90°, 120° and 150°. A simplified schematic of the acoustic setup can be seen in Figure 34.

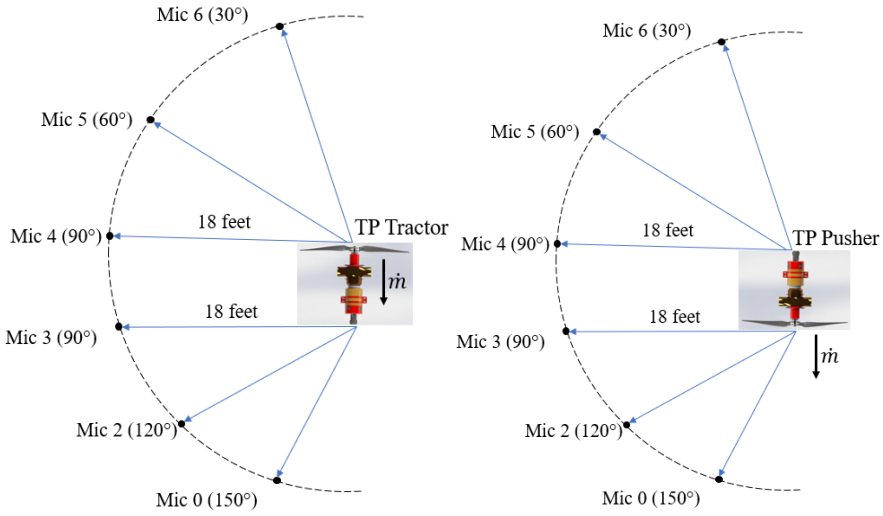

Figure 34. Microphone Schematic for TP Pusher and TP Tractor.

For the turboprop comparison to an electric motor and the K45 turbojet, a quarter-circle of microphones was used. The quarter-circle was effectively aft of the K45 and forward of the Electric Tractor configuration, as shown in Figure 35. K45TP data from the same microphones is extracted for the comparisons in Section 5.6. The same 20X12 two-bladed carbon fiber propeller was used when comparing the Electric Tractor and TP Tractor configuration.

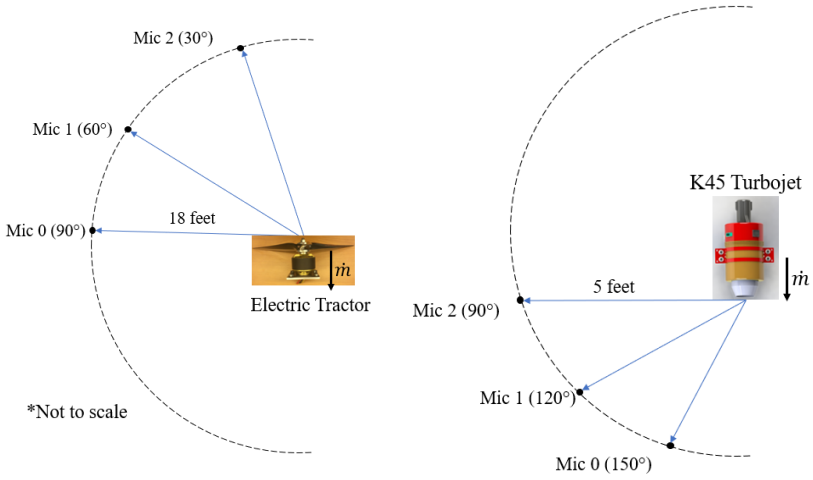

Figure 35. Microphone Schematic for Electric Tractor (left) and K45 (right).

4.4 Wind Tunnel Testing

Measurement of turbojet and turboprop exhaust properties took place in the Advanced Technology Research Center Wind Tunnel at Oklahoma State University [3]. A schematic of the wind tunnel can be seen in Figure 36 with arrows representing air flow. This tunnel has an open-loop configuration with a 3-ft by 3-ft test section. A flow straightener is located at the tunnel entrance, just ahead of the contraction section. The wind tunnel is controlled and monitored using a LabVIEW program that measures speed using a pitot-static probe located at the test section entrance. The wind tunnel was run at a notional air speed (5 mph) to vent exhaust. This is similar to the wind speeds on the acoustic tests although the air temperature was much warmer (50 °F).

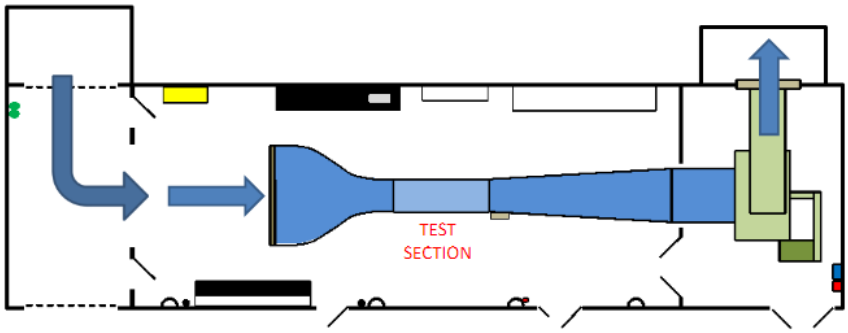

Figure 36. Oklahoma State Wind Tunnel Schematic.

To better understand their acoustic signature, velocity and temperature of the K45TP exhaust and K45TP propwash were made with a five-hole pitot probe and an accompanying thermocouple. The tubes from the pitot probe and the thermocouple are connected to an air data computer. Data is read at 50 Hz through Teraterm software. The thermocouple was friction fit into a plastic mount that slides into T-Slotted Aluminum Extrusion; this blue plastic mount can be seen in Figure 37 (left). For propwash and turbojet exhaust, the base of the thermocouple was taped to the moment arm stand so that the tip of the thermocouple was in the air flow. The pitot probe location

is controlled with a traverse system through the wind tunnel's LabVIEW software. The pitot probe can also be seen in Figure 37 (left).

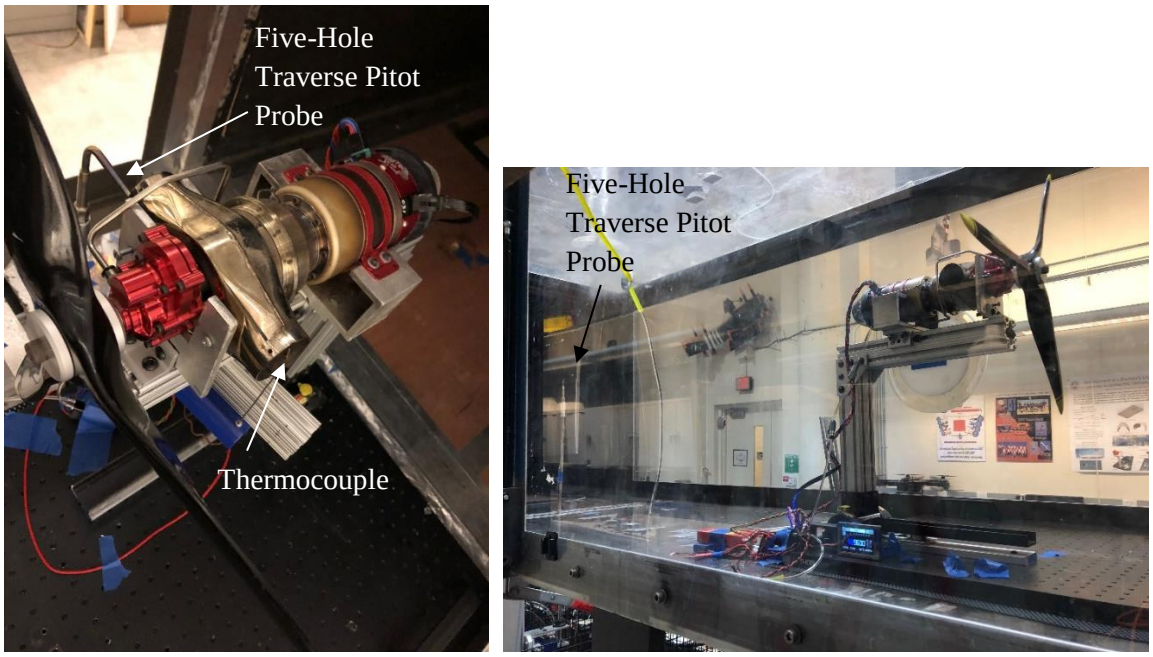

Figure 37. Five-Hole Pitot Probe and Thermocouple before Turboprop Testing.

During exhaust testing of the K45TP, the traverse system guided the pitot probe into the exhaust and stayed there for 5 seconds. The pitot probe then moved out of the exhaust for 5 seconds during which time the engine was throttled up. The process was repeated until data was gathered at 50%, 75% and 100% throttle. The pitot probe was less than 0.5 inches from the turboprop exhaust duct.

To measure velocity of the K45TP propwash, the moment arm stand was positioned such that the traverse was more than 3 propeller diameters aft of the propeller to ensure minimal radial variation in the velocity profile [20]. This setup can be seen in Figure 37 (right). The traverse was programmed to sweep through several points behind the propeller, and the entire survey was averaged to determine the approximate global velocity of the propwash. The survey points were

evenly distributed in a 90° sector behind the propeller. The traverse gathered data at each point for 5 seconds and Figure 38 shows the survey schematic.

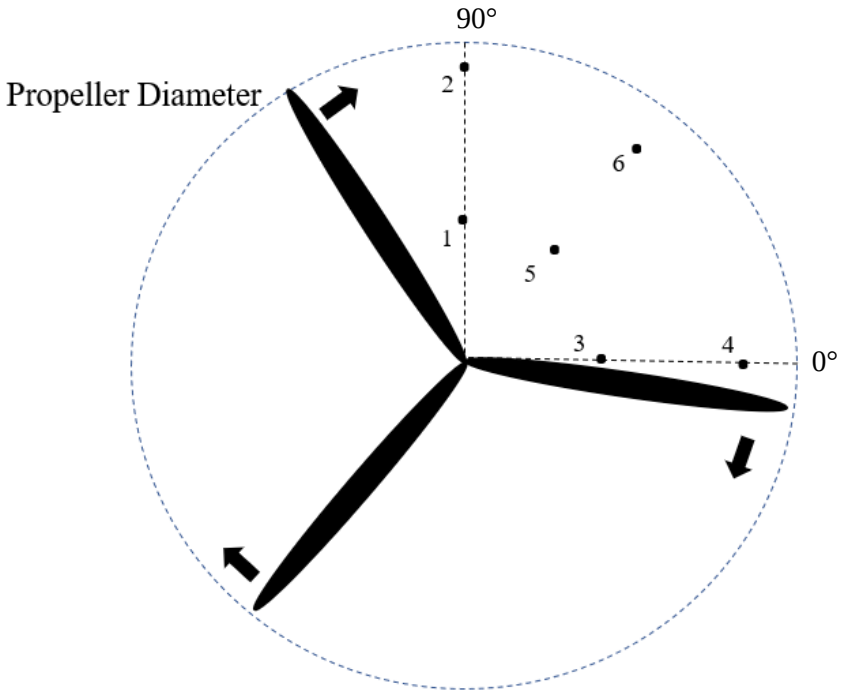

Figure 38. Propwash Traverse Pitot Survey.

Lastly, the fuel tank for the K45TP was placed on a digital scale during wind tunnel testing. While the traverse pitot probe was measuring exhaust properties, the change in weight of the fuel tank was noted every ten seconds. With that information, Equation 15 and Equation 1 can be used to calculate SFC.

$$\dot{m}_f = \frac{W_{t1} - W_{t2}}{\Delta t} \tag{15}$$

CHAPTER V

RESULTS

This chapter presents qualitative results from the variable cycle assemblies. Additionally, thrust and acoustic data are presented for the turboprop and baseline turbojet data is presented for a future comparison to a variable-cycle engine. Contributions of turboprop noise are studied in the acoustic data and also with respect to velocity and temperature data of the engines' exhaust and propwash. Lastly, comparisons between the thrust and acoustic signature of the propulsors are made; a summary of these comparisons can be seen in Table 4.

Comparisons	
K45 Turbojet and K45TP	Turbojet vs Turboprop with same gas turbine core
TP Tractor and Electric Tractor	Effect of gas turbine core
K45TP Pusher and Tractor	Pusher and Tractor Propeller on K45TP

Table 4. Comparisons Made between Propulsors.

5.1 Variable-Cycle Assembly Concept 1

The first step in studying the feasibility of Variable-Cycle Concept 1 was to drive the aft propeller assembly with a turbojet. This was effectively the turboprop mode for Concept 1. The K45TP can be partially disassembled into two parts: the aft propeller assembly and the gas turbine core. Figure 39 (left) shows the two parts of the K45TP used in Concept 1. Attaching a nozzle makes

the gas turbine core like the K45 turbojet but a fuel tap-off connector remains so some of the fuel acts as a lubricant for the aft propeller assembly gearbox. Figure 39 (right) shows Concept 1 fully assembled with the K45TP core (turbojet), bellmouth inlet, jet pipe, aft propeller assembly and fuel tap-off (lubricant) line.

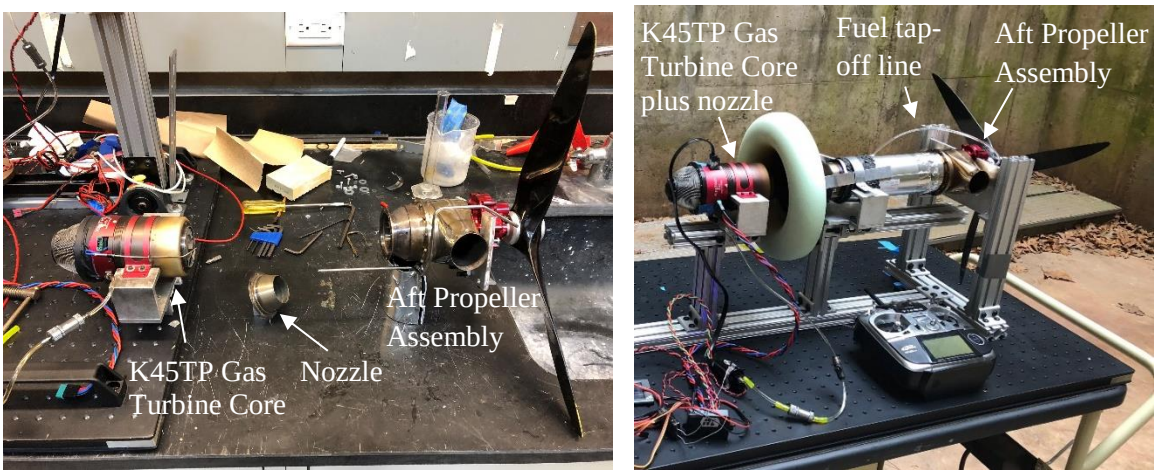

Figure 39. Disassembled K45TP (left) and Concept 1 Preliminary Test (right).

Initial tests of the setup shown in Figure 39 resulted in a sustained, blue flame at the nozzle of the turbojet through engine startup. Fuel flow was cut during startup to avoid damage to the jet pipe, wires and other components. This sustained flame was unlike a “hot-start” common to gas turbine engines during startup in which fumes or excess fuel are burnt off in short bursts of flames noticeable in the exhaust. It was thought that the exhaust, and therefore the fuel content of the air, in the jet pipe built up enough to hold a steady flame outside of the nozzle. This is likely due to an off-design condition for the aft propeller turbine that provides more resistance. To facilitate exhaust traveling through aft propeller assembly, a steel cone was fabricated on a computer numerical controlled (CNC) lathe. The cone was friction fit into the aft propeller assembly hub to provide a less tortuous flow path for the exhaust. The steel cone was used in the remainder of the Concept 1 operability tests and can be seen on the hub in Figure 40.

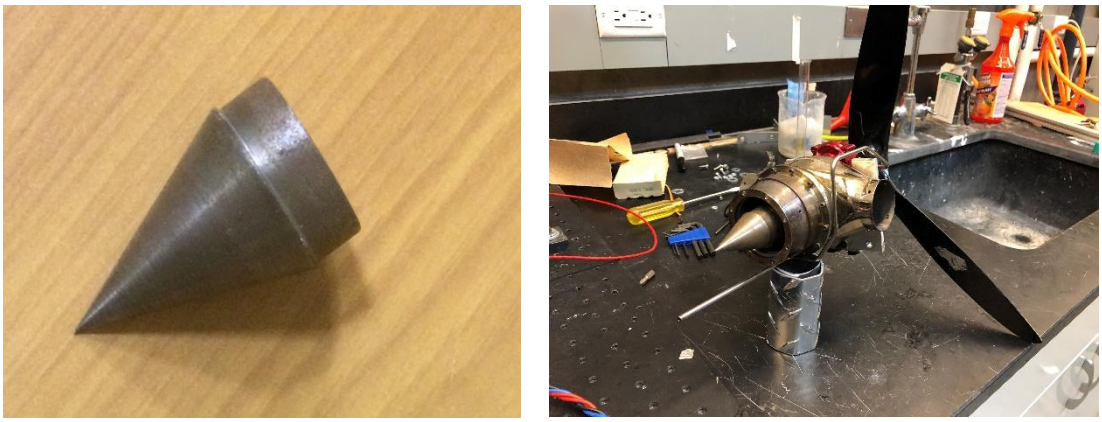

Figure 40. Stainless Steel Cone for Aft Propeller Assembly (left) and Cone in Hub of Aft Propeller Assembly (right).

With the addition of the cone, operability was tested:

1. Without the bellmouth (jet pipe only)
2. With less fuel injection during startup
3. With different jet pipe distances from the nozzle
4. Joining the jet pipe to the turbojet after turbojet startup
5. With a seal around the jet pipe/propeller assembly connection
6. With compressed air to spin start the aft propeller assembly
7. With a seal around the turbojet/jet pipe connection

All attempts resulted in different severities of sustained flames and testing was halted during or shortly after engine startup. Sustained flames can be seen in Figure 41. A detailed test log and the accompanying notes can be seen in Appendix C. This concept could be made feasible with an area-ruled duct in place of the jet pipe and turbine inlet guide vanes, but added complexity and weight are not practical for sUAS.

Figure 41. Sustained Flames at Nozzle (left) and at Turbojet/Jet Pipe Seal (right).

5.2 Variable-Cycle Assembly Concept 2

Operability for Concept 2 was initially tested by starting the K45TP in a way that the propeller, and therefore the free turbine, could not spin. Figure 42 shows the K45TP mounted so that the upper horizontal arm interfered with the propeller's rotational path and the propeller could not rotate. The engine successfully started and visual observations were compared to a nominal run in which the propeller was able to spin. Visual observations include a more active hot-start, and at 33% throttle, a faint, steady flame in the exhaust duct which was glowing red.

Figure 42. Turboprop with Propeller Locked.

Core RPM, Pump Power, Exhaust Gas Temperature and Throttle data from the KingTech engine logs were used to compare a nominal test to a test with the propeller locked. Figure 43 shows graphs from the entire test but values from a single data point on the right side of the photos. At approximately the same throttle setting (33-36%), the test with the propeller locked resulted in 16% higher exhaust gas temperature. This is still below standard, full-throttle exhaust gas temperatures that are approximately 548 °C.

Figure 43. Nominal Turboprop Startup (left) and Propeller Locked Startup (right).

In an attempt to produce thrust from turboprop exhaust, commercial exhaust ducts that feature a 70° turn were attached during tests with the propeller locked. This resulted in higher than nominal exhaust temperatures sooner in the startup sequence. Figure 44 shows multiple red hot components during startup. Engine startup was aborted soon after this instant. Future studying of exhaust conditions and engine operability with the propeller locked are recommended in Section 5.2.

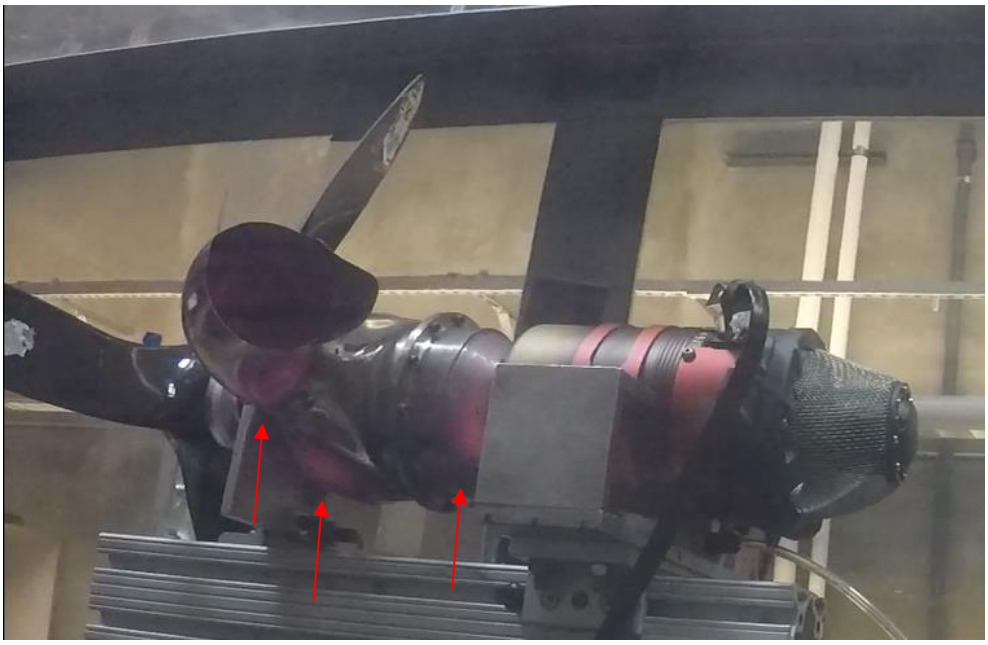

Figure 44. Red Hot Exhaust Ducts during Engine Startup.

5.3 Performance Data

Thrust data of the test configurations used in the current study was gathered simultaneously with acoustic data. Thrust data is presented as an average of the five seconds that data was collected during engine equilibrium. Figure 45 shows this data graphically for all configurations. Note that Figure 45 shows values for Propeller RPM on the upper x-axis and RPM of the gas turbine core for the turbojet on the lower x-axis. Since the turboprop engine has both a propeller and core RPM, propeller RPM can be read on the upper axis and core RPM is labeled on each point. Error bars are standard deviations of the averaged thrust. Electric Tractor can also be seen on the chart for the comparison to TP Tractor. K45 Turbojet data is included for an acoustic comparison to the K45TP as a baseline for a variable-cycle engine.

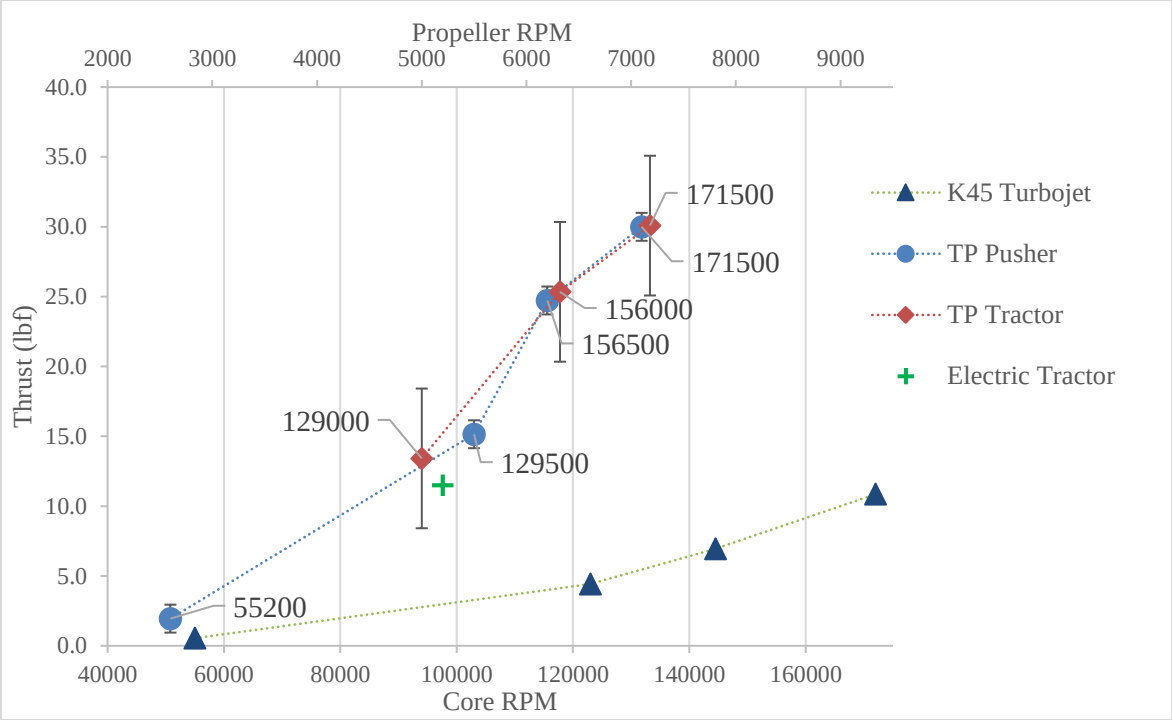

Figure 45. Thrust of All Tested Configurations.

The lower thrust range of the K45 turbojet compared to the K45TP can be seen in Figure 45. This is important to note because a similar thrust range can be expected from a variable-cycle turbojet mode.

Turbojet SFC data at full-throttle can be calculated from manufacturer specifications [2] and Equation 1, but K45TP SFC data was gathered in the current study. Using the same 3-bladed 20x10 propeller from acoustic tests, fuel consumption data was gathered during exhaust property testing of the K45TP. SFC of the K45TP was calculated for each throttle setting and can be seen in Figure 46. SFC can be calculated for the K45 turbojet from manufacturer data. The K45TP has 60% less SFC than the K45 turbojet. Using Equation 2, low-speed mission legs can result in approximately 65% more range and endurance by making use of a turboprop-like mode in a variable-cycle engine instead of a turbojet alone.

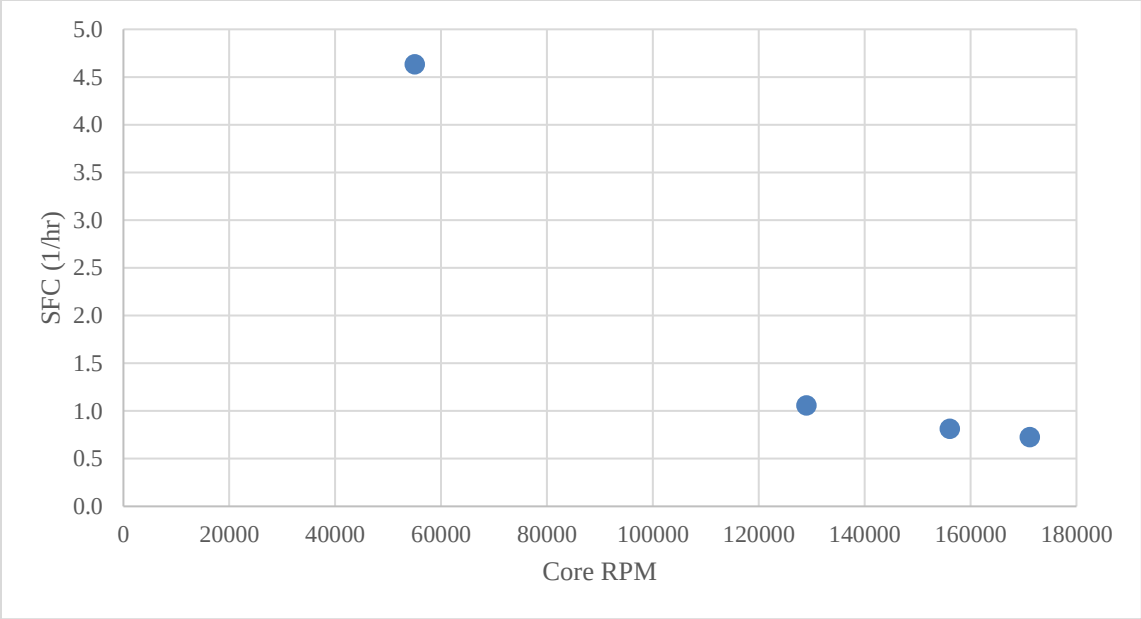

Figure 46. Turboprop SFC vs Throttle Setting (Core RPM).

5.3.1 Thrust Uncertainty

Sources of error in thrust data include drag on the moment arm stand from freestream conditions at the acoustic test facility. To counteract different effective preloads due to wind, thrust data is presented as a difference from an “engine off” reading. This ensures that thrust data does not include drag from the ambient wind. The drag force on the vertical arm of the moment arm stand does not unload the load cell because the air is deflected onto the same rigid body that holds the propeller. Stand interactions with the propeller wash could underestimate thrust, but the complexity of propeller wake and resultant effect on thrust is out of the scope of the current study and the stand was consistent between different configurations. Therefore, comparisons between propulsors are included.

Vibrations in the moment arm stand were present in the turboprop thrust data. These vibrations are presumably from a combination of the rotational degree of freedom present in the stand and also an unbalanced propeller. Uncertainty is assumed to predominately stem from stand

vibrations. Therefore, only precision uncertainty on the thrust averages at each throttle setting (idle, 50%, 75%, 100%) is presented in Table 5. Equation 15 was used with a 95% confidence.

$$s = \sqrt{\frac{1}{n-1}\sum_{i=1}^{n}(x_i - \bar{x})^2} \qquad P = \pm t_{\alpha/2}\left(\frac{s}{\sqrt{n}}\right) \tag{15}$$

	TP Pusher	TP Tractor
idle	0.82%	2.66%
50%	0.25%	1.26%
75%	0.16%	0.77%
100%	0.13%	0.57%

Table 5. Uncertainty in K45TP Thrust.

5.4 Acoustic Data

Narrowband data was acquired from 0-25.6 kHz with $\Delta f = 2$ Hz. Overall Sound Pressure Level (OASPL) calculations feature a summation of pressure levels from frequencies of 100 Hz to 20 kHz. Ambient data was contributing to noise at frequencies below 100 Hz, so those frequencies were neglected. Narrowband plots will frequently be seen without data below 100 Hz for clarity. Frequencies above 20 kHz were neglected because they are above the human threshold of hearing. Figure 47 shows a typical narrowband plot with acoustic turboprop and ambient data. The range of frequencies used for the OASPL calculation can be seen in the plot.

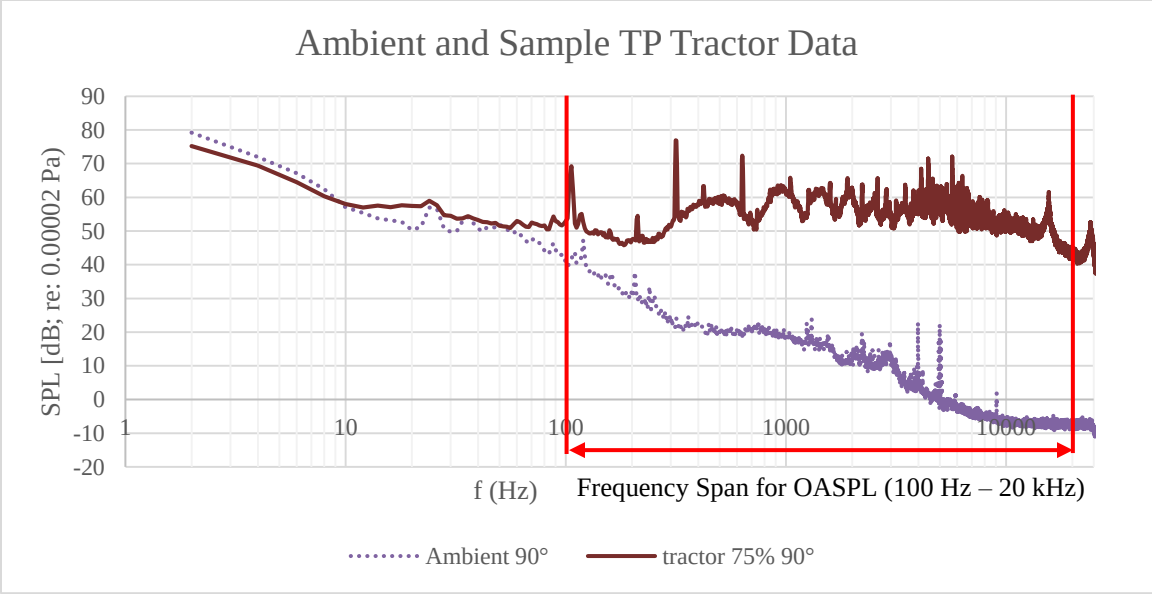

Figure 47. Sample Plot of Narrowband Data, Δf = 2 Hz.

5.4.1 OASPL Plots

Polar OASPL plots are a useful summary of noise at all angles. The radius of the points from center is representative of OASPL magnitude in dB and the angle of the point represents the physical angle of the microphone following the convention outlined in Sections 4.3.1 and 4.3.2. **Error! Reference source not found.** and Figure 48 show polar plots with all angles and all throttle settings for acoustic testing of the TP Tractor and TP Pusher configurations. The engines are pictured in the plots as they were setup.

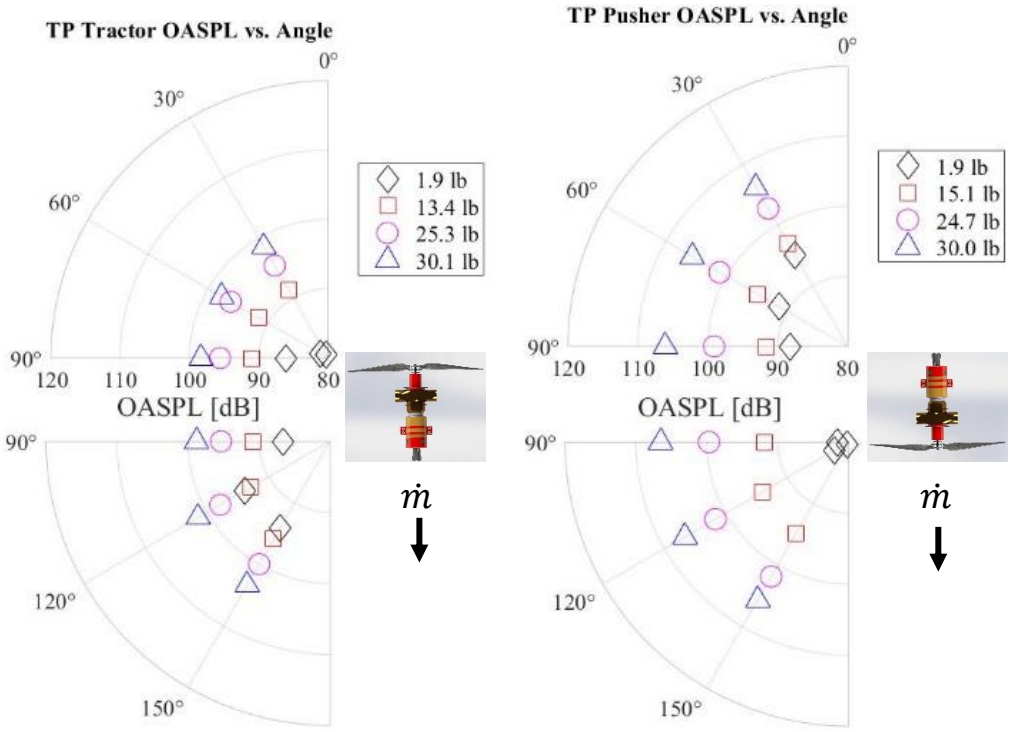

Figure 48. OASPL vs. Angle and Thrust for TP Pusher and TP Tractor.

Figure 48 shows the polar plots for the TP Tractor and TP Pusher configurations. The noise measured consists of the internal noise sources, jet noise from the exhaust and propeller noise. The OASPL is higher for TP Pusher on average. To better understand contributions to K45TP noise, a simplified schematic of the microphone placement and air flow around the TP Pusher and TP Tractor configurations can be seen in Figure 49.

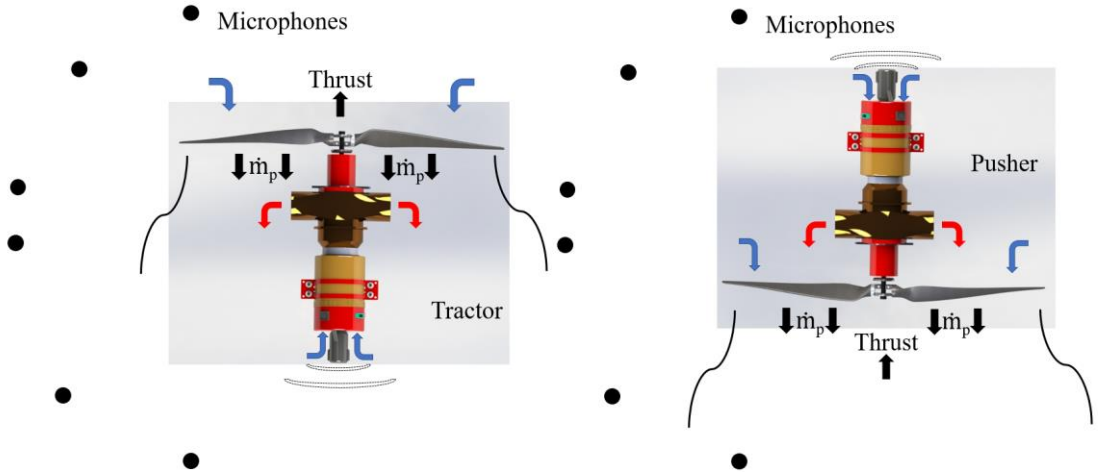

Figure 49. Simplified Air Flow and Microphone Schematic of TP Tractor (left) and TP Pusher (right).

While Figure 49 is not to scale, one can see that the pusher propeller ingests turboprop exhaust. This is a noise source unique to the TP Pusher configuration and may partially explain the higher OASPL measured. Another cause of higher OASPL is likely the higher propeller RPM achieved by the pusher propeller. This can be seen in the narrowband data. The final noise source to note is turbomachinery noise emanating from the gas turbine core inlet. Compressor noise can explain relatively high OASPL at 120°-150° for the TP Tractor configuration and 30°-60° for TP Pusher at the lowest thrust value. Compressor noise will be studied further in the narrowband data.

5.4.2 Narrowband Data

Figure 50 shows narrowband data from 3 angles of the TP Tractor and TP Pusher data. Propeller blade passing frequency (BPF) is evident in the narrowband data from both configurations. For example, at a propeller RPM of 5000, the BPF is 2 x rpm x number of blades or 250 times per second. This means that one can expect to see a peak in the spectra at approximately 183 Hz; all other peaks are harmonics of that frequency. BPF peaks are labeled in Figure 50. It can also be seen that the amplitude of the peak is highest at 90° and decreases at other angles, as expected

[21]. Although one thrust value is shown, this trend was the case for all thrust values of the TP Tractor and TP Pusher configurations. Unabridged narrowband data can be found in Appendix E.

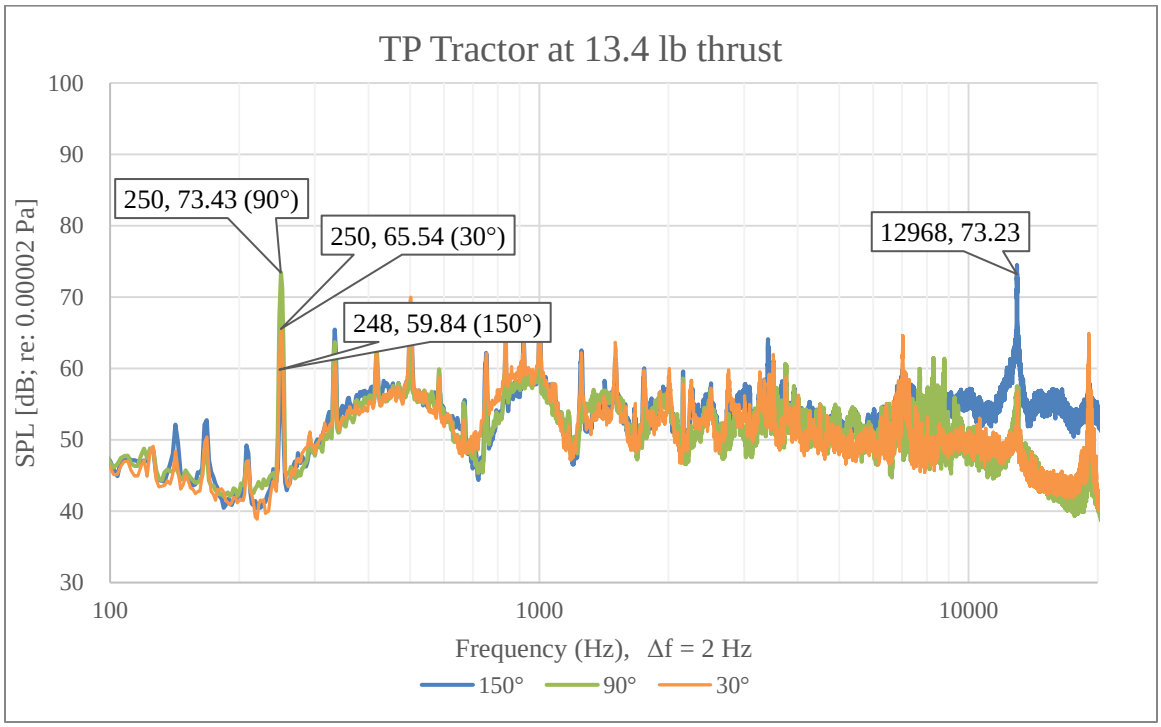

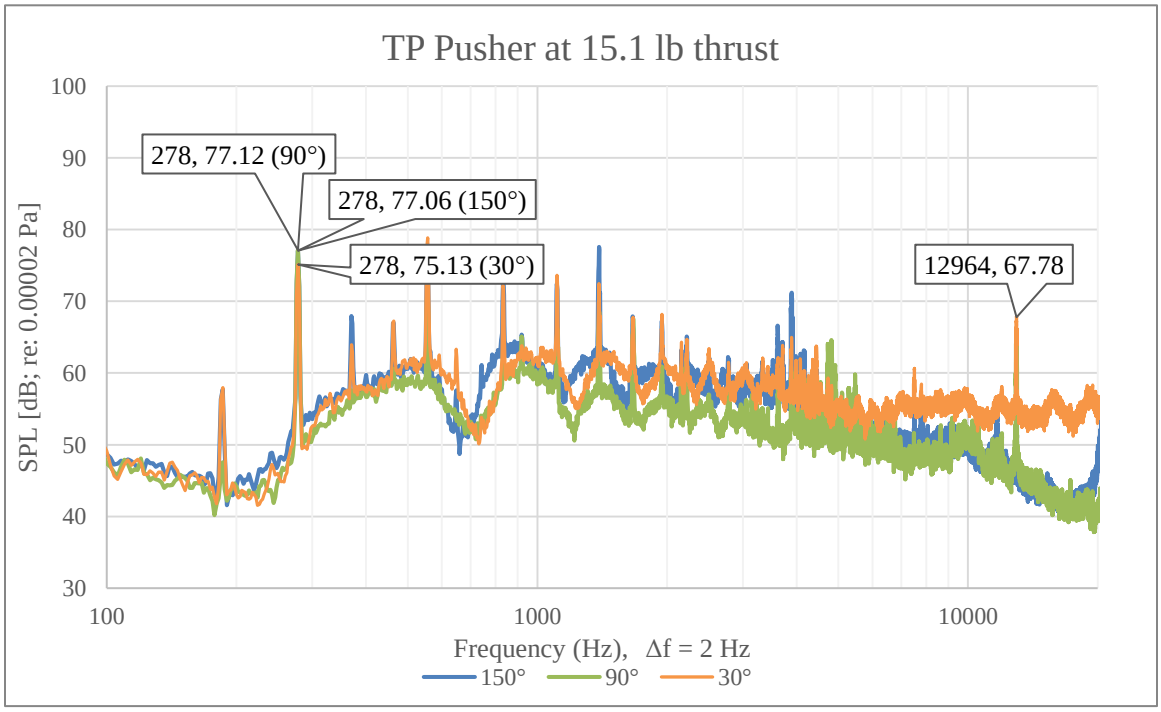

Figure 50. Narrowband Spectra of TP Tractor and TP Pusher at 50% Throttle.

Compressor BPF is also labeled in Figure 50. The K45TP turbojet has 6 compressor blades, so with the knowledge of Core RPM at each throttle setting, compressor BPF in narrowband data can be seen to match expectation. A summary of all expected BPF is provided in Table 6. Figure 51 shows the TP Tractor 150° microphone data at all throttle settings. The compressor noise is clear and in agreement with the expected values. Turbine BPF is not present in the narrowband data and is likely overpowered by propeller noise since the turboprop exhaust is close to the propeller.

TP Tractor	Prop RPM	Prop BPF	Core RPM	comp BPF	avg thrust (lb)
idle	1750	87.5	55500	5550	1.9
50%	5000	250	129000	12900	13.4
75%	6320	316	156000	15600	25.3
100%	7180	359	171500	17150	30.1
TP Pusher					
idle	2600	130	55200	5520	1.9
50%	5500	275	129500	12950	15.1
75%	7100	355	156500	15650	24.7
100%	8050	402.5	171500	17150	30.0

Table 6. Expected BPF during Acoustic Testing.

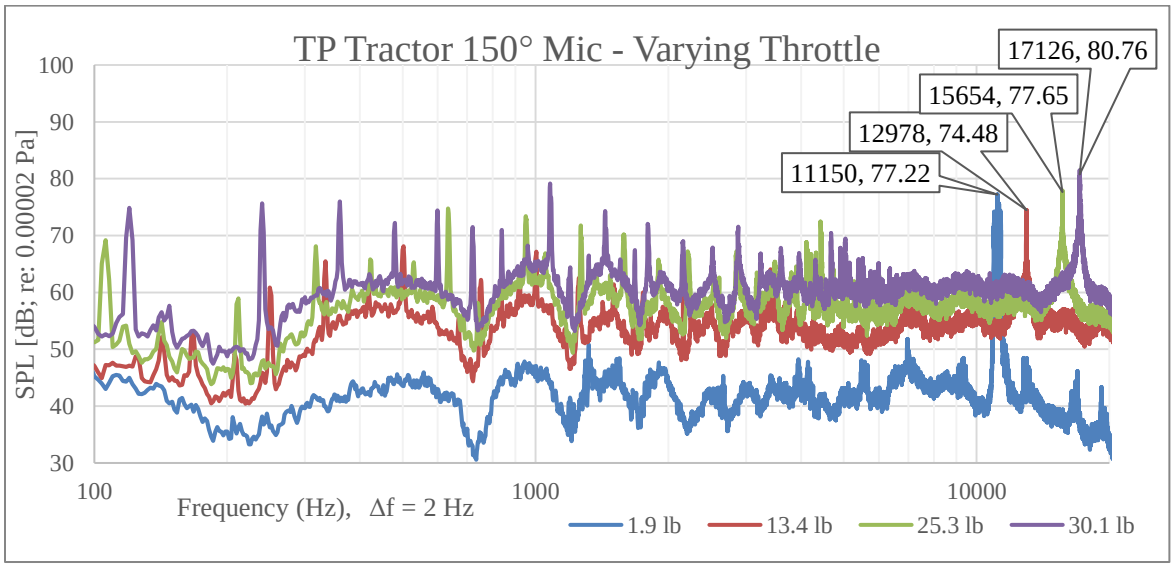

Figure 51. TP Tractor Narrowband Data Varying Throttle.

The concept of BPF frequency spikes is important for the detectability UAS, and therefore variable-cycle design. For example, high SPL of BPF could be easily distinguished with detection devices like the microphones used in the current study. The results of this study show that turboprops have several distinct tones due to propeller and turbomachinery BPF, but turbojets have significantly less. While the turbojet tones are higher frequency and may be less noticeable to the human hear, other methods of detection may find them just as detectable.

5.4.3 Acoustic Sources of Error

Sources of error for acoustic data are not quantified but could include differing ambient conditions and microphone bias. However, acoustic measurements were taken on the same day or in similar conditions, therefore observations drawn are acceptable for comparisons.

5.5 Exhaust Property Testing

Figure 52 shows exhaust properties from traverse pitot probe measurements in the wind tunnel. These properties are useful for identifying contributions of noise. The K45TP exhaust changes only slightly with increased throttle, so broadband noise stemming from exhaust should be nearly constant. Turboprop exhaust properties are also useful in future design of a variable-cycle propulsion system. For example, the notional nozzle from VC Concept 2 could be optimized to ensure proper flow acceleration for thrust production.

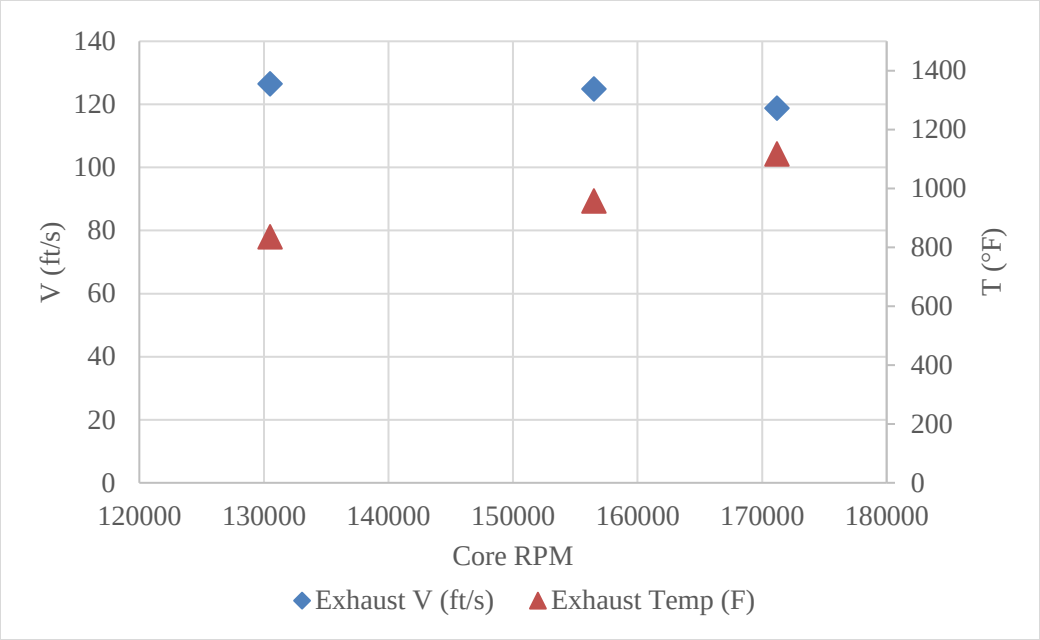

Figure 52. Exhaust Properties of K45TP.

Using Equation 11, exhaust temperature and the turboprop exhaust velocity, T_9 for the nominal turboprop can be calculated. Holding T_9 constant and plugging in the higher exhaust gas temperature (T_{t9}) from the propeller locked configuration, Equation 11 shows V_9 to be 1266 ft/s. This high exhaust velocity should be experimentally verified but matches the turbojet PCA from Section 3.1. This prediction is promising for appreciable thrust in turbojet mode in Variable-Cycle Concept 2.

Figure 53 shows propwash velocity of the 20x10 3-bladed propeller with increased turboprop throttle. Error bars are standard deviations of the averaged velocity. Broadband noise from the TP configurations increases, so it is likely that the broadband noise is caused mostly by propwash and not turboprop exhaust.

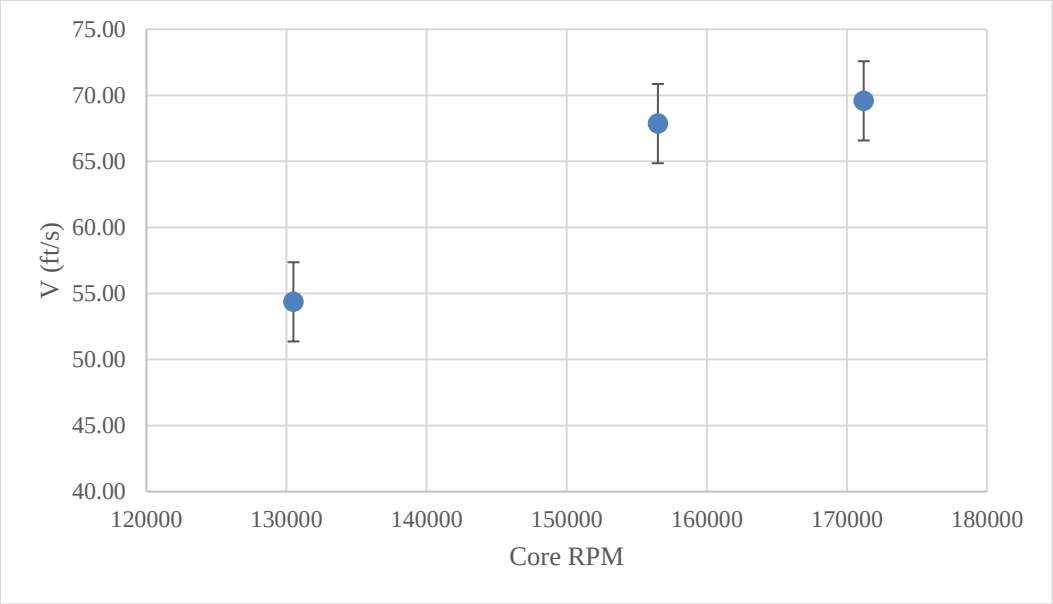

Figure 53. K45TP Propwash Velocity vs Throttle.

5.5.1 Propwash Uncertainty

The propwash caused large vibrations in the traverse pitot probe which is only supported from its base. This is expected to be the primary cause of uncertainty on the propwash velocity measurement. Therefore, uncertainty on the propwash measurement is presented as precision error on the average taken during the survey. Equation 15 was used with a 95% confidence. Table 7 shows the precision error as a percentage of the average.

Throttle	Velocity (ft/s)
50%	54.36±0.35%
75%	67.86±0.47%
100%	69.58±0.60%

Table 7. Precision Error of Propwash Average.

5.6 Additional Comparisons

5.6.1 TP Tractor vs Electric Tractor

To examine the propeller noise contribution from the turboprop, the noise from the TP Tractor and Electric Tractor configuration were compared [22]. In the Electric Tractor tests, RPM was matched to the previously tested TP Tractor RPM. Figure 54 and Figure 55 show the peaks and some harmonics of the propeller noise matching for the two configurations as expected. Another peak can be seen at half of the BPF on the Electric Tractor configuration only. Since the propeller is two-bladed, half of that frequency would be a noise source that happens once per revolution.

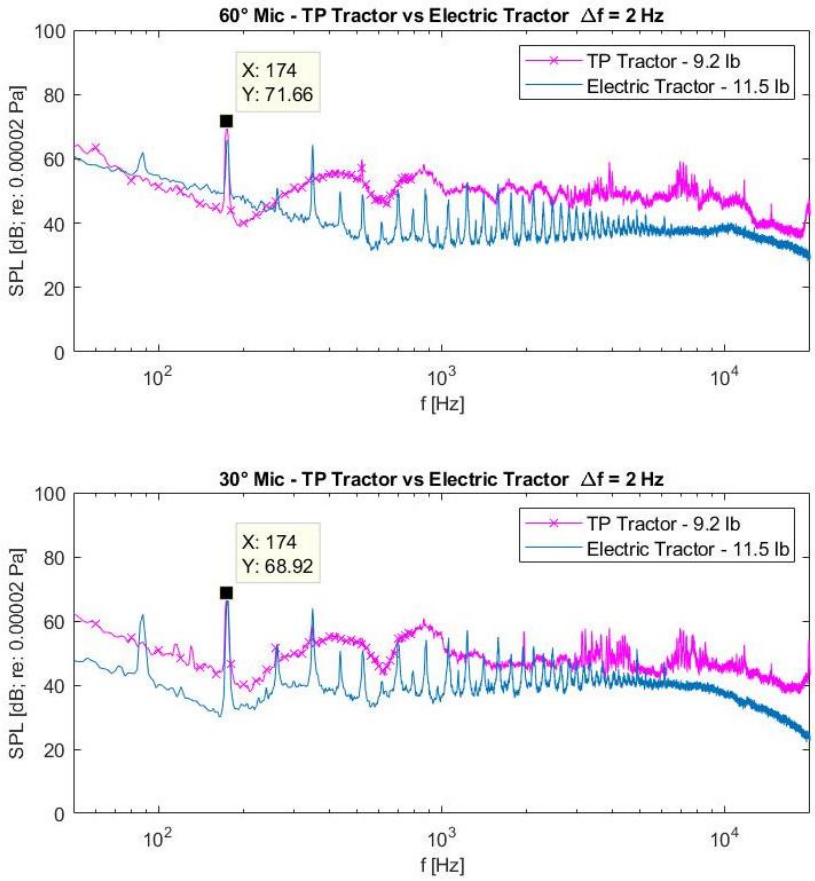

Figure 54. Narrowband Data of TP Tractor vs Electric Tractor [22].

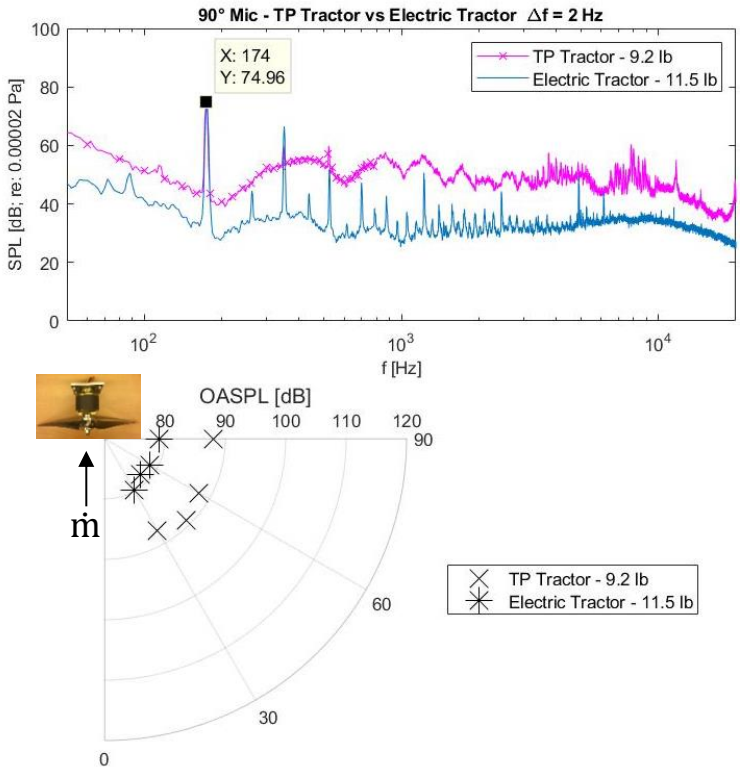

Figure 55. Narrowband Data and OASPL of TP Tractor vs Electric Tractor [22].

The same trends with a maximum SPL of the BPF frequency at 90° can be seen in Figure 55. Additionally, the broadband component of the turboprop follows similar trends to the broadband noise of the turbojet with a maximum SPL at 30°. This data underscores that the propeller noise signature is dominating noise below 300 Hz.

5.6.2 TP Pusher vs K45 Turbojet

To observe the potential acoustic signature of the turbojet mode of a variable-cycle engine, a small turbojet is compared to the K45TP [22]. This comparison is shown in Figure 56 and makes use of the smaller K45 turbojet on which the K45TP is based. Thrust values are similar even though the K45 was at full throttle and the K45TP was at approximately 50% throttle. Microphones were placed 5 feet from the K45 turbojet, so acoustic data was therefore scaled down according to the inverse square law [23]. The K45TP propeller noise is above the K45

broadband. This comparison is included as a baseline for the variable-cycle concepts whose turbojet modes would resemble a K45 turbojet.

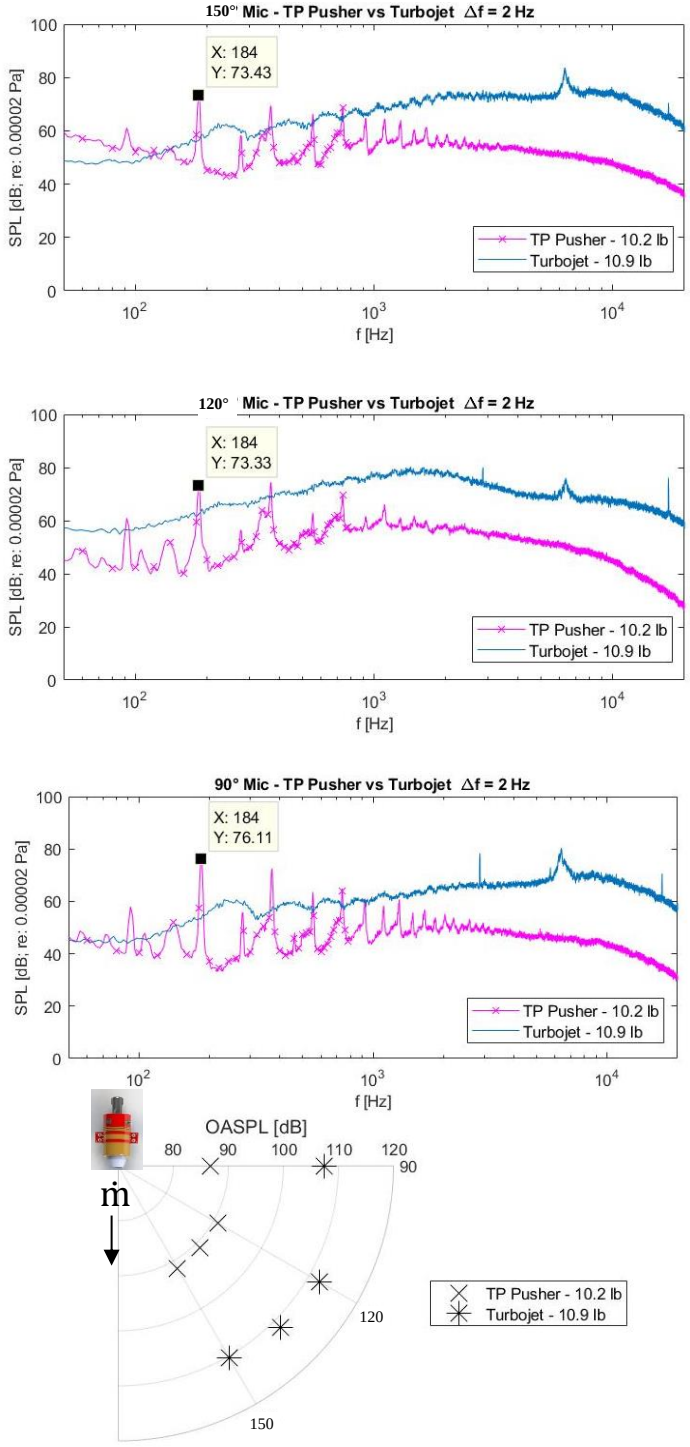

Figure 56. Narrowband Data and OASPL of TP Pusher vs K45 Turbojet [22].

Figure 56 shows that most of the noise from the turbojet is between 120-150° and falls off as the observer moves from 120° to 90°. If the measured noise was solely from jet noise, one could expect to see a peak level in the 150° observer angle [15]. However, the turbojet engine has numerous noise sources inside the jet itself, such as turbomachinery and combustion noise. These internal noise sources will tend to exit the nozzle closer to the 60° observer. The resultant measured noise was a combination of internal noise sources and external jet noise. This comparison shows that turbojet noise is composed primarily of broadband noise near 1000 Hz and turboprop noise is primarily BPF and harmonics. An engine that switches between variable-cycle modes may avoid detection with the use of different modes that provide a less obvious acoustic signature.

5.6.3 Tractor and Pusher Comparison

The final comparison features polar plots of similar thrust values from the TP Tractor and TP Pusher configurations, shown in Figure 57. From a UAS design perspective, it is important to note that directivity at the idle setting is dominated by the orientation of the gas turbine core. This may be relevant for a turboprop sUAS loitering at very low throttle. Also, the TP Tractor configuration is quieter than TP Pusher at higher throttle settings. Narrowband data in Figure 58 shows that both components of propeller noise (BPF and broadband) are higher in the pusher configuration. The X-axes in Figure 58 show narrowband frequency divided by BPF because of the different propeller RPM. Higher OASPL may be related to a higher propeller RPM from the pusher propeller compared to the tractor propeller caused by effectively opposite freestream conditions after switching the configuration. However, thrust was matched between the pusher and tractor propellers, so the higher OASPL may dissuade a designer from choosing a pusher propeller on the K45TP or in a variable-cycle arrangement.

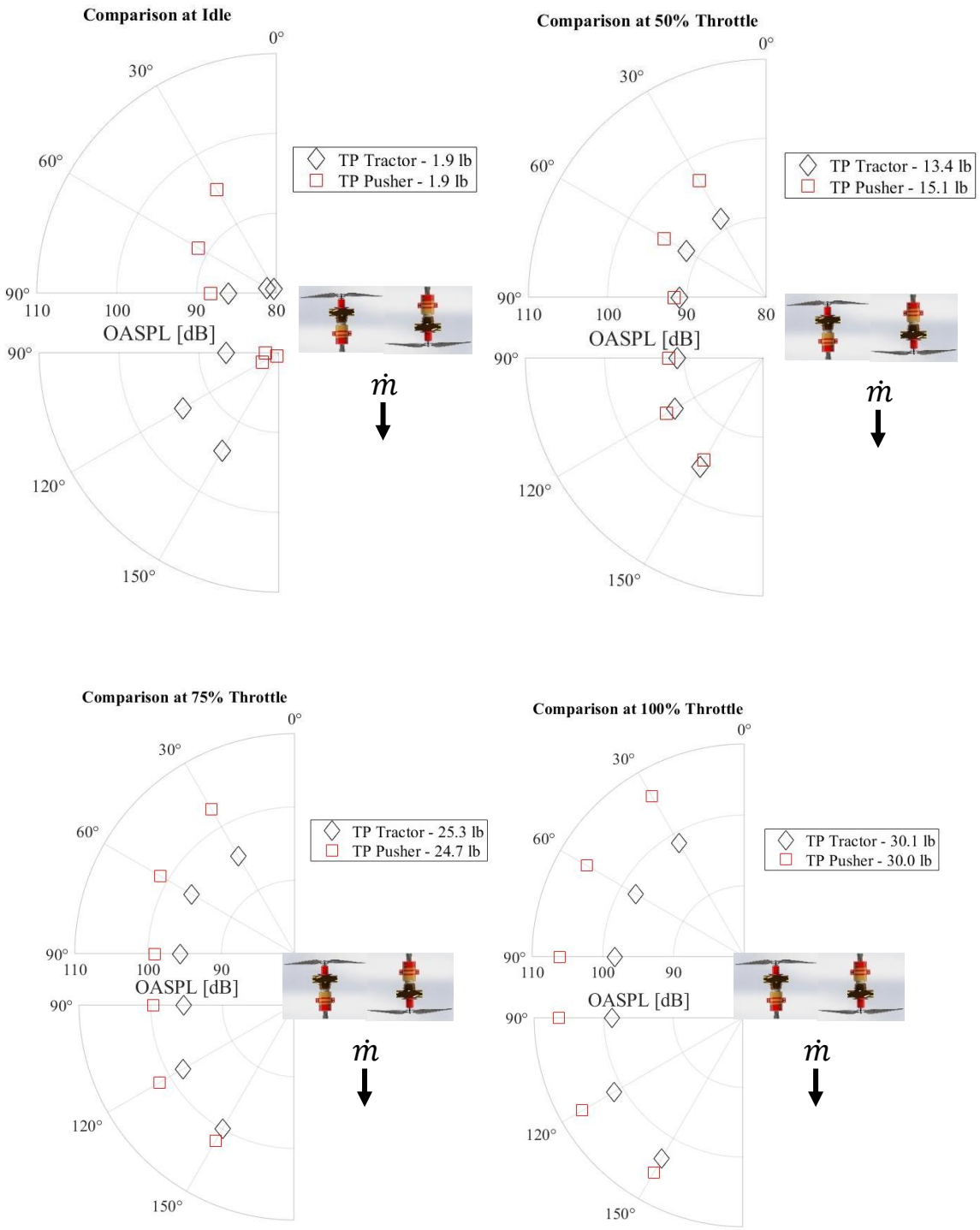

Figure 57. Comparison of TP Tractor and TP Pusher at Similar Thrust Levels.

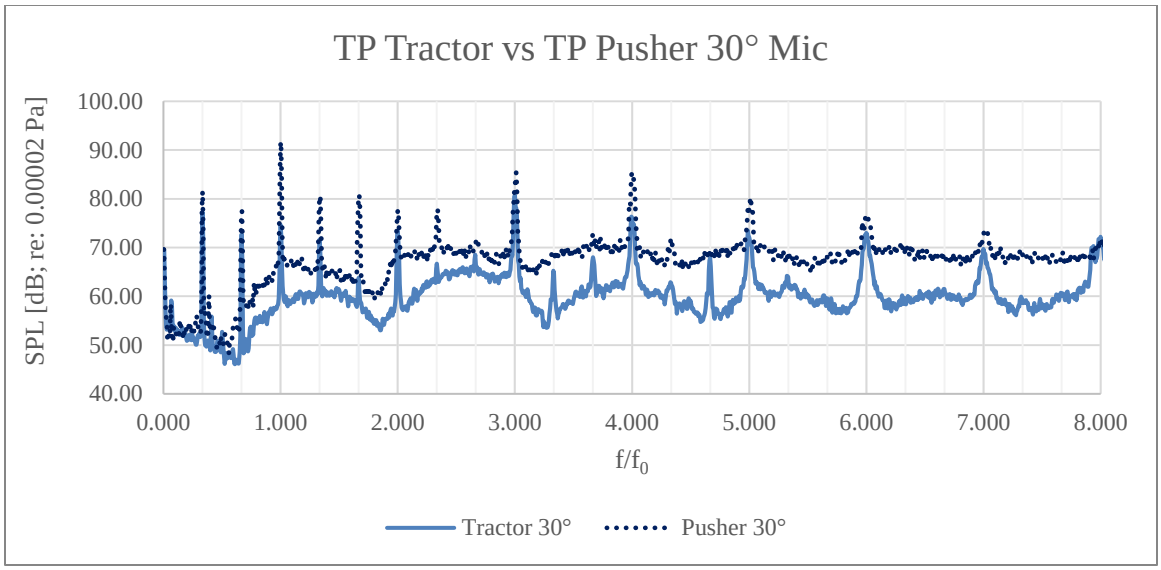

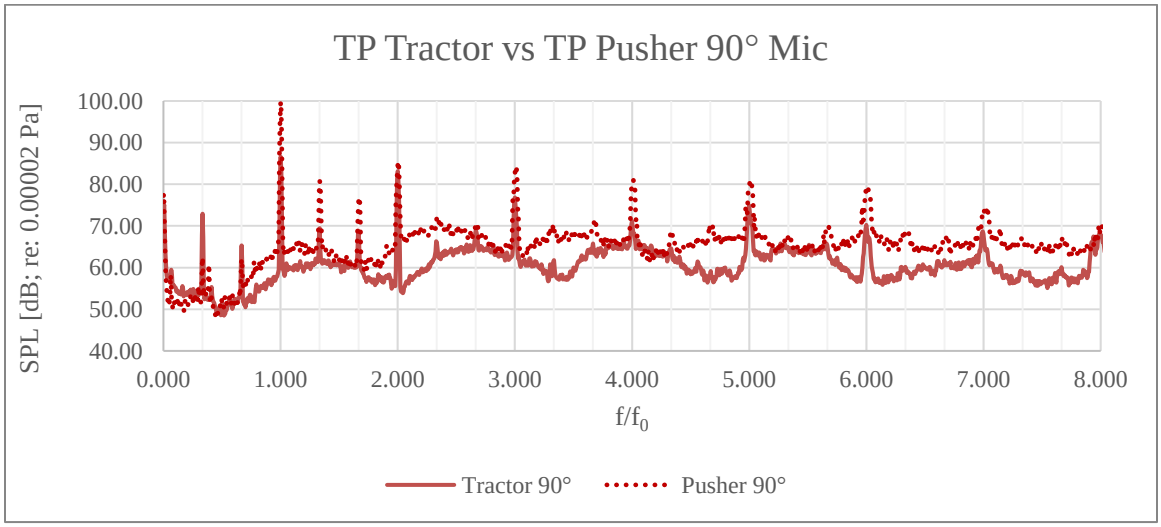

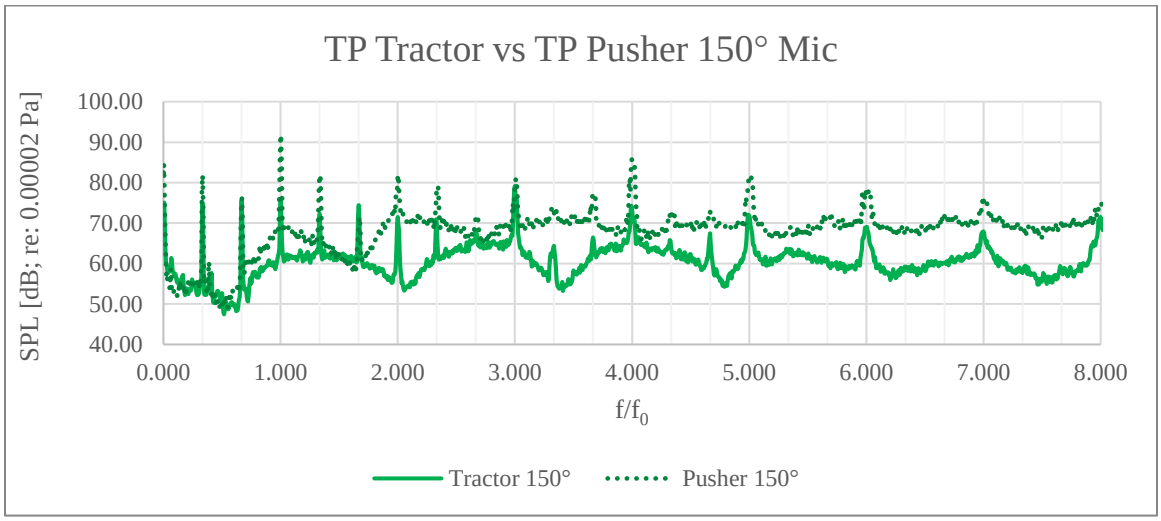

Figure 58. Narrowband TP Tractor vs TP Pusher Comparison at 50% Throttle.

CHAPTER VI

CONCLUSION

This chapter presents a summary of the current study and recommendations for future design and study of a variable-cycle propulsion system.

6.1 Summary

Results of this study present and test two concepts for a sUAS variable-cycle engine that can function as a turboprop or turbojet. Concepts were comprised of primarily commercial off-the-shelf components and some custom fittings. Concept 1 features a jet pipe for optional guiding of exhaust into a turbine that drives a propeller; this resulted in flames in the jet pipe and damaged components. Flames were presumably caused by difficulties in venting exhaust out of the aft propeller assembly. Concept 2 makes use of a commercial turboprop engine in its stock configuration. The propeller was locked to examine feasibility of using exhaust for thrust in turbojet mode. This resulted in a successful engine start but higher than nominal exhaust temperatures. Concept 2 is promising for future work toward a variable-cycle engine.

Performance and far-field acoustic data for Concept 2 turboprop mode (the stock turboprop engine) is also presented. During turboprop testing, a comparison to a turbojet and a propeller with an electric motor was made. Important results are:

1. Parametric cycle analysis shows that small turbojet thrust is heavily dependent on nozzle pressure ratio.
2. A variable-cycle engine could widen operating envelopes of sUAS with diverse mission requirements.
3. Novel operational methods for small gas turbines show a thin operating envelope.
4. The K45 Turbojet has about 12 dB higher OASPL than the K45TP at similar thrust levels.
5. The turboprop with a pusher propeller results in 8 dB higher OASPL than with tractor propeller.
6. Noise in the frequency bands below 500 Hz are dominated by the propeller of the turboprop, and noise in the bands above 1000 Hz are dominated by the turbojet.

6.2 Future Recommendations

The most open-ended section of the current study is the design and performance of Concept 2. The turboprop mode of Concept 2 has been studied. Although a locked propeller results in very high temperature exhaust, the turbojet mode for Concept 2 could be optimized and studied. For example, a turbojet mode exhaust nozzle should be finalized and fabricated to accelerate exhaust flow and produce thrust when the propeller is locked. Lastly, an actuation mechanism for releasing the propeller clutch would allow study of the transition from turbojet to turboprop mode. With an operational variable-cycle propulsion system, performance and acoustics of the turbojet mode can be compared to the turbojets in the current study. Assuming favorable performance results, a vehicle can be developed, and the effect of aircraft integration on performance and acoustics should be studied.

REFERENCES

[1] Desert Aircraft DA-100L Twin Cylinder RC Gas Engine. (2017, November 28). Retrieved from AeroBeez: aerobeez.com/Desert-Aircraft-DA-100L-Twin-Cylinder-RC-Gas-Engine.html.

[2] *KingTech Turbines - Engine Manual*. N.p.: KingTech Turbines, 2016. Print.

[3] Durkee et al., "Turbojet Ejector and Propeller Aft Assembly for Small Unmanned Aircraft Systems," 56th AIAA Aerospace Sciences Meeting & Exhibit, AIAA, 2018.

[4] Mattingly, J. D., Elements of Propulsion: Gas Turbines and Rockets, American Institute of Aeronautics and Astronautics, 2006.

[5] Wood, Alan, and Pericles Pilidis. "A Variable Cycle Jet Engine for ASTOVL Aircraft." *Aircraft Engineering and Aerospace Technology* 69.6 (1997): 534-39. Web.

[6] The Superjet: Building the Ultimate Flying Machine. (2016, February 23). Retrieved from https://www.ge.com/reports/post/78469596586/the-superjet/

[7] Hager., R. D. and Vrabel, D., "Advanced Turboprop Project," Sp-495, NASA, 1988.

[8] Bevilaqua, Paul M. "Genesis of the F-35 Joint Strike Fighter." Journal of Aircraft 46.6 (2009): 1825-836. Web.

[9] McCormick, Barnes W. Aerodynamics, Aeronautics, and Flight Mechanics. 2nd ed. N.p.: Pennsylvania State U, 1994. Print.

[10] Heiser, W. H. Ejector Thrust Augmentation. Tech. 6th ed. Vol. 26. Colorado: U. S. Air Force Academy, 2010. Print. Journal of Propulsion and Power.

[11] P, B. G. and Cahoon, W. M., "Design of an Intake Bellmouth. Rep. Prof Blair and Associates/Volvo Penta of the Americas," Race Engine Technology, 2006.

[12] Oglesby, Britt A. *Experimental Study of a Small Turbojet for Use in an Unmanned Aircraft System*. Tech. Stillwater: Oklahoma State U, 2014. Print.

[13] Matthew Durkee and Kurt P. Rouser, "Small-Scale Turbojet Thrust Augmentation from a Jet Pipe with a Bellmouth Inlet", AIAA 2018-0004, 56th AIAA Aerospace Sciences Meeting, Kissimmee, FL, 2018.

[14] Lighthill, M. (1952). On Sound Generated Aerodynamically. I. General Theory. *Proceedings of the Royal Society of London. Series A, Mathematical and Physical Sciences (1934-1990), 211*(1107), 564-587.

[15] Ahuja & Bushell. (1973). An experimental study of subsonic jet noise and comparison with theory. Journal of Sound and Vibration, 30(3), 317, IN1-341, IN1.

[16] Sinibaldi & Marino. (2013). Experimental analysis on the noise of propellers for small UAV. *Applied Acoustics, 74*(1), 79-88.

[17] Clark, B., & Scott, J. (1986). Coupled aerodynamic and acoustical predictions for turboprops - NASA-TM-87094.

[18] Jet Cat Data Sheet. (2019, April 2). Retrieved from https://www.chiefaircraft.com/pdf/jetcat-data.pdf

[19] KC, Real et al., “Investigation of a Geared Turbofan for Small Unmanned Aircraft Systems,” 57th AIAA Aerospace Sciences Meeting & Exhibit, AIAA, 2019.

[20] Hamill, G.A., Kee, C., Predicting axial velocity profiles within a diffusing marine propeller jet. Ocean Eng. (2016).

[21] Hubbard, Harvey H. Aeroacoustics of Flight Vehicles: Theory and Practice. Acoustical Society of America, 1995.

[22] Durkee and Gaeta, “Characterization of Thrust and Noise of Small Turboprop and Turbojet Engines,” 57th AIAA Aerospace Sciences Meeting & Exhibit, AIAA, 2019.

[23] Kinsler, Lawrence E., Fundamentals of Acoustics. Wiley, 1982.

APPENDICES

APPENDIX A
ANALYTICAL CALCULATIONS

PARAMETRIC CYCLE ANALYSIS

$\pi_{c.ref} := 2.1$ https://www.chiefaircraft.com/pdf/jetcat-data.pdf $V_{dash} := 150mph$

<Level of Tech (1): $T_{t4.ref} := 1400\,°F = 1860\,R$ $mdot := 0.3\,\frac{lbm}{s}$

Level of Tech (2): $\pi_b := 0.92$ $\eta_b := 0.94$

Level of Tech (3): $\pi_n := 0.98$ $\pi_{d.max} := 0.96$ $e_c := 0.88$ $e_t := 0.89$ $\eta_{mech} := 0.99$

Assume: $\gamma_c := 1.4$ $\gamma_t := 1.36$ $c_{pc} := 0.24\,\frac{BTU}{lbm \cdot R}$ $c_{pt} := 0.275\,\frac{BTU}{lbm \cdot R}$ $h_{PR} := 18400\,\frac{BTU}{lbm}$

Atmospheric Conditions: Altitude = 2000 ft

$a_{0.ref} := 756.06mph$ $P_{0.ref} := 13.66\,\frac{lbf}{in^2}$ $T_{0.ref} := 52\,°F$ $M_{0.ref} := \frac{V_{dash}}{a_{0.ref}} = 0.2$

$g_c := 32.2\,\frac{lbm \cdot ft}{lbf \cdot s^2}$ $P0\_P9 := 1$ (Perfectly expanded, nozzle design)

Analysis:

Step 1) Bundle

$Tt0ref\_T0ref := 1 + \frac{\gamma_c - 1}{2} \cdot M_{0.ref}$ $Tt0ref\_T0ref = 1.04$ $\tau_{r.ref} := Tt0ref\_T0ref = 1.04$

$T_{t0.ref} := T_{0.ref}$ $T_{t0.ref} = 511.67\,R$

$Pt0ref\_P0ref := Tt0ref\_T0ref^{\frac{\gamma}{\gamma - 1}}$ $Pt0ref\_P0ref = 0.95$ $\pi_{r.ref} := Pt0ref\_P0ref = 0.95$

$V_{0.ref} := M_{0.ref} \cdot a_{0.ref} = 220 \cdot \frac{ft}{s}$ $P_{t0.ref} := P_{0.ref}$ $P_{t2.ref} := P_{t0.ref} = 13.66\,psi$

Step 2) Inlet

$\eta_r := 1$ (subsonic) $\pi_d := \pi_{d.max} \cdot \eta_r = 0.96$ $T_{t2.ref} := T_{t0.ref} = 511.67\,R$

Step 3) Compressor

$$\tau_{c.ref} := \pi_{c.ref}^{\frac{\gamma_c - 1}{\gamma_c \cdot e_c}} = 1.27 \qquad P_{t3.ref} := \pi_{c.ref} \cdot P_{t2.ref} \qquad T_{t3.ref} := \tau_{c.ref} \cdot T_{t2.ref} \qquad P_{t3.ref} = 28.686 \cdot \frac{lbf}{in^2}$$

Step 4) Burner 1st Law Analysis

$$f_{ref} := \frac{c_{pt} \cdot T_{t4.ref} - c_{pc} \cdot T_{t3.ref}}{h_{PR} \cdot \eta_b - c_{pt} \cdot T_{t4.ref}} = 0.02 \qquad mdot_f := f_{ref} \cdot mdot = 0.0063 \cdot \frac{lbm}{s}$$ <--should be ~0.0057 lbm/s

Step 5) Turbine: Power balance $Wdot_{turb}\ \eta_{mech} = Wdot_{compr}$

$$T_{t5.ref} := T_{t4.ref} - \frac{c_{pc} \cdot (T_{t3.ref} - T_{t2.ref})}{(1 + f_{ref}) \cdot \eta_{mech} \cdot c_{pt}} = 1739.36\,R$$

$$\tau_{t.ref} := \frac{T_{t5.ref}}{T_{t4.ref}} = 0.94 \qquad \pi_{t.ref} := \left(\frac{T_{t5.ref}}{T_{t4.ref}}\right)^{\frac{\gamma_t}{(\gamma_t - 1) \cdot e_t}} = 0.75$$

Step 6) Nozzle Exit Properties

$$Pt9ref\_P9ref := \pi_{r.ref} \cdot \pi_d \cdot \pi_{c.ref} \cdot \pi_b \cdot \pi_{t.ref} \cdot \pi_n \cdot P0\_P9 = 1.3$$

$$Tt9ref\_T9ref := Pt9ref\_P9ref^{\frac{\gamma_t - 1}{\gamma_t}} = 1.07 \qquad T_{t9.ref} := T_{t5.ref}$$

so $$T_{9.ref} := \frac{T_{t9.ref}}{Tt9ref\_T9ref} = 1623.46\,R \qquad a_9 := 1374mph$$

$$V_{9.ref} := \sqrt{(T_{t9.ref} - T_{9.ref}) \cdot 2 \cdot g_c \cdot c_{pt}} = 1263.8 \frac{ft}{s} \qquad M_9 := \frac{V_{9.ref}}{a_9} = 0.63$$

$$\theta_{0.ref} := \frac{T_{t0.ref}}{518.69R} = 0.99$$

Step 5) Figures of Merit

$$F\_mdot_{0.ref} := \frac{(1 + f_{ref}) \cdot V_{9.ref} - V_{0.ref}}{g_c} = 33.25 \cdot \frac{lbf}{\frac{lbm}{s}}$$

$$Thrust := F\_mdot_{0.ref} \cdot mdot = 10\,lbf$$ <---- should be ~10 lbf

$$SFC_{ref} := \frac{f_{ref} \cdot g}{F\_mdot_{0.ref}} = 2.29 \cdot \frac{1}{hr} \qquad \frac{SFC_{ref} - \frac{2.05}{hr}}{\frac{2.05}{hr}} = 0.12$$ <— %diff from published SFC

$$\eta_{th.ref} := \frac{(1 + f_{ref}) \cdot V_{9.ref}^{\ 2} - V_{0.ref}^{\ 2}}{2 \cdot g_c \cdot f_{ref} \cdot h_{PR}} = 0.08$$

$$\eta_{p.ref} := \frac{2 \cdot g_c \cdot V_{0.ref} \cdot F\_mdot_{0.ref}}{(1 + f_{ref}) \cdot V_{9.ref}^{\ 2} - V_{0.ref}^{\ 2}} = 0.3$$

$$\eta_{o.ref} := \eta_{th.ref} \cdot \eta_{p.ref} = 0.02$$

MISSION ANALYSIS

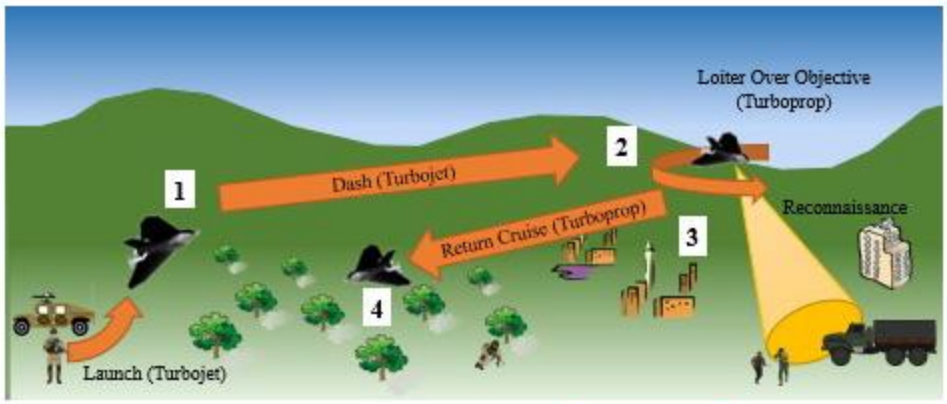

GIVEN *Aircraft Data:* $W_E := 12lbf$ $W_F := 6lbf$ $S_{wing} := 3ft^2$ $No\_Engines := 1$

Drag Polar: $K_1 := \frac{1}{\pi \cdot .9 \cdot 2} = 0.18$ $C_{D0} := .013$

Mission Data $W_{factor\_4} := 1.02$

$M_{cruise} := M_{0.ref}$ $R_{cruise} := 50mi$ $Alt_{cruise\_loiter} = 2000ft$ $M_{loiter} := 0.05$

Atmospheric Data

$P_{2kft} := P_{0.ref}$ $T_{2kft} := T_{0.ref}$ $\rho_{2kft} := 0.0749 \frac{lbm}{ft^3}$ $a_{2kft} := a_{0.ref}$

Installation Loss Model: $\phi_{cruise} := 0.05$ $\phi_{loiter} := 0.05$

Take-Off Weight: $W_1 := W_E + W_F = 18lbf$

Initial Dash Starting Weight: $W_1 = 18 \cdot lbf$

Return Cruise Ending Weight: $W_4 := W_{factor\_4} \cdot (W_E)$ $W_4 = 12.24 \cdot lbf$

Dash Velocity: $V_{cruise} := M_{cruise} \cdot a_{2kft}$ $V_{cruise} = 220 \frac{ft}{s}$

Initial Cruise Lift Coefficient: $C_{L1} := \frac{2 \cdot W_1}{\rho_{2kft} \cdot V_{cruise}^2 \cdot S_{wing}}$ $C_{L1} = 0.11$

Initial Cruise Drag Coefficient: $C_{D1} := C_{D0} + K_1 \cdot C_{L1}^2$ $C_{D1} = 0.015$

Initial Cruise Uninstalled Thrust Required: $F_{min\_3} := \frac{\frac{1}{2} \rho_{2kft} \cdot V_{cruise}^2 \cdot C_{D1} \cdot S_{wing}}{(1 - \phi_{cruise}) \cdot No\_Engines}$

$F_{min\_3} = 3 \cdot lbf$

Initial Cruise Uninstalled SFC: $SFC_{1\_2} := SFC_{ref} \cdot \frac{g_c}{g} = 2.29 \cdot \frac{lbm}{hr \cdot lbf}$

Initial Cruise Ending Weight: $W_2 := \left[\sqrt{W_1} - \sqrt{\frac{\rho_{2kft} \cdot S_{wing}}{2 \cdot C_{L1}}} \cdot \left(\frac{R_{cruise}}{2} \cdot \frac{SFC_{1\_2} \cdot g}{1 - \phi_{cruise}} \cdot C_{D1} \right) \right]^2$

$W_2 = 16.02 \cdot lbf$

Return Cruise Lift Coefficient: $C_{L4} := \frac{2 \cdot W_4}{\rho_{2kft} \cdot V_{cruise}^2 \cdot S_{wing}}$ $C_{L4} = 0.07$

Return Cruise Drag Coefficient: $C_{D4} := C_{D0} + K_1 \cdot C_{L4}^2$ $C_{D4} = 0.0139$

Return Cruise Uninstalled SFC: $SFC_{3\_4} := 1 \cdot \frac{lbm}{hr \cdot lbf}$ (turboprop partial throttle estimate, KC et al.)

Return Cruise Starting Weight: $W_3 := \left[\sqrt{W_4} + \sqrt{\frac{\rho_{2kft} \cdot S_{wing}}{2 \cdot C_{L4}}} \cdot \left(\frac{R_{cruise}}{2} \cdot \frac{SFC_{3\_4} \cdot g}{1 - \phi_{cruise}} \cdot C_{D4} \right) \right]^2$

$W_3 = 13 \cdot lbf$

Return Cruise Lift Coefficient: $C_{L3} := \frac{2 \cdot W_3}{\rho_{2kft} \cdot V_{cruise}^{2} \cdot S_{wing}}$ $C_{L3} = 0.08$

Return Cruise Drag Coefficient: $C_{D3} := C_{D0} + K_1 \cdot C_{L3}^{2}$ $C_{D3} = 0.0141$

Return Cruise Uninstalled Thrust Required: $F_{min\_3} := \frac{\frac{1}{2} \rho_{2kft} \cdot V_{cruise}^{2} \cdot C_{D3} \cdot S_{wing}}{(1 - \phi_{cruise}) \cdot No\_Engines}$

$F_{min\_3} = 2.5 \cdot lbf$

Fuel Available for Loiter: $W_{fuel\_loiter} := W_2 - W_3$ $W_{fuel\_loiter} = 3 \cdot lbf$

Loiter Velocity: $V_{loiter} := M_{loiter} \cdot a_{2kft}$ $V_{loiter} = 55.4 \cdot \frac{ft}{s}$

Loiter Initial Lift Coefficient: $C_{L2} := \frac{2 \cdot W_2}{\rho_{2kft} \cdot V_{loiter}^{2} \cdot S_{wing}}$ $C_{L2} = 1.49$

Loiter Initial Drag Coefficient: $C_{D2} := 2 \cdot K_1 \cdot C_{L2}^{2}$ $C_{D2} = 0.7874$

Loiter Uninstalled Thrust Required: $F_{min\_2} := \frac{\frac{1}{2} \rho_{2kft} \cdot V_{loiter}^{2} \cdot S_{wing} \cdot (C_{D2})}{(1 - \phi_{loiter}) \cdot No\_Engines}$ $F_{min\_2} = 8.9 \cdot lbf$

Loiter Maximum Endurance: $E_{loiter} := \frac{1}{g} \cdot \frac{(1 - \phi_{loiter})}{SFC_{3\_4}} \cdot \frac{C_{L2}}{C_{D2}} \cdot \ln\left(\frac{W_2}{W_3}\right)$

$E_{loiter} = 21.9 \cdot min$

APPENDIX B
CALIBRATION CURVES

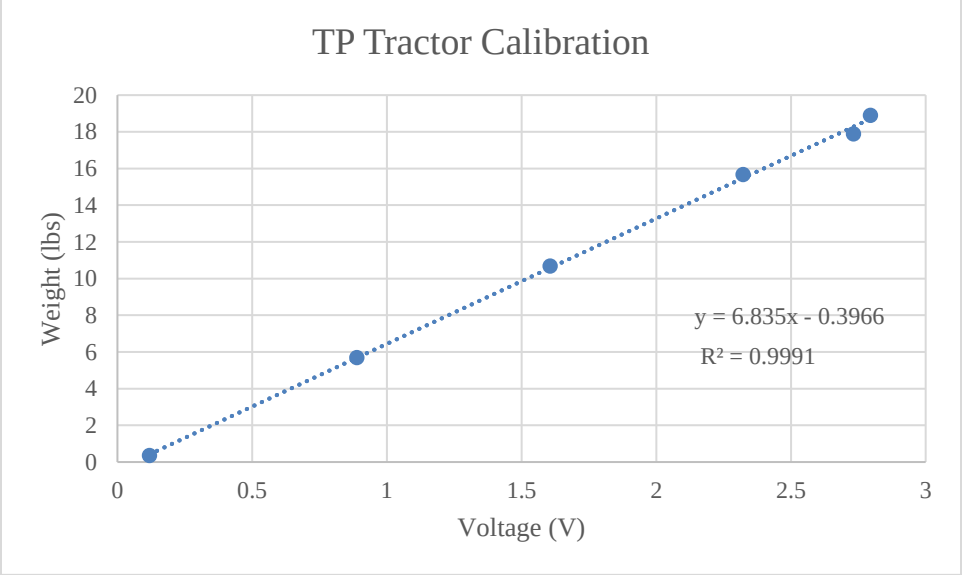

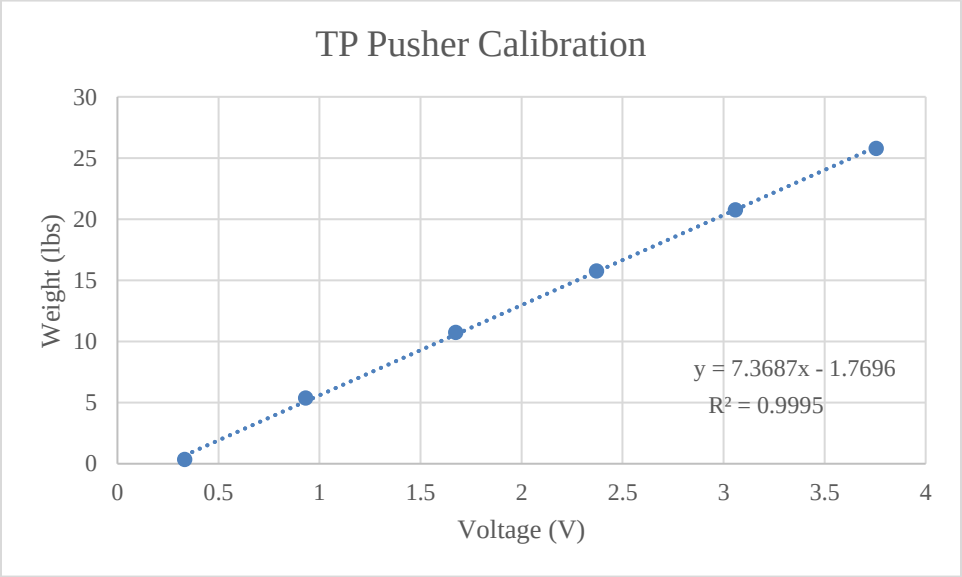

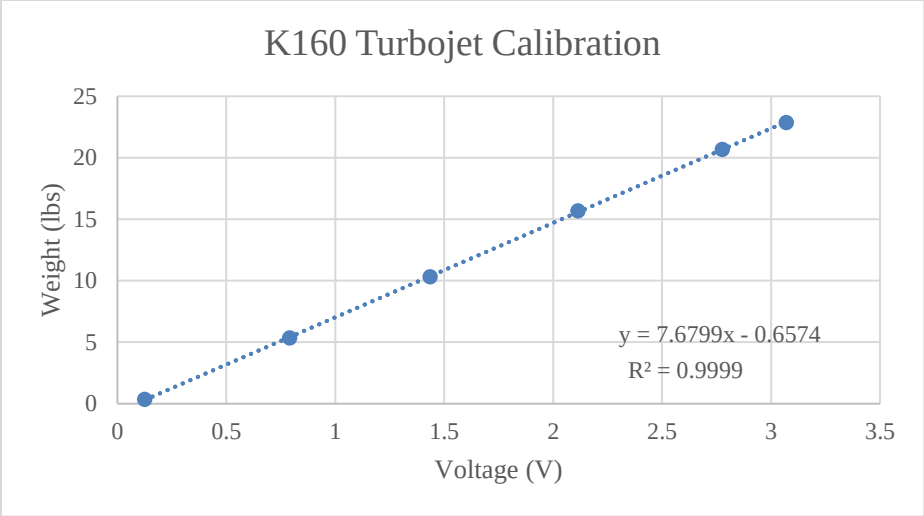
K160 Turbojet Calibration
Weight (lbs)
Voltage (V)
y = 7.6799x - 0.6574
R² = 0.9999
0
5
10
15
20
25
0
0.5
1
1.5
2
2.5
3
3.5

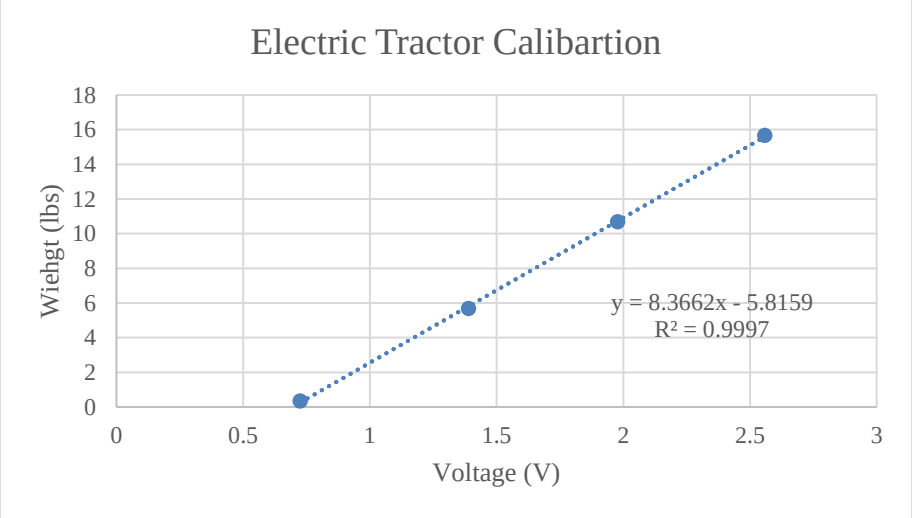
Electric Tractor Calibartion
Wiehgt (lbs)
Voltage (V)
y = 8.3662x - 5.8159
R² = 0.9997
0
2
4
6
8
10
12
14
16
18
0
0.5
1
1.5
2
2.5
3

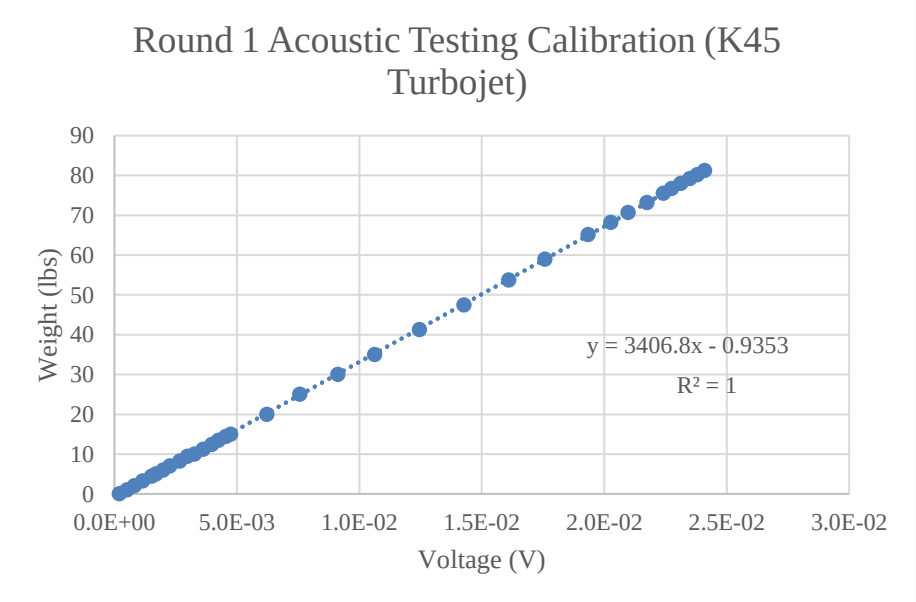
Round 1 Acoustic Testing Calibration (K45 Turbojet)
Weight (lbs)
Voltage (V)
y = 3406.8x - 0.9353
R² = 1
0
10
20
30
40
50
60
70
80
90
0.0E+00
5.0E-03
1.0E-02
1.5E-02
2.0E-02
2.5E-02
3.0E-02

APPENDIX C
CONCEPT 1 TEST LOG

	K45	K45TP	K45TP Core	Bellmouth	Jet Pipe	Cone	Jet Pipe Aft Seal	Ram Air	Gradual Mating of K45	Startup Fuel
3/28/2018	x									31%
		x								31%
			x							31%
	x			x	x					31%
3/30/2018			x		x	x				31%
			x		x	x				31%
4/2/2018			x	x	x	x	x		x	20%
			x	x	x	x	x	x		20%
			x	x	x	x	x	x		20%
			x		x	x	x	x		20%
4/24/2018			x		direct connect					20%

Concept 1 Detailed Test Log.

Notes
Nominal
Nominal
Nominal
Blue flame coming out of nozzle. Cut during startup
Jet pipe 1.5 in forward of nozzle exit plane. Blue flame sustained around nozzle. Cut during startup
Jet pipe in-line with nozzle exit plane. Blue flame sustained around nozzle. Cut during startup
Made it through startup normally before mating. Sustained flame out of nozzle upon mating.
Ejector ~1in forward. Smaller flame out of the nozzle during startup. Large flame once ram air was cut after startup
Throttled up after startup. Same flame
Let idle after startup. Steady blue flame through jet pipe during idle.
Fire at Turbojet/Jet Pipe seal, fire extinguisher discharged

Test Log Notes Column.

APPENDIX D
MATLAB POLAR PLOTTER CODE

```
%Useful for OASPL graphs in acoustic testing
%insert mic setup in deg
%insert corresponding OASPL data in r1, r2, r3...


clear all
deg = [150 120 90 90 60 30];
th = deg2rad(deg);
r1 = [103.33 101.43 98.81 98.31 97.75 98.53];
r2 = [105.67 106.66 106.48 106.07 105.66 106.20];
r3 = [117.51 115.05 109.05 107.98 108.19 108.39];
%r4 = [105.67 106.66 106.48 106.07 105.66 106.20];
subplot(2, 1, 1)
polarplot(th(4:6), r1(4:6), 'dk', 'markers',13)
hold on
polarplot(th(4:6), r2(4:6), 'sr', 'markers',13)
rlim([80 120])
pax = gca;
pax.ThetaZeroLocation = 'top';
pax.ThetaLim = [0 90];
polarplot(th(4:6), r3(4:6), 'om', 'markers',13)
%polarplot(th(4:6), r4(4:6), '^b', 'markers',13)
legend({'TP Tractor - 30.1 lb', 'TP Pusher - 30.0 lb', 'Turbojet - 31.7
lb'})
set(findall(gcf,'-property','FontSize'),'FontSize',14)
set(findall(gca,'-property','FontName'),'FontName','Times New Roman')
title('Comparison at 100% Throttle')
thetaticklabels({'0°','30°','60°', '90°'})

subplot(2, 1, 2)
polarplot(th(1:3), r1(1:3), 'dk', 'markers', 13)
hold on
polarplot(th(1:3), r2(1:3), 'sr', 'markers', 13)
rlim([80 120])
pax = gca;
pax.ThetaZeroLocation = 'top';
pax.ThetaLim = [90 180];
polarplot(th(1:3), r3(1:3), 'om', 'markers', 13)
%polarplot(th(1:3), r4(1:3), '^b', 'markers', 13)
set(findall(gcf,'-property','FontSize'),'FontSize', 14)
set(findall(gca,'-property','FontName'),'FontName','Times New Roman')
pax.RAxis.Label.String = 'OASPL [dB]';
thetaticklabels({'90°','120°','150°'})
rticklabels([])
```

APPENDIX E
ALL GRAPHS FROM ACOUSTIC TESTING

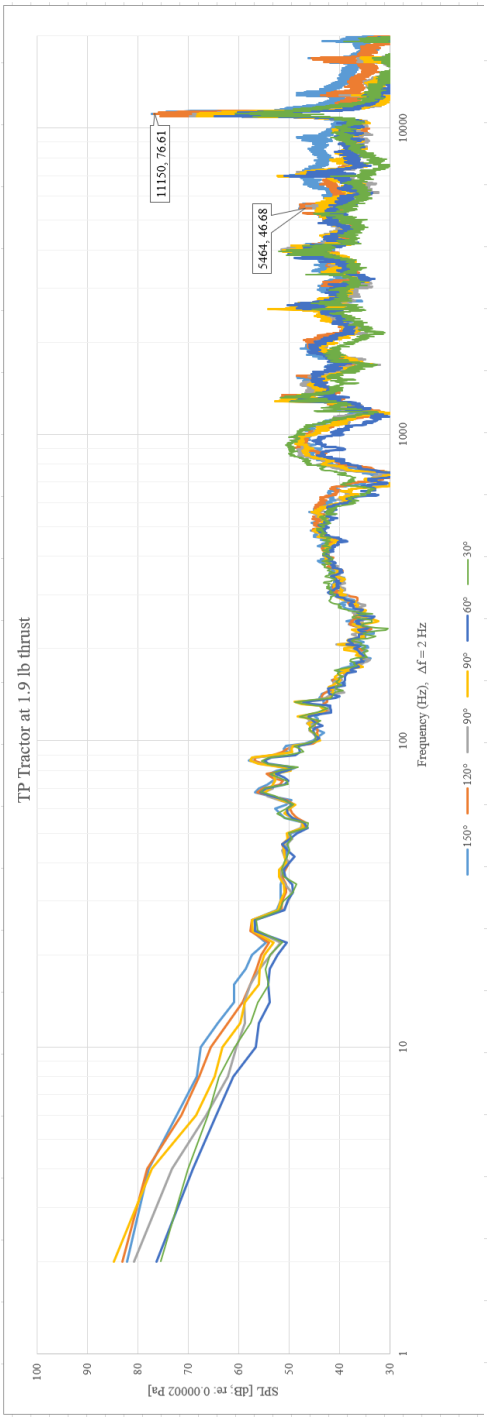

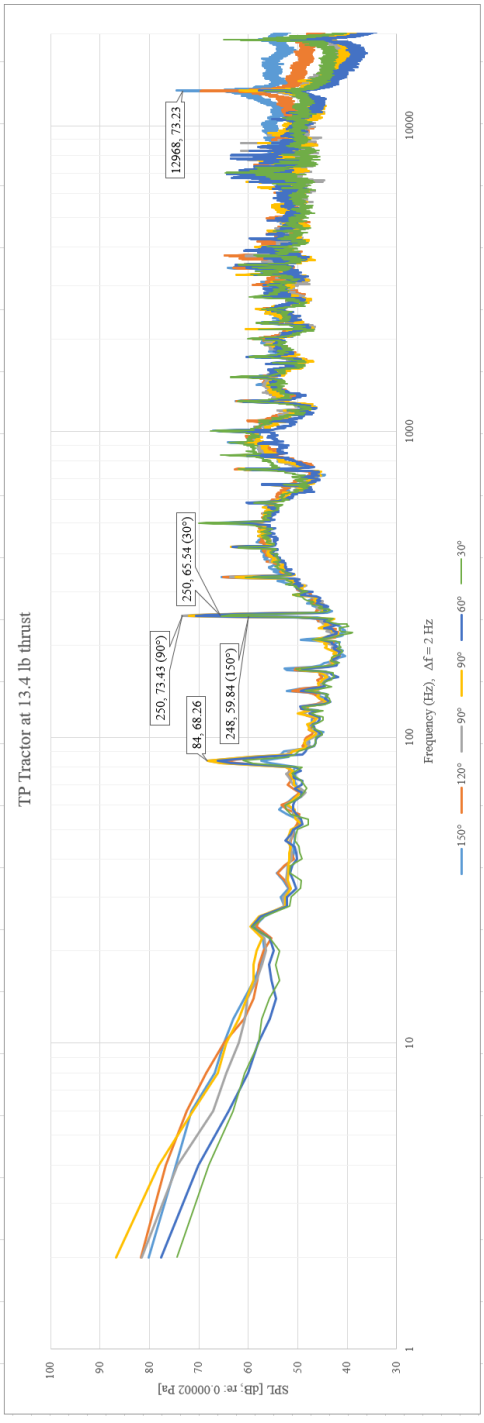

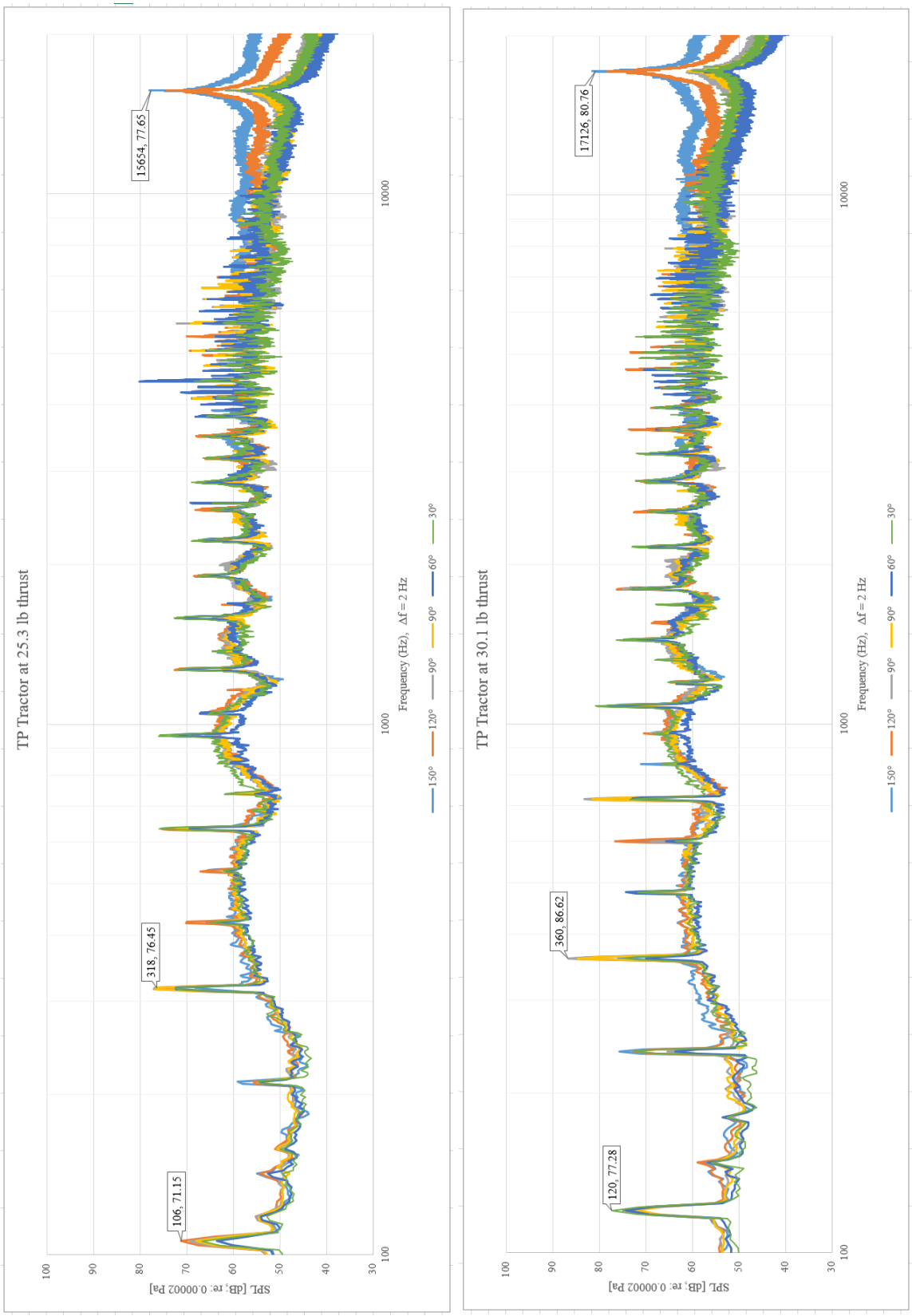
TP Tractor at 25.3 lb thrust
SPL [dB; re: 0.00002 Pa]
Frequency (Hz), Δf = 2 Hz
106, 71.15
318, 76.45
15654, 77.65
150°
120°
90°
90°
60°
30°
TP Tractor at 30.1 lb thrust
SPL [dB; re: 0.00002 Pa]
Frequency (Hz), Δf = 2 Hz
120, 77.28
360, 86.62
17126, 80.76
150°
120°
90°
90°
60°
30°

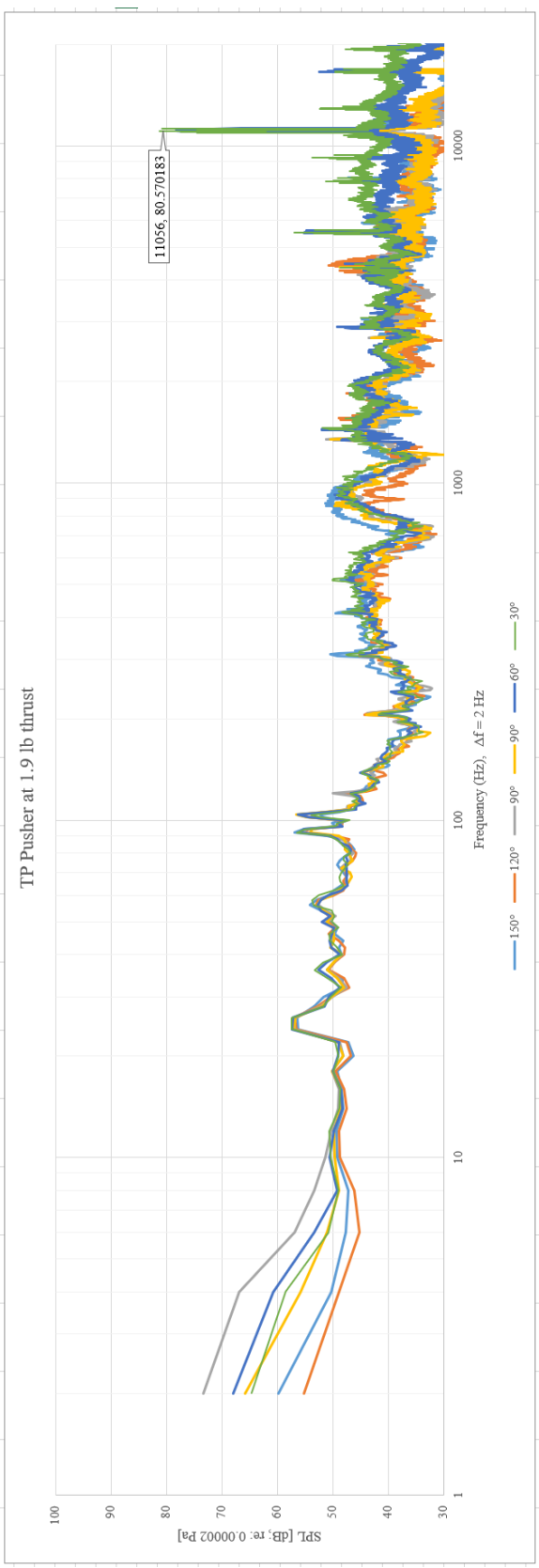
TP Pusher at 1.9 lb thrust
11056, 80.570183
SPL [dB; re: 0.00002 Pa]
Frequency (Hz), Δf = 2 Hz
150° 120° 90° 90° 60° 30°

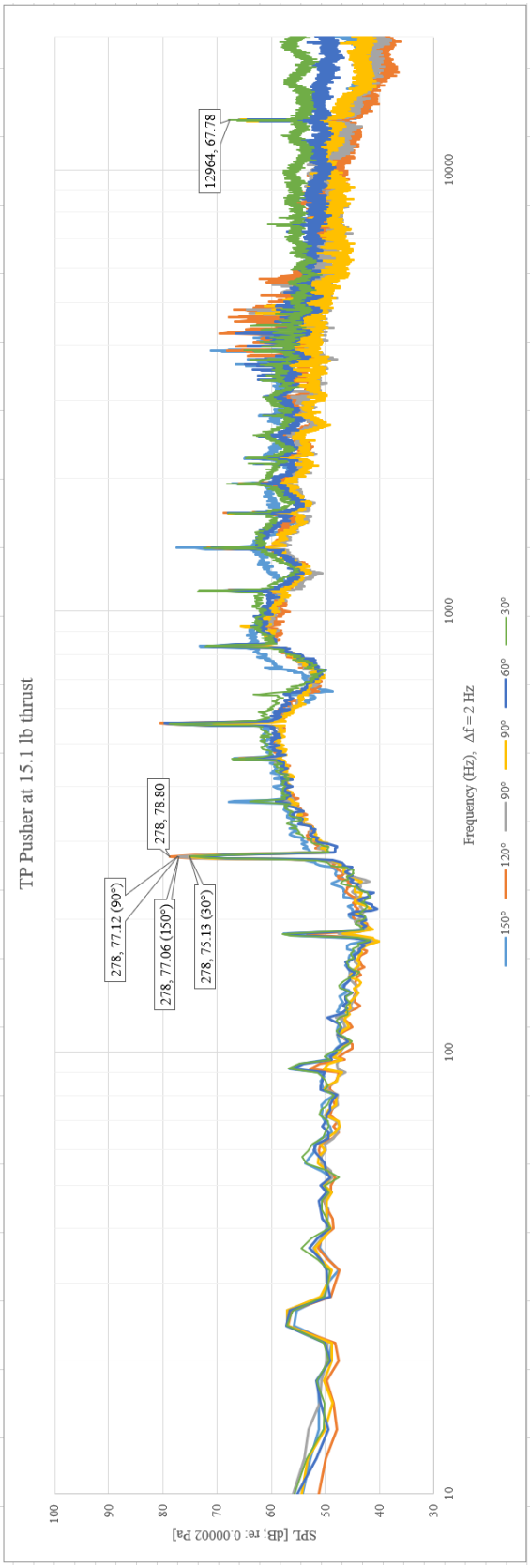
TP Pusher at 15.1 lb thrust
12964, 67.78
278, 78.80
278, 77.12 (90°)
278, 77.06 (150°)
278, 75.13 (30°)
SPL [dB; re: 0.00002 Pa]
Frequency (Hz), Δf = 2 Hz
150° 120° 90° 90° 60° 30°

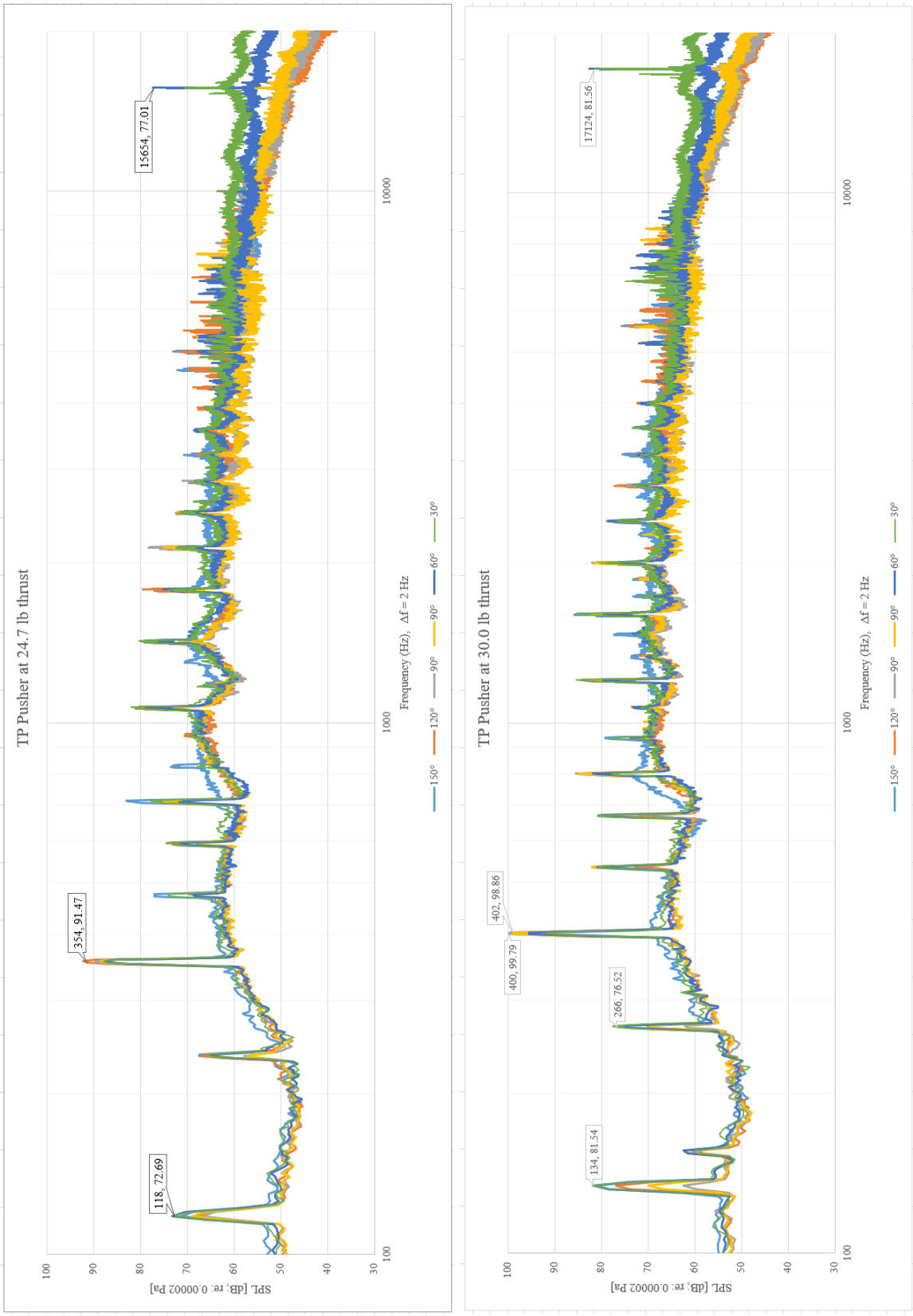
TP Pusher at 24.7 lb thrust
15654, 77.01
354, 91.47
118, 72.69
SPL [dB; re: 0.00002 Pa]
Frequency (Hz), Δf = 2 Hz
150°
120°
90°
60°
30°
TP Pusher at 30.0 lb thrust
17124, 81.56
402, 98.86
400, 99.79
266, 76.52
134, 81.54
SPL [dB; re: 0.00002 Pa]
Frequency (Hz), Δf = 2 Hz
150°
120°
90°
60°
30°

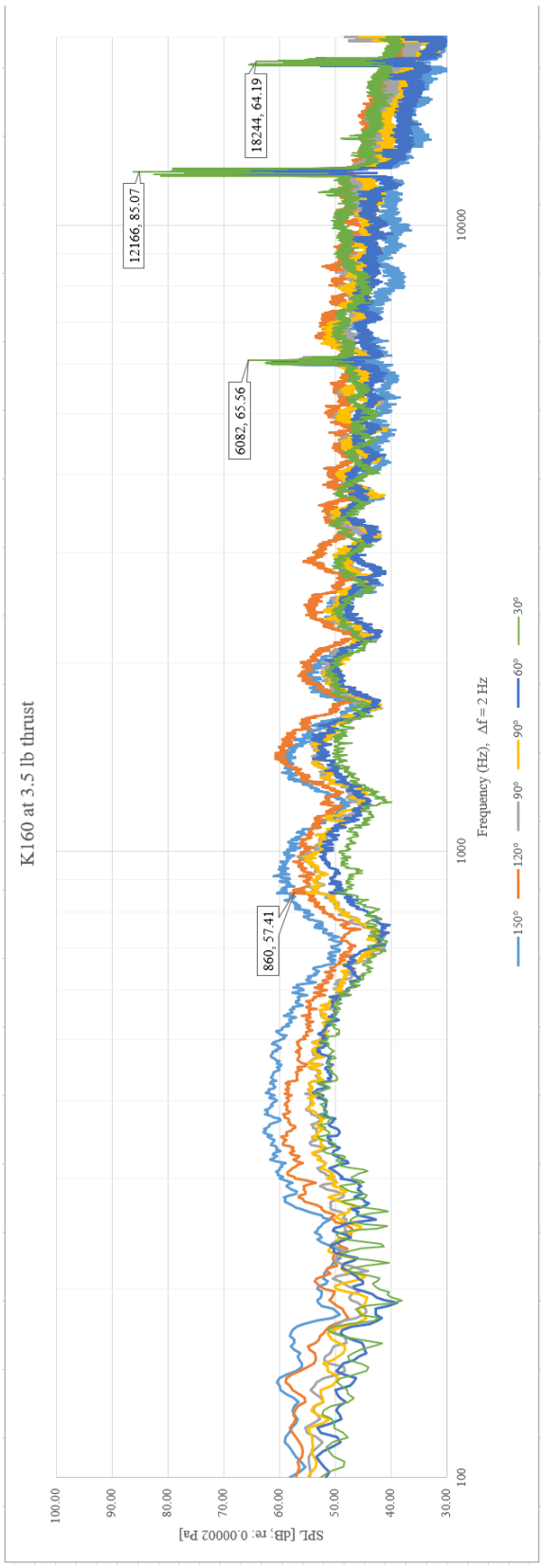
K160 at 3.5 lb thrust
SPL [dB; re: 0.00002 Pa]
100.00
90.00
80.00
70.00
60.00
50.00
40.00
30.00
100
1000
10000
Frequency (Hz), Δf = 2 Hz
150°
120°
90°
60°
30°
860, 57.41
6082, 65.56
12166, 85.07
18244, 64.19

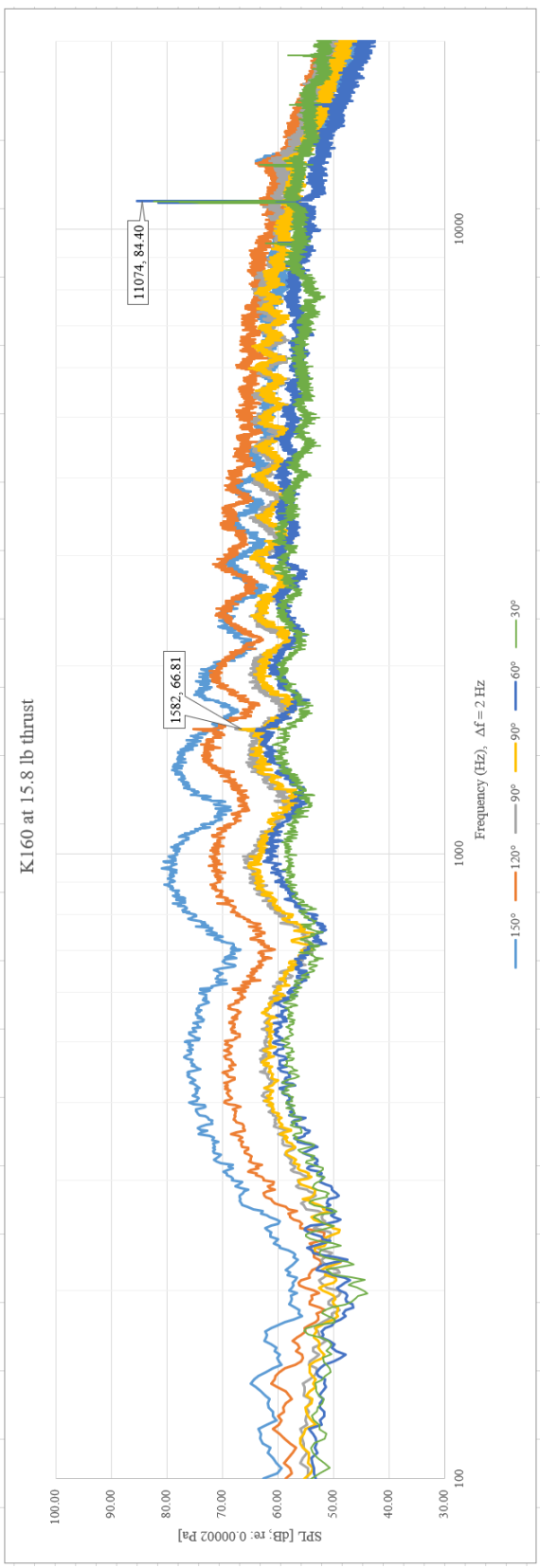
K160 at 15.8 lb thrust
SPL [dB; re: 0.00002 Pa]
100.00
90.00
80.00
70.00
60.00
50.00
40.00
30.00
100
1000
10000
Frequency (Hz), Δf = 2 Hz
150°
120°
90°
60°
30°
1582, 66.81
11074, 84.40

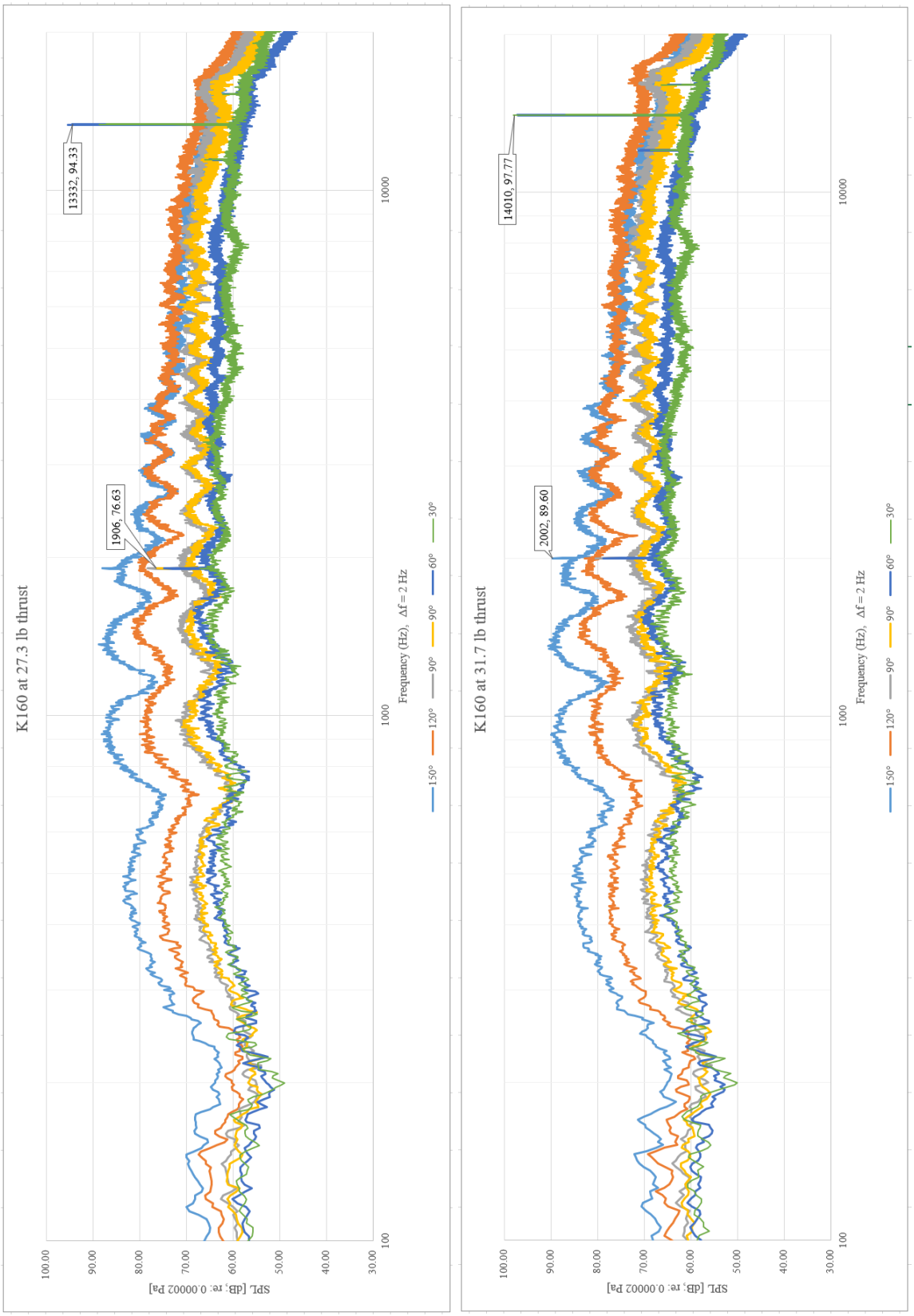
K160 at 27.3 lb thrust
13332, 94.33
1906, 76.63
SPL [dB; re: 0.00002 Pa]
Frequency (Hz), Δf = 2 Hz
150°
120°
90°
90°
60°
30°
K160 at 31.7 lb thrust
14010, 97.77
2002, 89.60
SPL [dB; re: 0.00002 Pa]
Frequency (Hz), Δf = 2 Hz
150°
120°
90°
90°
60°
30°

APPENDIX F
K160 TURBOJET ACOUSTIC TESTING

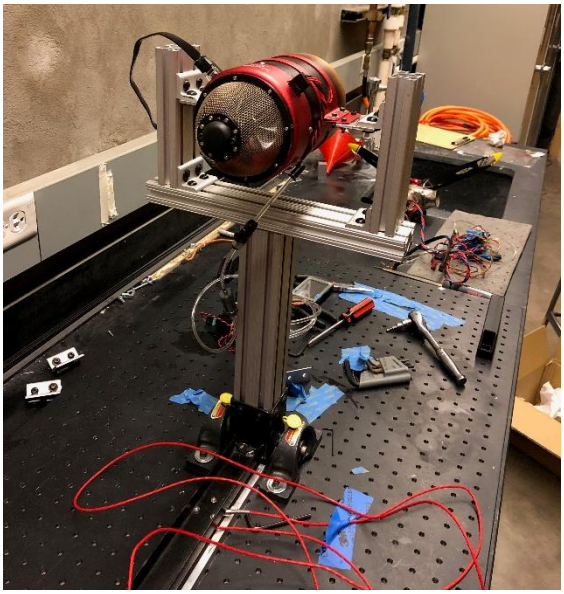

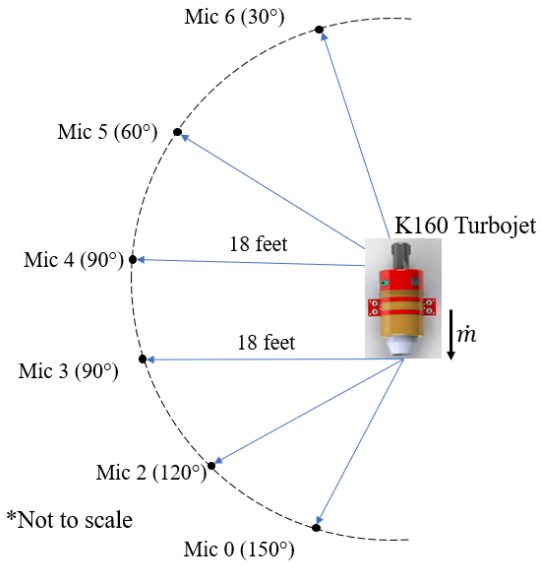

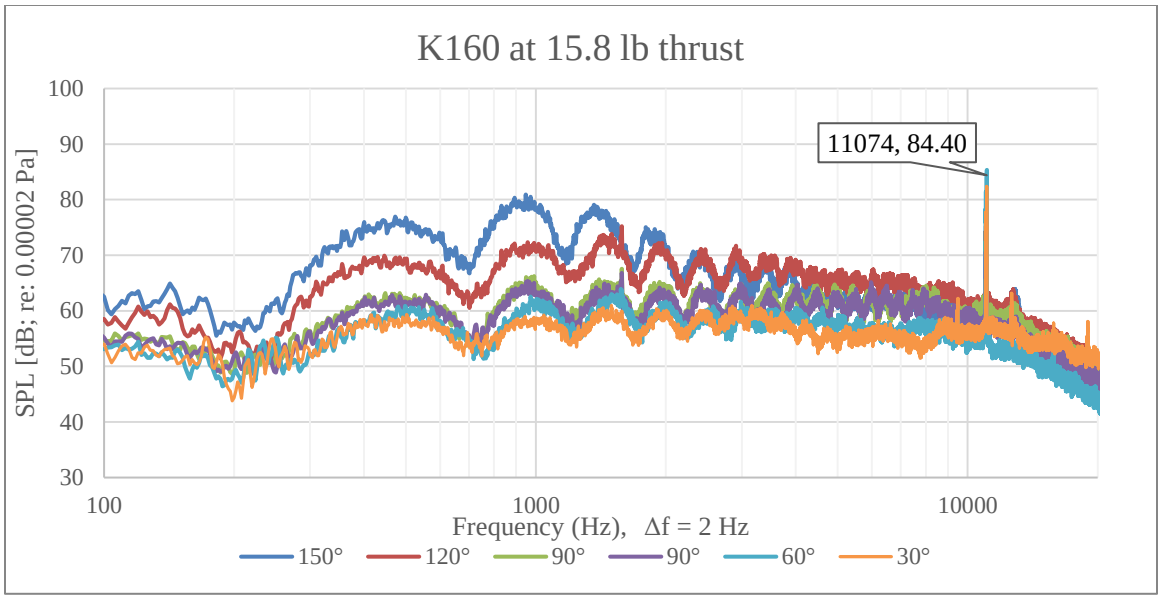
K160 at 15.8 lb thrust
SPL [dB; re: 0.00002 Pa]
100
90
80
70
60
50
40
30
11074, 84.40
100
1000
10000
Frequency (Hz), Δf = 2 Hz
150°
120°
90°
90°
60°
30°

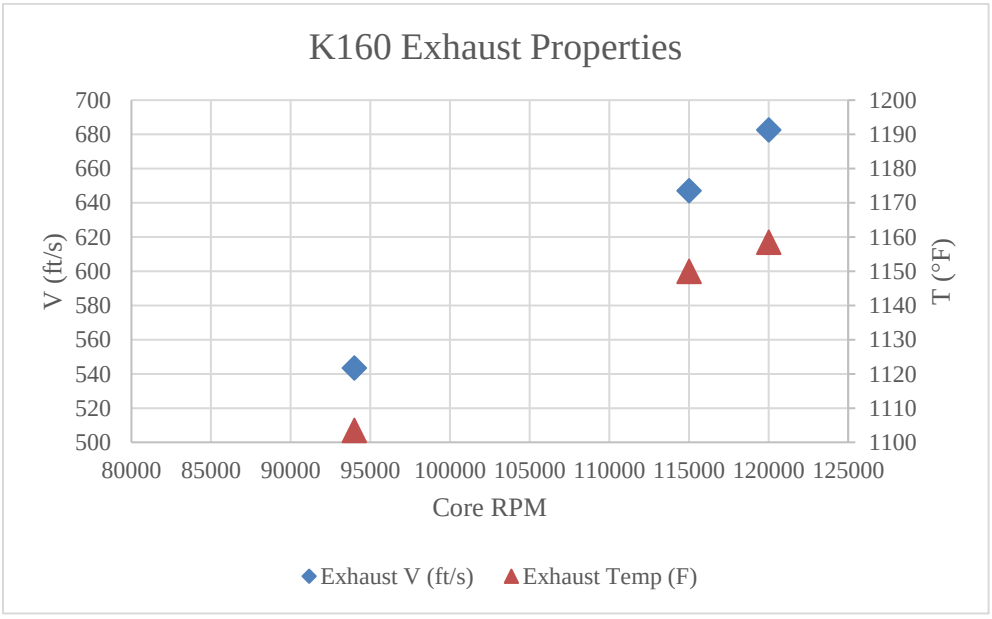
K160 Exhaust Properties
V (ft/s)
700
680
660
640
620
600
580
560
540
520
500
T (°F)
1200
1190
1180
1170
1160
1150
1140
1130
1120
1110
1100
80000
85000
90000
95000
100000
105000
110000
115000
120000
125000
Core RPM
Exhaust V (ft/s)
Exhaust Temp (F)

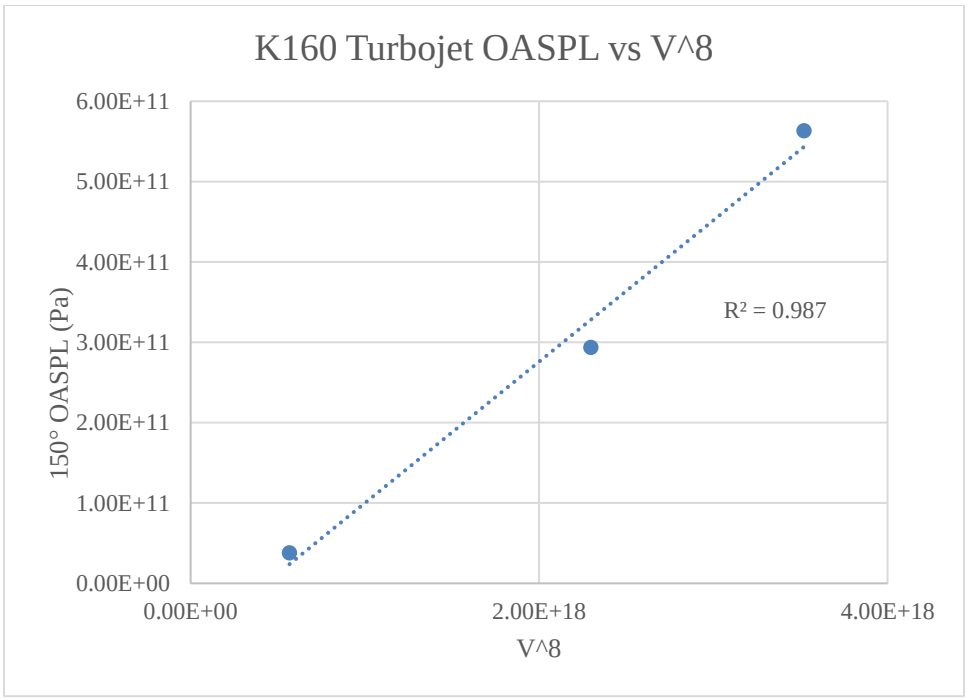
K160 Turbojet OASPL vs V^8
6.00E+11
5.00E+11
4.00E+11
3.00E+11
2.00E+11
1.00E+11
0.00E+00
150° OASPL (Pa)
R² = 0.987
0.00E+00
2.00E+18
4.00E+18
V^8

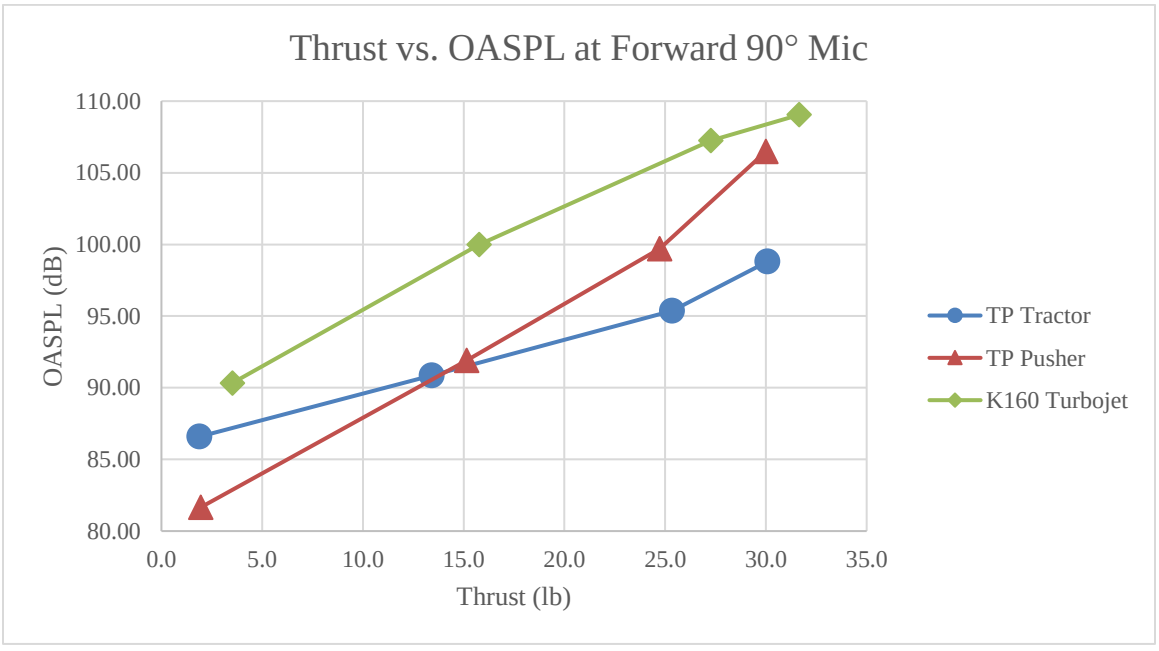
Thrust vs. OASPL at Forward 90° Mic
110.00
105.00
100.00
95.00
90.00
85.00
80.00
OASPL (dB)
0.0
5.0
10.0
15.0
20.0
25.0
30.0
35.0
Thrust (lb)
TP Tractor
TP Pusher
K160 Turbojet

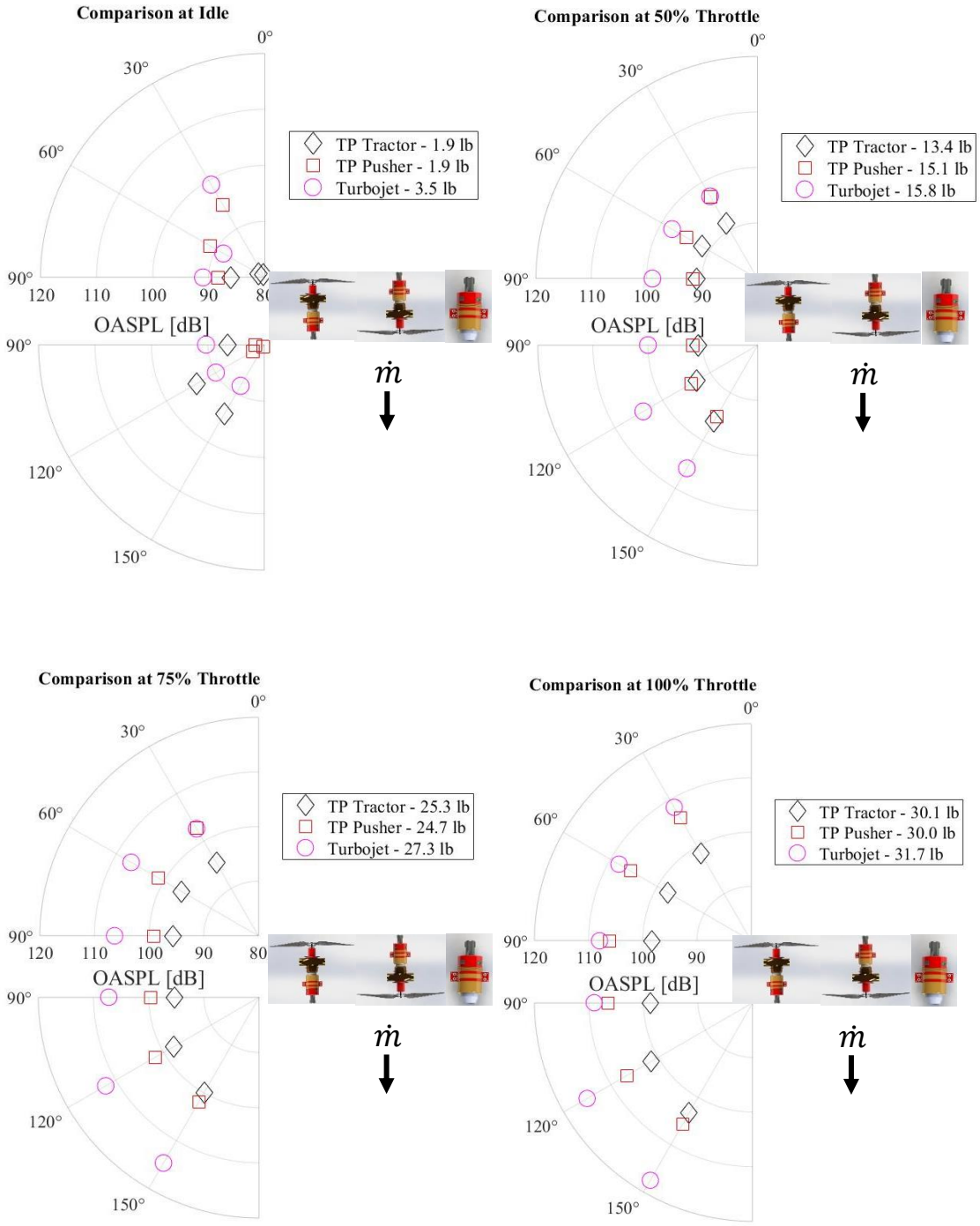
Comparison at Idle
0°
30°
60°
90°
120°
150°
120
110
100
90
OASPL [dB]
TP Tractor - 1.9 lb
TP Pusher - 1.9 lb
Turbojet - 3.5 lb
$\dot{m}$
Comparison at 50% Throttle
TP Tractor - 13.4 lb
TP Pusher - 15.1 lb
Turbojet - 15.8 lb
Comparison at 75% Throttle
TP Tractor - 25.3 lb
TP Pusher - 24.7 lb
Turbojet - 27.3 lb
Comparison at 100% Throttle
TP Tractor - 30.1 lb
TP Pusher - 30.0 lb
Turbojet - 31.7 lb

VITA

Matt R. Durkee

Candidate for the Degree of

Master of Science

Thesis: TURBOPROP PERFORMANCE AND ACOUSTIC EVALUATION FOR A SMALL UNMANNED AIRCRAFT VARIABLE-CYCLE ENGINE

Major Field: Mechanical and Aerospace Engineering

Biographical:

Education:

Completed the requirements for the Master of Science in Mechanical and Aerospace Engineering at Oklahoma State University, Stillwater, Oklahoma in May, 2019.

Completed the requirements for the Bachelor of Science in Mechanical Engineering and Aerospace Engineering at Oklahoma State University, Stillwater, Oklahoma in 2017.

Experience:

Graduate Research Assistant – Oklahoma State University, Stillwater, OK
Graduate Teaching Assistant – Oklahoma State University, Stillwater, OK
Propulsion Development Intern – SpaceX, Hawthorne, CA
Powerplant Engineering Intern – Southwest Airlines, Dallas, TX

Professional Memberships:

AIAA